DTIC
ELECTE
JAN 03 1994
S D
F

DESIGN, FABRICATION, MODELING, AND OPTICAL CHARACTERIZATION OF ORGANIC POLYMER NONLINEAR DIRECTIONAL COUPLERS

THESIS

John Nathan Berry, Captain, USAF

AFIT/GEO/ENP/94D-01

19941228 005

This document has been approved for public release and sale; its distribution is unlimited.

DEPARTMENT OF THE AIR FORCE
AIR UNIVERSITY
AIR FORCE INSTITUTE OF TECHNOLOGY

Wright-Patterson Air Force Base, Ohio

AFIT/GEO/ENP/94D-01

DTIC
ELECTE
JAN 03 1994
S D
F

Accesion For
NTIS CRA&I ☒
DTIC TAB ☐
Unannounced ☐
Justification
By
Distribution /
Availability Codes
Dist | Avail and / or Special
A-1

DESIGN, FABRICATION, MODELING, AND OPTICAL CHARACTERIZATION OF ORGANIC POLYMER NONLINEAR DIRECTIONAL COUPLERS

THESIS

John Nathan Berry, Captain, USAF

AFIT/GEO/ENP/94D-01

DTIC QUALITY INSPECTED 2

Approved for public release; distribution unlimited.

AFIT/GEO/ENP/94D-01

DESIGN, FABRICATION, MODELING, AND OPTICAL CHARACTERIZATION OF ORGANIC POLYMER NONLINEAR DIRECTIONAL COUPLERS

THESIS

Presented to the Faculty of the School of Engineering

of the Air Force Institute of Technology

Air University

In Partial Fulfillment of the

Requirements for the Degree of

Master of Science in Electrical Engineering

John Nathan Berry, B.S.E.E.
Captain, USAF

December 1994

Approved for public release; distribution unlimited.

To my Parents

Preface

This work on organic polymer-based integrated optic devices is a direct extension of work done by Captain Carl A. Kutsche at the Air Force Institute of Technology during 1990-91. His investigation of processing techniques for the polymers under study was an essential step toward the design, fabrication, and optical characterization of working devices. Captain Kutsche's work concentrated on developing the processing steps needed to fabricate optical waveguides from thin polymer films. This thesis is the next logical step. The devices were designed using the dimensions of the existing lithographic mask and the measured optical indices of the polymers under study. Fabrication of the waveguides was carried out using the techniques developed by Captain Kutsche. Modeling of the resulting devices was accomplished using previously developed approximate analytical methods. The optical characterization of the devices under study was accomplished through an end-fired input coupling technique. The results of this thesis demonstrate that the organic polymers under investigation have applications in the fields of integrated optics, optical signal processing, and all-optical computing.

There were, of course, many people involved in this thesis research. I owe a debt of gratitude to Captain Kutsche, then of WL/ELR, for his advice and time during the fabrication of devices. His experience in this area was invaluable and is greatly appreciated. Dr. Hoa Jiang and Dr. Pete Haaland of Lawrence Associates, WL/MLPJ, were responsible for the growth of the thin polymer films under investigation. I thank them for their help and cooperation. I would also like to thank my advisor, Captain (Dr.) Jeffrey Grantham, and my committee members, Major (Dr.) Paul Ostdiek and Dr. Victor M. Bright. My conversations with them and their editorial comments made this thesis a far better document than it would have been otherwise. Major Richard Bagnell's help in the laboratory and contribution of a format conversion program were essential to the successful

collection of data and I owe him a debt of gratitude. I would also like to thank Chris O'Brien and Bill Trop for their help in wafer preparation and Joe Williams for his excellent work with the scanning electron microscope. My friend, Eric Baenen, also deserves my thanks for making me laugh and keeping me company while at AFIT. His companionship made this ordeal much more tolerable than it would have been otherwise. Finally, I would like to thank my wife, Laurel; my parents, Michael and Mary Hamm; our dogs, Bandit and Noel; and the cats, Alaska and Doobie. Without their love, patience, and understanding this research would not have been accomplished.

John N. Berry
19 October 1994

Table of Contents

Preface ii

List of Figures vi

List of Tables viii

List of Symbols ix

Abstract xi

I. Introduction 1-1

Background 1-1
Problem Statement 1-5
Scope 1-5
Approach and Presentation 1-5

II. Theory of Optical Directional Couplers 2-1

Theory of Dielectric Waveguides 2-1
The Ray-Optic Approach 2-2
The Electromagnetic Development 2-7
Coupling Between Waveguides Made from Linear Media 2-11
Optical Nonlinearity in Polymers 2-18
Coupling Between Waveguides Made from Nonlinear Media 2-22

III. Design and Modeling of Waveguide and Coupler Structures 3-1

Confinement in Two Dimensions and Marcatili's Method 3-1
Effective Index Method 3-5
Calculation of Coupling Coefficients 3-9
Estimation of the Critical Power for an NLDC 3-12
Models of Fabricated Coupler Structures 3-14
Modeling of Strip-Loaded Waveguides 3-16
Modeling of Rib Waveguides 3-18
Modeling of Embedded Channel Waveguides 3-21
Observations Concerning the Modeling of Waveguides 3-21

IV. Fabrication of Waveguiding Structures 4-1

Strip-Loaded Waveguides 4-2
Rib Waveguides 4-13
Channel Waveguides 4-17

V. Experimental Apparatus 5-1

End-Fire Coupling Method 5-1
Overview of Experimental Apparatus 5-2
Alignment of the Optical Components 5-4

VI. Experimental Procedure 6-1

Sample Preparation and Alignment 6-1

VII. Experimental Results and Analysis 7-1

Guiding of Light Through a Polyphenylene Slab Waveguide 7-1
Coupling in a Multi-channel Directional Coupler 7-4
Lateral Confinement of Light and Coupling Between Guides 7-5
Nonlinear Effects 7-10
Waveguide Losses 7-12

VIII. Summary and Recommendations 8-1

Appendix A: Waveguide Dimensions for Single-mode Operation A-1

Appendix B: Slab Waveguide Electric Field Profiles B-1

Appendix C: The Effective Index Method for Strip-Loaded Waveguides C-1

Appendix D: The Effective Index Method for Rib Waveguides D-1

Appendix E: Marcatili's Method for Embedded Waveguides E-1

Bibliography Bib-1

Vita Vita-1

Figures

1-1. Basic geometry of an optical directional coupler. 1-3

1-2. The two-dimensional distribution of electric field within the coupling region of an optical directional coupler. 1-4

2-1. Radiation of optical energy into the cover and substrate in a "slab" waveguide structure. 2-2

2-2. Path of a ray undergoing total internal reflection (TIR) in a dielectric slab waveguide structure. 2-5

2-3. Some possible modes in a slab waveguide. 2-10

2-4. Dielectric slab waveguide geometry used as a model for the development of the coupled-mode equations. 2-12

2-5. The periodic exchange of power with $\Delta\beta \neq 0$. 2-15

2-6. The periodic exchange of power when $\Delta\beta = 0$. 2-16

2-7. Dependence of the power-transfer ratio, $\mathfrak{I}$, on the phase mismatch. 2-17

2-8. Self-defocusing and self-focusing in nonlinear materials. 2-19

2-9. Uncoupled nonlinear waveguides. 2-20

2-10. The response of an NLDC to various input powers. 2-24

2-11. An NLDC functioning as an all-optical logic gate. 2-26

3-1. Cross section of a guide region embedded in lower refractive index materials. 3-2

3-2. A channel waveguide used for two dimensional confinement of optical energy. 3-5

3-3. Typical strip-loaded and ridge waveguide structures. 3-6

3-4. Guide geometry used to analyze the strip-loaded guide by Marcatili's method. 3-8

3-5. Typical coupled waveguide structure and mode profiles. 3-10

3-6. The photolithographic mask used to define the dimensions of the waveguide structures. 3-15

3-7. Typical mode profiles in a strip-loaded waveguide. 3-18

3-8. Electric field profiles for $p = 1$ and $p = 2$ in a rib waveguide..... 3-20

4-1. The photolithographic mask used in fabrication of waveguide structures..... 4-1

4-2. The major steps in the fabrication of strip-loaded waveguide structures..... 4-5

4-3. Side wall roughness of the strip-loaded waveguide structures..... 4-7

4-4. Two different techniques for cleaving of samples..... 4-8

4-5. Resulting sample interfaces for different cleaving techniques..... 4-9

4-6. Typical SEM photograph used in the measurement of film thicknesses and waveguide features..... 4-12

4-7. Major steps in the fabrication of the rib waveguide structures..... 4-14

4-8. Structures resulting from rib waveguide fabrication attempt..... 4-15

4-9. The major steps in the fabrication of channel waveguides..... 4-17

4-10. Channel waveguides fabricated by etching silicon dioxide and deposition of polyphenylene..... 4-19

4-11. Close-up of the polyphenylene channel waveguides..... 4-20

5-1. The basic geometry of the end-fire coupling method..... 5-1

5-2. Test setup for the optical characterization of NLDCs..... 5-4

6-1. The "sunrise" pattern seen on the output monitor from the diffraction of the input light..... 6-2

7-1. Guiding of light through the polyphenylene film..... 7-2

7-2. Measured (a) and modeled (b) intensity profiles for a polyphenylene slab waveguide..... 7-3

7-3. Flow of injected power in a multi-channel directional coupler..... 7-4

7-4. Observed confinement of light in the lateral direction and coupling between adjacent strip-loaded guides..... 7-6

7-5. Observed guiding and coupling of light injected into a $W = 5$ μm strip-loaded waveguide..... 7-8

7-6. Coupling of light between adjacent strip-loaded waveguides..... 7-10

7-7. Output intensities for "low" and "high" peak injected powers..... 7-11

8-1. Proposed lithographic mask for further NLDC research..... 8-3

Tables

3-1. Modeling results for the strip-loaded waveguides. 3-17

3-2. Modeling results for the rib waveguides. 3-19

4-1. Parameters used for growth of polymer thin-films. 4-3

4-2. Nominal dimensions of the strip-loaded waveguide layers and features. 4-13

List of Symbols

Symbol	Definition
$a_1(z)$, $a_2(z)$	functions describing the amplitudes of the electric fields in coupled waveguides
$2a$	separation distance between guides in the coupled slab waveguide structure
C	arbitrary constant used in the normalization of the electric field profiles
d	width of the guide regions in the coupled slab waveguide structure
h	field parameter that describes the mode structure in the guide region
I	intensity of the light within a guide
k_o	propagation constant of an electromagnetic wave in free-space
k_x, k_y, k_z	propagation constant of a waveguide mode in direction specified by the subscript
L_o	interaction length of a directional coupler that results in complete coupling of the energy from one guide to the other
m_c	parameter used as a measure of input power in *Jensen*'s NLDC model
N_1, N_2	effective indices of the guides in the coupled slab waveguide structure
n	index of the media around the guides in the coupled slab waveguide structure
n_c, n_g, n_s	refractive index of the cover (c), guide (g), or substrate (s) layer in a slab waveguide structure
Δn	change in index due to nonlinear properties of material and intensity of light propagating within the material
n_2	coefficient that describes the intensity-dependent index shift
$P_1(z)$, $P_2(z)$	functions describing the power in the waveguides of a directional coupler
P_c	injected power level in a nonlinear directional coupler that results in the power being split equally between the two output ports
p	field parameter that describes the decay of the electric field in the cover layer; also, integer mode number in x direction for *Marcatili*'s method
q	field parameter that describes the decay of the electric field in the guide layer; also, integer mode number in y direction for *Marcatili*'s method
t_g	thickness of the guide layer in a slab waveguide structure
$u_1(x)$, $u_2(x)$	functions describing the spatial distribution of the modes in the coupled slab waveguide structure
W	width of waveguide in *Marcatili*'s method
Z	normalized coupler length in *Jensen*'s NLDC model
β_m	propagation constant in the z direction of the mth mode

$\Delta\beta$	difference in the propagation constant between two waveguides (also called the phase-mismatch between guides)
$\varepsilon_x(y)$	transverse function that describes the profile of the x-directed electric field in the y-direction.
η_2, η_4	decay coefficients of the fields in regions 2 and 4, respectively, in *Marcatili*'s method
θ_m	bounce angle, as measured from the interface, of the mth mode
θ_c	critical angle for the interface between two media as measured from the interface normal
θ_{cgc}, θ_{cgs}	critical angle at the guide/cover (gc) or guide/substrate (gs) interfaces, measured from the interface normal
κ, κ_{12}, κ_{21}	coupling coefficient between linear waveguides
λ_o	free-space wavelength of operation
ξ_3, ξ_5	decay coefficients of the fields in regions 3 and 5, respectively, in *Marcatili*'s method
ϕ_m	angle of incidence, as measured from the interface normal, for a ray of the mth mode
ϕ_{gc}, ϕ_{gs}	Goos-Hänchen phase shift experienced upon reflection from the guide/cover (gc) or guide/substrate (gs) interface.
$\chi^{(3)}$	a material parameter (chi-three) that describes third-order nonlinear properties
$\mathfrak{I}$	power-transfer ratio between coupled guides
$\ominus$	symbol used for the "bar" or straight-through channel in an optical coupler
$\otimes$	symbol used for the "cross" or adjacent channel in an optical coupler

Abstract

This research was an investigation into the suitability of a recently developed polymer, polyphenylene, as a material for integrated optical circuits (IOCs). Polymers show great promise in the area of IOCs because of material processing advantages, compatibility with most existing integrated circuit technology, and relatively strong nonlinear optical characteristics. This thesis contains an overview of: dielectric waveguides, linear and nonlinear directional coupler theory; various models useful in the design and analysis of optical waveguides; the fabrication of three different waveguide designs; the experimental apparatus and procedure used to optically characterize the waveguides; and the experimental results of the characterization.

Waveguiding of near infrared light through polyphenylene, in both a slab waveguide and strip-loaded guides, was observed for the first time in this polymer. Coupling of light between guides of a multi-channel directional coupler was also observed. No definitive conclusions concerning nonlinear effects are possible due to the non-identical, multi-channel nature of the fabricated waveguides. The results of this research indicate that polyphenylene is a candidate for use in IOCs and that the polymer should be the topic of further research.

Design, Fabrication, Modeling, and Optical Characterization of Organic Polymer Nonlinear Directional Couplers

I. Introduction

This thesis reports on research that was conducted on optical directional couplers (DCs). These devices are important integrated optic (IO) components of modern optical information processing systems. Recent advances in organic polymers indicate that these materials could be suited for use in IO devices such as linear and nonlinear directional couplers (NLDCs). Polymers may have cost, processing, and material property advantages over traditional optical materials used for waveguiding. During the course of this thesis research, optical DCs were designed, fabricated, modeled, and optically characterized.

Background

Light has been used to communicate information since prehistoric times. Perhaps the first instance of this was the caveman's use of campfire light and shadow puppets to play out the stalking of animals. Other historical examples abound: signal fires and lighthouses used to warn ships of dangerous coast lines, land- and ship-based optical telegraphs, and Paul Revere's famous "one if by land, two if by sea" signal from the Old North Church bell tower. All of these communication methods rely on the modulation of light to convey information. Modern optical communication networks use this same concept; information is encoded and transmitted using changes in optical intensity, frequency, or phase (10:124).

The Information Age is characterized by the transmission and processing of large amounts of data. This flow of information has created the need for communication

networks and processing systems with very fast data through-put rates. Traditional communication links are limited by the bandwidth available within the radio frequency spectrum. Fiber optic data networks and optical processing systems have overcome this limitation by using light as the carrier of information (11:2).

The electronic equipment used to transmit, receive, and process the information carried by an optical link is the bandwidth-limiting factor in modern optical data networks. With current electronic equipment, the information carried by an optical network must be converted into an electrical signal before it can be processed. After processing, the information is often reconverted into an optical signal so that it can be retransmitted to another system. On a relative time scale, the conversion process and electrical processing are slow. Great efforts are being made to produce hybrid electrical-optical and all-optical computers; processing systems that can carry out operations on information that is in an optical format. All-optical systems could be capable of data rates on the order of 10^{16} bits/sec, an exciting prospect when current electro-optical systems have achieved data rates on the order of 10^{9} bits/sec (25:864).

The DC (Fig. 1-1) is an essential element in an all-optical information processing system. A DC is composed of two optical waveguides brought into close proximity. A waveguiding region, shown as a gray line in the figure, is simply an optically suitable material surrounded by a material or materials of relatively lower refractive index. The difference in refractive index between the materials leads to total internal reflection of the optical energy within the waveguiding region.

The electric field of the optical energy traveling though a waveguide is concentrated within the guide material but some of the field, the so-called evanescent tail of the mode, extends into the material surrounding the waveguide. The adjacent waveguide is placed so close to the "excited" guide (the guide carrying the light) that the evanescent tail of the mode

overlaps into this second waveguide (Fig. 1-2). This results in the light being coupled from the excited waveguide into the adjacent waveguide.

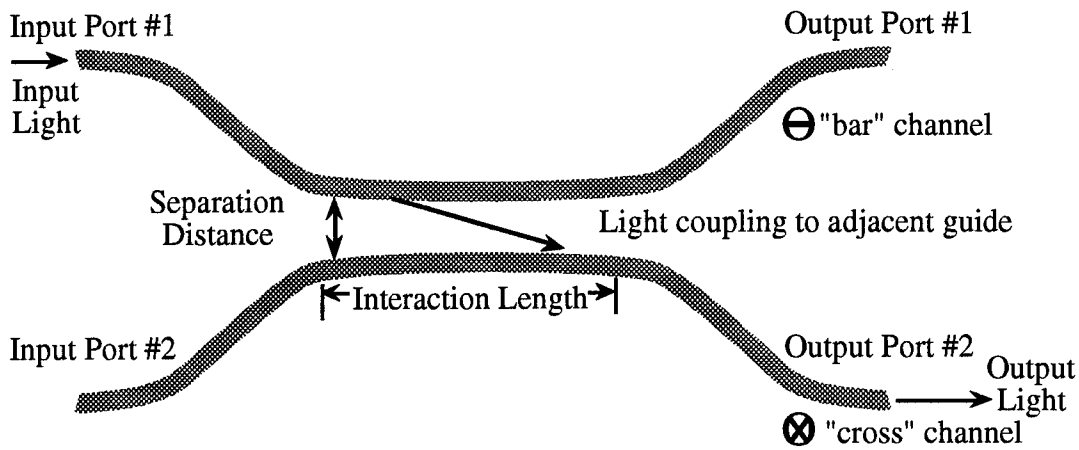

Fig. 1-1. Basic geometry of an optical directional coupler. Light injected into the input of the "bar" channel is coupled to the output of the "cross" channel (after 25:708).

The amount of coupling between two waveguides is a function of field confinement within the guide material, the separation distance between waveguides, the length of the interaction region, and the geometry of the guides. The first parameter, the confinement of the optical energy, is a function of the difference in refractive index between the guide material and the surrounding media. The smaller the index difference, the less the optical energy is confined to the guide material. In a linear directional coupler, the index difference between the coupler materials is fixed and the coupling becomes largely a function of the interaction length (25:266). In a nonlinear directional coupler, the index difference between the coupler materials is not fixed, and is instead a function of the intensity of the light traveling within the waveguides of the coupler. An NLDC works by changing the difference in optical indices between the guide material and the surrounding media. The polymers under investigation in this thesis exhibit this intensity-dependent index

characteristic, also known as the optical Kerr effect. The optical index "seen" by light traveling though the polymer depends on the intensity of the beam (4). Thus, as the intensity of the beam is changed, the index difference between the guide material and the surrounding media is changed. This change in index modifies the confinement of the optical energy and changes the amount of coupling between the two guides. In this way, the flow of the light from the bar channel to the cross channel of a coupler (Fig. 1-1) can be controlled by the intensity of the light itself - light controlling light (13:1582).

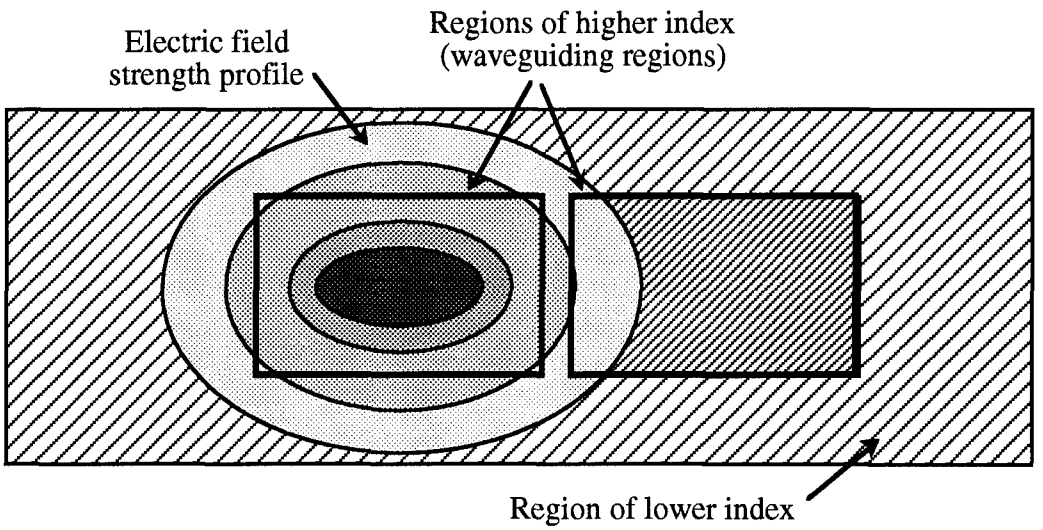

Fig. 1-2. The two-dimensional distribution of electric field within the coupling region of an optical directional coupler. The two waveguides are so close together that the optical energy in the excited guide overlaps into the second waveguide region (after 11:111).

An NLDC can function as an optically controlled switch, a signal-splitting network, or as a logic gate (13:1583). In order to ease the transition to all-optical computing and to facilitate an interface with electronic equipment, an NLDC should be fabricated with methods that are compatible with current integrated circuit manufacturing. Traditional

nonlinear optical materials such as gallium-arsenide (GaAs) or lithium-niobate ($LiNbO_3$) are not easily incorporated into standard silicon integrated-circuit processing steps (11:9).

Organic polymer films have many advantages over the materials currently used in all-optical systems. Cost for materials and processing may be lower than they are for GaAs or $LiNbO_3$. Unlike most nonlinear optical materials, the growth and processing of polymer materials is compatible with most commonly used silicon integrated circuit fabrication techniques. Polymers can also exhibit higher nonlinear coefficients than most commonly used materials, resulting in lower optical switching powers and smaller devices. Finally, the composition of organic films can be easily altered to produce the characteristics desired by a device designer (28:246; 32:778, 23).

Problem Statement

This thesis involved the design, fabrication, modeling, and optical characterization of directional couplers fabricated from optically nonlinear organic polymers.

Scope

Design tools such as the effective index method (11:37-42), the field-shadow method (21:2071-2102), and modal analysis (25:248-252) were used to design three waveguide structures. Using the results of previous work (18), micron-scale polymer films were grown on silicon substrates and lithographically patterned to produce optical waveguides. The material properties and waveguide dimensions were used to model the coupling between adjacent waveguides and the results of the modeling were compared with the experimental results. The coupling characteristics of the resulting devices were investigated using an optical test setup. Suggestions for further work in this area were considered.

Approach and Presentation

The main goal of this research was to fabricate and optically characterize directional couplers that used polyphenylene and a similar polymer, polythiophene, as waveguide

materials. The fabrication of devices heavily utilized previous work (18) and the modeling of devices relied principally on theoretical work by (11, 25, 13, and 17).

Chapter II gives a brief overview of the theory of optical waveguides and directional couplers. Chapter III details the modeling of the coupling structures that were investigated. The fabrication of the polymer films and devices is covered in Chapter IV. Chapter V describes the setup used to optically characterize the waveguide structures. Chapter VI outlines the procedures used to align the system and characterize the devices. Chapter VII reports on the results of the experimental investigations and contains a qualitative discussion of the experimental observations. Chapter VIII contains a summary of this thesis and recommendations for further work.

II. Theory of Optical Directional Couplers

This chapter covers the basic theory of dielectric waveguides and optical directional couplers. For a more detailed treatment see, for example, (11, 25, 17, 29, and 13). The phenomenon of total internal reflection and waveguiding in dielectric media is examined. Next, the coupling between two adjacent waveguides is discussed. This discussion is used to analyze the case of a linear directional coupler. The concept of an intensity-dependent index, a nonlinear effect, is presented and, along with the development concerning a linear directional coupler, is used to explain how a nonlinear directional coupler functions.

Theory of Dielectric Waveguides

This development assumes that the waveguide and surrounding media are made from lossless, non-magnetic, homogenous, linear material. The linear constraint will be lifted in the section concerning coupling between waveguides made from nonlinear media. The two common approaches to explaining the phenomenon of waveguiding, the ray-optic approach and the electromagnetic treatment, will be presented. The ray-optic approach is a useful introduction to the phenomenon of waveguiding because it provides intuitive, physical insight into how light is confined within a waveguiding region. In this approach, light is modeled by rays that bounce off the media interfaces, obeying simple rules of reflection, refraction, and resonance. However, the ray-optic approach does not provide insight into the spatial distribution of the light's electric field. This spatial distribution of the electric field is needed to explain and model the coupling that occurs between adjacent waveguides. The electromagnetic treatment provides this spatial distribution of the electric field and is essential for a full understanding of waveguiding and the coupling between adjacent guides.

The Ray-Optic Approach

The ray-optic approach treats light as a bundle of rays that travel through a medium, reflecting and refracting at interfaces. In this way, the path of the optical energy can be traced through a structure like the one shown in Fig. 2-1.

In Fig. 2-1, a simple "slab" waveguide structure, consisting of a layer of guide material with semi-infinite layers of different materials on either side, is shown. The top layer is referred to as the cover and has a refractive index of n_c. The bottom layer is called the substrate and has a refractive index of n_s, while the middle layer, the waveguiding region, has a refractive index of n_g. The cover and substrate are considered to be semi-infinite in the y direction so that reflections occurring at cover-air and substrate-air interfaces may be neglected. All layers have infinite extent in the x and z directions. This slab waveguide structure can provide confinement in one dimension, the y direction.

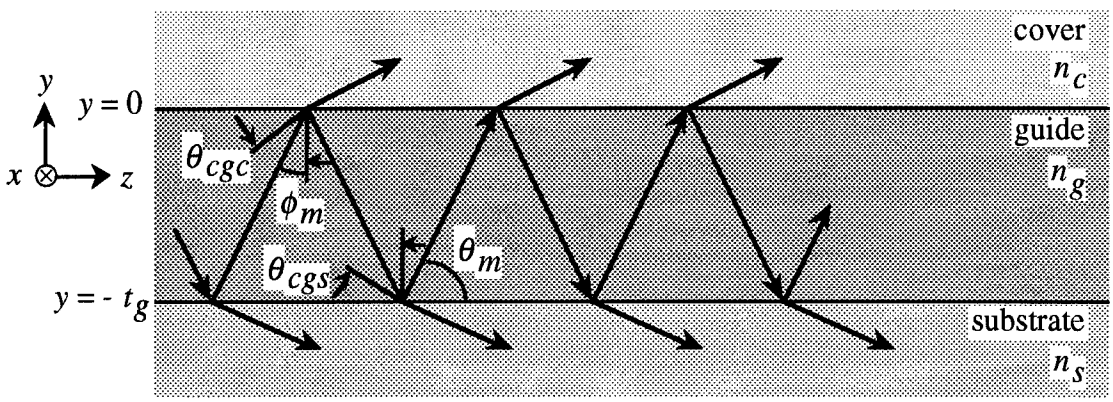

Fig. 2-1. Radiation of optical energy into the cover and substrate in a "slab" waveguide structure. Note that θ_m, the bounce angle associated with this ray, is measured from the interface while the critical angles and angle of incidence, ϕ_m, are measured from the normal to the interface. The ray strikes the cover and substrate interfaces at an angle less than the critical angles for the two interfaces. The cover and substrate layers have refractive indices that are lower than the refractive index of the guide layer and are semi-infinite in the y direction. All layers are assumed infinite in the x and z directions (after 17:35, 11:25).

For a ray traveling through the guide layer and striking either the cover or substrate layer interface, there is a **critical angle** at which **total internal reflection** (**TIR**) occurs. The critical angle is the smallest angle from the interface normal at which total internal reflection can occur. The critical angles are given as (25:11)

$$\theta_{cgc} = \sin^{-1}\left(\frac{n_c}{n_g}\right) \tag{2-1a}$$

and

$$\theta_{cgs} = \sin^{-1}\left(\frac{n_s}{n_g}\right) \tag{2-1b}$$

where the angles are measured from the normals to the interfaces. Note that for a critical angle to exist, and thus TIR and waveguiding to occur, n_g must be greater than n_c and n_s.

If a ray travels through the waveguide media and encounters an interface at either the cover or substrate at an angle of incidence less than the critical angle, there will be both reflection and refraction of the ray at the interface. That is, some of the optical energy will be reflected back into the waveguiding region and some will be transmitted through the interface and refracted. Fig. 2-1 shows a ray striking the interfaces at an angle less than the critical angles for the two interfaces. For a ray propagating in this way, some energy is lost into the cover and substrate during reflections from the interface. This type of ray is called a **cover** and **substrate radiation mode** and will die out after propagating a short distance down the guide. The optical energy is not guided but rather is lost into the layers surrounding the guide.

When a ray is reflected from an interface, there will be a shift in the phase of the wave-front represented by the ray. If the indices of the cover and substrate layers are different then the phase shift upon reflection will be different for each interface. The phase shifts can be interpreted as a slight penetration of the ray into the cover and substrate layers.

A more detailed discussion of these shifts in phase, commonly called the **Goos-Hänchen** phase shifts, can be found in (17:27).

Assuming a transverse-electric (TE) wave (electric field perpendicular to the plane of incidence) having components E_x, H_y, and H_z, the phase shifts upon reflection from the cover and substrate interfaces are given as (11:28, 25:204)

$$\tan \phi_{gs} = \frac{\left[n_g^2 \cos^2 \theta_m - n_s^2\right]^{1/2}}{n_g \sin \theta_m} \tag{2-2a}$$

and (TE modes)

$$\tan \phi_{gc} = \frac{\left[n_g^2 \cos^2 \theta_m - n_c^2\right]^{1/2}}{n_g \sin \theta_m} \tag{2-2b}$$

where ϕ_{gs} is the phase shift at the guide-substrate interface; ϕ_{gc} is the phase shift at the guide-cover interface; and θ_m is the bounce angle, as measured from the interface, of the ray in the guide medium.

If a ray strikes an interface at an angle of incidence greater than the critical angle then the ray will be entirely reflected back into the waveguide region. The "zig-zag" path for a ray propagating in this way is shown in Fig. 2-2.

A ray that undergoes TIR can be a **guided mode** if the ray also meets the **transverse resonance condition** (16:20). This condition states that for a ray to be guided through the structure, the wave front must reproduce itself as it propagates along the guide. Mathematically this implies that the net phase shift from a substrate-cover-substrate trip through the guide medium and the Goos-Hänchen phase shifts from reflections must equal a multiple of 2π. The condition for a **guided mode** can be stated as (11:27):

$$2k_o n_g t_g \sin \theta_m - 2\phi_{gs} - 2\phi_{gc} = 2m\pi \tag{2-3}$$

where k_O is the free-space propagation constant ($k_O = \omega/c$), t_g is the thickness of the guiding layer, and m is the mode number ($m = 0, 1, 2, ...$).

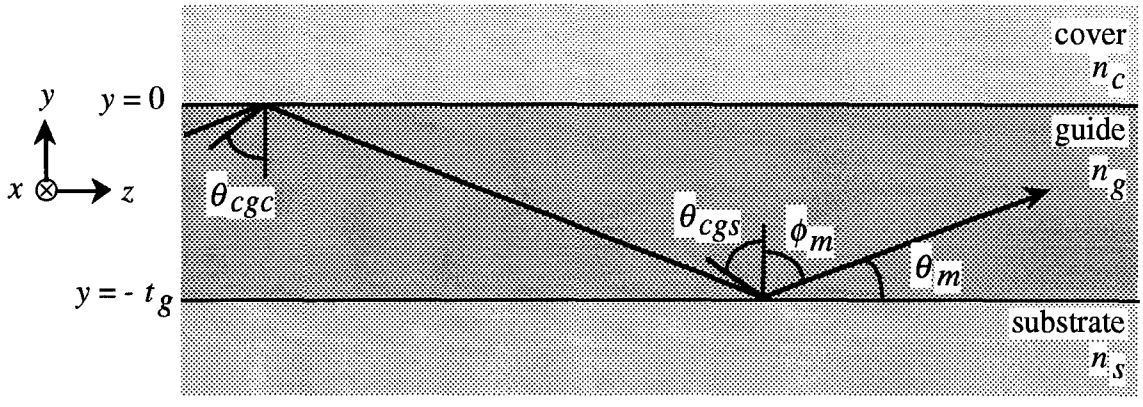

Fig. 2-2. Path of a ray undergoing total internal reflection (TIR) in a dielectric slab waveguide structure. Note that θ_m, the bounce angle associated with this ray, is measured from the interface while the critical angles and angle of incidence, ϕ_m, are measured from the normal to the interface (after 17:35).

The transverse resonance condition, eqn. (2-3), leads to the idea of allowed modes within the waveguide. Only a discrete set of bounce angles will satisfy this condition and result in optical energy propagating down the waveguide. Rays that are incident at angles greater than the critical angle but do not met the transverse resonance condition are lost through self-interference and their power is reflected back out of the guide. Rays at angles of incidence that are greater than the interface critical angles and that are allowed by the transverse resonance condition result in total internal reflection and the guiding of energy along the z direction. For a given set of n_c, n_g, n_s, t_g, and ω (or free-space wavelength of operation, λ_O), the set of bounce angles (θ_m, $m = 1, 2, ...$) that correspond to guided modes can be calculated using eqns. (2-3) and (2-2). The **cut-off condition** for a mode is the point where the angle of incidence (ϕ_m) becomes equal to the cut-off angle, which is

the larger of the two critical angles for the interfaces. A mode with an angle of incidence that is smaller than this cut-off angle will not propagate down the guide region and is said to be "cut-off."

The propagation constant in the z direction for a mode, β_m, is given by (25:250)

$$\beta_m = n_g k_o \cos(\theta_m) \tag{2-4}$$

Since the propagation constant of each mode is different, a given mode propagates down the guide at a group velocity different from the group velocity of any other mode. All rays travel through the guide media at the same phase velocity. The difference in group velocities between the modes is due to the fact that a large part of the energy in higher order modes actually travels in the cover and substrate layers. One interpretation of the Goos-Hänchen phase shifts replaces the shifts in phase upon reflection with an additional distance traveled along z at the speed of light in the material across the interface (either the cover or substrate), which is greater than the speed of light within the guide region (25:257). Higher-order modes in a dielectric waveguide undergo greater Goos-Hänchen phase-shifts and thus travel down the guide faster than lower-order modes (25:255-258).

A waveguide is called **multi-mode** if propagation of more than one mode is supported by the guide. In a multi-mode guide, a pulse of light that excites a large number of modes will be broadened or spread in time as it travels down the guide because the modes are not propagating down the guide with the same group velocity. This **pulse spreading** - also sometimes called **modal dispersion** - is due to the differing group velocities of the modes within the waveguide (25:284-286).

A **single-mode waveguide** is a waveguide that allows only one guided mode to propagate. Generally, waveguide dimensions must be small (on the order of the wavelength of operation) for a waveguide to be single-mode. In a single-mode waveguide,

any mode other than the zero-order mode ($m = 0$) results in an angle of incidence that is less than the cut-off angle, indicating an unguided mode. Single-mode operation of a waveguide has many advantages in optical communication systems and IO circuits. The pulse spreading experienced by light in a multi-mode guide can be a bandwidth-limiting factor; short duration pulses are "blurred" by the spreading of the pulses. Single-mode guides, because of less pulse spreading and other effects from higher-order modes, are capable of data transmission rates that are significantly higher than the rates achievable with multi-mode guides (25:286). In addition, the analysis of the coupling between single-mode waveguides is greatly simplified since the light propagates down the guide in only one mode. Appendix A is a Mathcad® (version 3.1 for the Macintosh, published by MathSoft, Inc.) file that uses the transverse resonance condition to calculate the waveguide dimensions required for single-mode operation.

The Electromagnetic Development

This section contains a brief development of the electromagnetic equations that govern the propagation of light through waveguiding structures. The solution of these equations results in a function that describes the spatial distribution of the energy in the waveguide structure. As previously mentioned, this spatial distribution is need to fully analyze the coupling between adjacent waveguides. The section also discusses how these equations lead to a cut-off condition for modes within a waveguide. This development principally follows the work presented in (11, 34).

The geometry of the simple slab waveguide, as shown in Fig. 2-1, is the starting point for the development of the electromagnetic equations governing the guiding of light through dielectric structures. Note that n_g is assumed to be greater than both n_c and n_s, indicating that the light is guided by the structure.

Any traveling electromagnetic field can be represented by a combination of transverse magnetic (TM) and transverse electric (TE) waves. In this analysis, a purely TE wave,

consisting of only E_x, H_y, and H_z components, is assumed for simplicity. For such a TE wave traveling in the z direction, Maxwell's wave equation can be stated as (11:30)

$$\nabla^2 E_x = \frac{n_p^2}{c^2}\frac{\partial^2 E_x}{\partial t^2} \tag{2-5}$$

where n_p is the index of the media that the wave is propagating through (n_c, n_g, and n_s for the slab waveguide structure of Fig. 2-1), and E_x is the x component of the electric field propagating in the z direction. Note that since we are assuming a TE wave, the E_y and E_z components of the electric field are zero.

Equation (2-5) has solutions in the form of (11:30)

$$E_x(y,z,t) = \varepsilon_x(y)e^{i(\omega t-\beta z)} \tag{2-6}$$

where $\varepsilon_x(y)$ is the transverse function, a function that describes the spatial distribution of the x directed electric field in the y direction; ω is the angular frequency of the radiation; and β is the propagation constant in the z direction. The transverse function, $\varepsilon_x(y)$, has only y dependence since we are assuming that the waveguide structure is infinite in the x and z directions.

The transverse function has the general form of (34:921)

$$\varepsilon_x(y) = \begin{cases} C\ \exp(-qy) & 0 \le y < \infty \quad \text{cover layer} \\ C\left[\cos(hy) - (q/h)\ \sin(hy)\right] & -t_g \le y \le 0 \quad \text{guide layer} \\ C\left[\cos(ht_g) + (q/h)\ \sin(ht_g)\right]\exp[p(y+t_g)] & -\infty < y \le -t_g \quad \text{substrate layer} \end{cases} \tag{2-7}$$

where C, h, q, and p are all constants that describe the spatial distribution of the electromagnetic energy within the waveguide structure. Note that the field in the cover and

substrate layers decays exponentially because the optical energy is concentrated in the guide layer for a guided mode.

Equation (2-7) for the different regions can be substituted into eqns. (2-6) and (2-5) to determine q, h, and p (11:31, 34:921):

$$h = \left(n_g^2 k_o^2 - \beta^2\right)^{1/2} \tag{2-8b}$$

$$q = \left(\beta^2 - n_c^2 k_o^2\right)^{1/2} \tag{2-8a}$$

$$p = \left(\beta^2 - n_s^2 k_o^2\right)^{1/2} \tag{2-8c}$$

where k_O, previously defined as ω/c, can also be expressed as $k_O = 2\pi/\lambda_O$, where λ_O is the wavelength of the electromagnetic energy in free space.

The constants q, h, and p are all given in terms of β, the propagation constant in the z direction and the material constants. Imposing the boundary conditions that ε_x and $\partial\varepsilon_x/\partial y$ must be continuous at the guide-cover and guide-substrate interfaces leads to a condition on β (34:921). In the resulting transcendental equation, eqn. (2-9), both the left and right hand sides are functions of β, k_O (and thus the wavelength of the electromagnetic energy), and the material constants (11:31-32):

$$\tan\left(ht_g\right) = \frac{q+p}{h\left(1-\frac{pq}{h^2}\right)} \tag{2-9}$$

Solving eqn. (2-9) results in a set of discrete values of β that correspond to allowed modes within the waveguide structure. For each value of β_m, the values of p_m, h_m, and q_m for each allowed mode can be calculated using eqn. (2-8). Some possible modes for a slab waveguide structure are shown in Fig. 2-3.

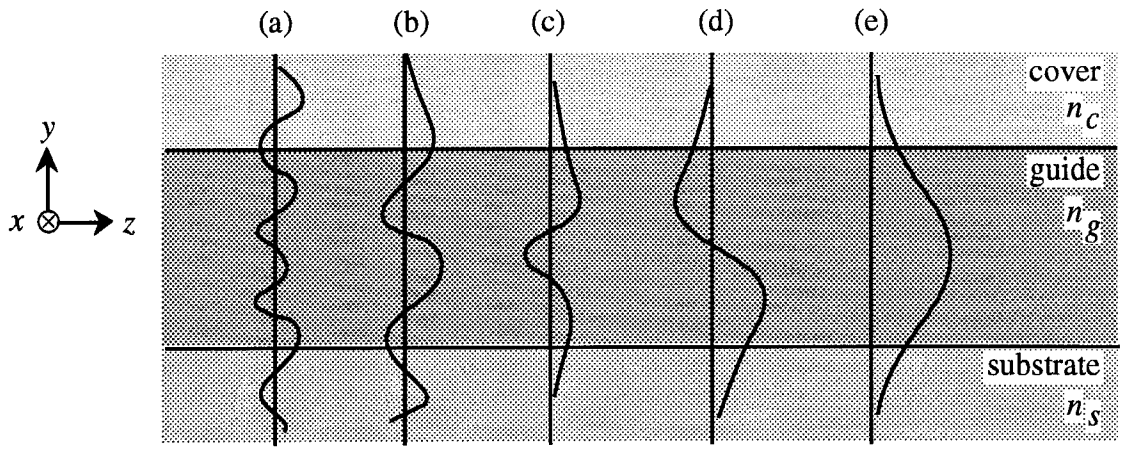

Fig. 2-3. Some possible modes in a slab waveguide. The profiles depict the spatial distribution of the electric field and are: (a) a higher-order, non-guided mode; (b) a substrate radiation mode; (c) the TE_2 mode; (d) the TE_1 mode; (e) the TE_0 mode. The subscript of TE indicates the value of m for that mode and corresponds to the number of nulls in the electric field profile (after 11:18).

When a mode is "cut-off," the field in either the cover or substrate layers becomes oscillatory instead of exponentially decaying. Cut-off occurs when the appropriate field parameter, q or p, becomes imaginary. There are equations that can be used to find the number of modes that either a symmetric ($n_C = n_S$) or highly asymmetric ($n_S >> n_C$) waveguide will support (11:34-36). Note that in an asymmetric guide, the lowest order mode in the TE case can be cut-off. That is, there is a minimum guide layer thickness required to support the lowest-order for a given set of materials. This is in contrast to the case of the symmetric guide where the lowest order mode has no cut-off. However, a guided mode will be poorly confined if the refractive index difference between the guide and the cover or substrate layers is very small (11:34). The Mathcad® document in Appendix B can be used to model the profile of the electric field in a slab waveguide.

Coupling Between Waveguides Made from Linear Media

The basic geometry of a typical directional coupler is shown in Fig. 1-1. Here, two optical waveguides are brought into close proximity and allowed to run parallel to each other before separating. Each of the waveguides is assumed to be single-mode and made from a material whose optical response is linear. The separation distance between guides is assumed to be small enough such that the evanescent tail of the field pattern in one guide overlaps into the other guide (Fig. 1-2).

The interaction region, the area where the two guides are close together and coupling is facilitated, can be modeled by two slab waveguides as shown in Fig. 2-4. The two guide regions have refractive index of n_g and the surrounding medium has a refractive index of n. For guiding purposes, n is assumed to be less than n_g. The width of the guide regions is d and they are separated by a distance $2a$. All materials are assumed lossless. The interaction length needed for complete transfer of optical energy from guide 1 to guide 2 is designated as L_O.

Note that following analysis does not account for the confinement of the energy in two dimensions, as would be the case in most practical IO circuits. In that case, the spatial description of the field of the mode would be a function of both the x and y coordinates. Even though the analysis presented in this section ignores confinement in the x direction, it is still illustrative of the concept of optical coupling (25:264-267).

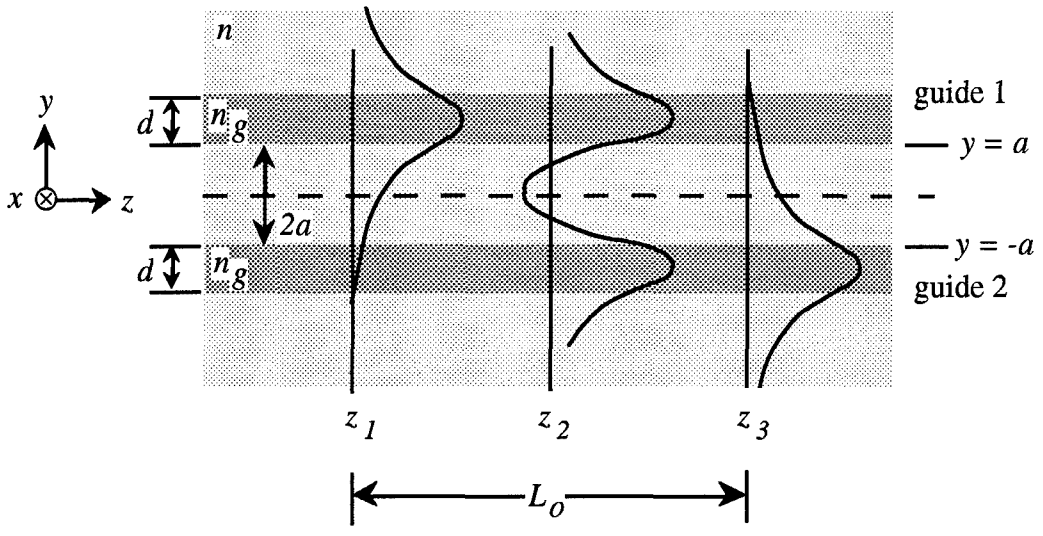

Fig. 2-4. Dielectric slab waveguide geometry used as a model for the development of the coupled-mode equations. The profiles represent the distribution of the electric field. At z_1 the light is mostly in guide 1, at z_2 the light is equally divided between the two waveguides, and at z_3 the light has coupled into guide 2 (after 25:264).

Coupled-mode theory, also known as the weak-coupling approximation, is a common simplified approach to solving the problem of two closely-spaced waveguides (25:264). The theory assumes that the spatial shape of the waveguide modes is not affected by the coupling and that coupling affects only the amplitudes of the fields in the waveguides. Therefore, the amplitudes of the electric fields are a function of the z direction, and are designated as $a_1(z)$ and $a_2(z)$. The functions $a_1(z)$ and $a_2(z)$ describe how the optical energy is distributed between the two guides along the propagation direction, z. It can be shown (25:264-265) that the amplitude functions $a_1(z)$ and $a_2(z)$ obey the coupled-mode equations (25:265):

$$\frac{d a_1}{dz} = -j\kappa_{21} \exp(j\Delta\beta z) a_2(z) \tag{2-10a}$$

and

$$\frac{d a_2}{dz} = -j\kappa_{12} \exp(j\Delta\beta z) a_1(z) \tag{2-10b}$$

where κ_{21} and κ_{12} are coupling coefficients that describe how strongly the modes in the two guides interact, and $\Delta\beta$ is the difference between the propagation constants of the two guides (also called the phase mismatch). If the modes in the two guides are identical, then $\Delta\beta = 0$ and $\kappa_{21} = \kappa_{12} = \kappa$. In general, the coupling coefficients are (25:265)

$$\kappa_{21} = \frac{1}{2}\left(n_g^2 - n^2\right)\frac{k_o^2}{\beta_1}\int_a^{a+d} u_1(y) u_2(y) dy \tag{2-11a}$$

and

$$\kappa_{12} = \frac{1}{2}\left(n_g^2 - n^2\right)\frac{k_o^2}{\beta_2}\int_{-a-d}^{-a} u_2(y) u_1(y) dy \tag{2-11b}$$

where $u_1(y)$ and $u_2(y)$ are functions that describe the transverse profiles of the modes within waveguides 1 and 2, respectively. They are examples of the transverse mode profile function, eqn. (2-7). β_1, β_2 are the propagation constants in the z direction of the modes within waveguides 1 and 2, respectively.

The constant, C, appearing in the spatial distribution functions $u_1(y)$ and $u_2(y)$ is arbitrary (11:32, 34:921). In this development, the normalization condition for these two functions is taken as (25:253)

$$\int_{-\infty}^{\infty} u_m^2(y) dy = 1 \tag{2-12}$$

where $u_m(y)$ is the spatial distribution of the electric field in the mth guide. Eqn. (2-12) can be used to determine a normalized value of the arbitrary constant C in eqn. (2-7).

The phase mismatch per unit length between the two guides is given by (25:265)

$$\begin{aligned}\Delta\beta &= \beta_1 - \beta_2 \\ &= \frac{2\pi}{\lambda_o}(N_1 - N_2)\end{aligned} \tag{2-13}$$

where $N_1 = n_1\cos(\theta_1)$; $N_2 = n_2\cos(\theta_2)$; and N_1, N_2 are the effective indices for guides 1 and 2, respectively; θ_1, θ_2 are the bounce angles of the modes in guides 1 and 2, respectively; and λ_o is the wavelength of the electromagnetic energy in free space (25:265). The concept of an effective index will be discussed in more detail in Chapter III. Again, for the special case of identical guides, $\Delta\beta = 0$ (25:266).

From eqns. (2-10a) and (2-10b), the coupled-mode equations, it can be seen that the variation of the optical energy in a guide depends on the amount of optical energy in the other guide and the coupling coefficient. For the case of an initial optical power launched into waveguide 1 and no light entering waveguide 2 at $z = 0$, these equations can be solved to give the optical power in the waveguides as a function of z, the direction of propagation (25:266):

$$P_1(z) = P_1(0)\left[\cos^2\gamma z + \left(\frac{\Delta\beta}{2\gamma}\right)^2 \sin^2\gamma z\right] \tag{2-14a}$$

and

$$P_2(z) = P_1(0)\frac{|\kappa_{12}|^2}{\gamma^2}\sin^2\gamma z \tag{2-14b}$$

where $P_1(z)$, $P_2(z)$ are the optical powers in guides 1 and 2, respectively; $P_1(0)$ is the initial power launched into waveguide 1 at $z = 0$; $\gamma^2 = (\Delta\beta/2)^2 + \kappa^2$; and $\kappa = \sqrt{\kappa_{12}\kappa_{21}}$.

If the two guides are not identical then, in general, the phase mismatch will not be zero and the power will be exchanged between the two guides as shown in Fig. 2-5. Note that because of the phase mismatch, the power exchange is not complete. That is, there is no interaction length such that all of the power in guide 1 is transferred over to guide 2.

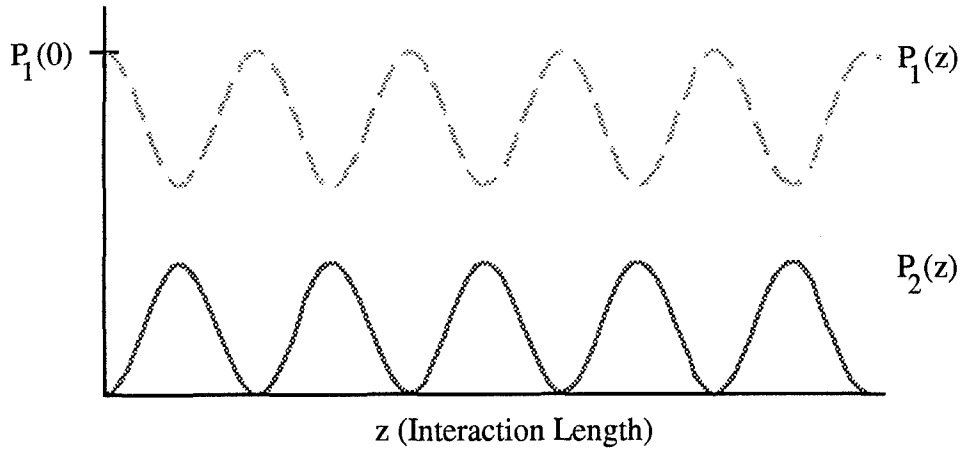

Fig. 2-5. The periodic exchange of power with $\Delta\beta \neq 0$. The period of the exchange along the z axis is $2\pi/\gamma$ (after 25:266).

If the guides are identical then they have identical propagation constants and $\Delta\beta = 0$. In this case the eqns. (2-14a) and (2-14b) simplify to (25:266)

$$P_1(z) = P_1(0)\cos^2 \kappa z \tag{2-15a}$$

and

$$P_2(z) = P_1(0)\sin^2 \kappa z \tag{2-15b}$$

This results in complete power transfer between the two guides. At $z=\pi/2\kappa$ the optical power in guide 1 is zero and the optical power in guide 2 is $P_1(0)$, the power that was initially launched into guide 1. This interaction length, $z=\pi/2\kappa$, is shown as L_O in Figs. 2-4 and 2-6. The periodic nature of the complete power exchange between guide 1 and guide 2 is shown in Fig. 2-6.

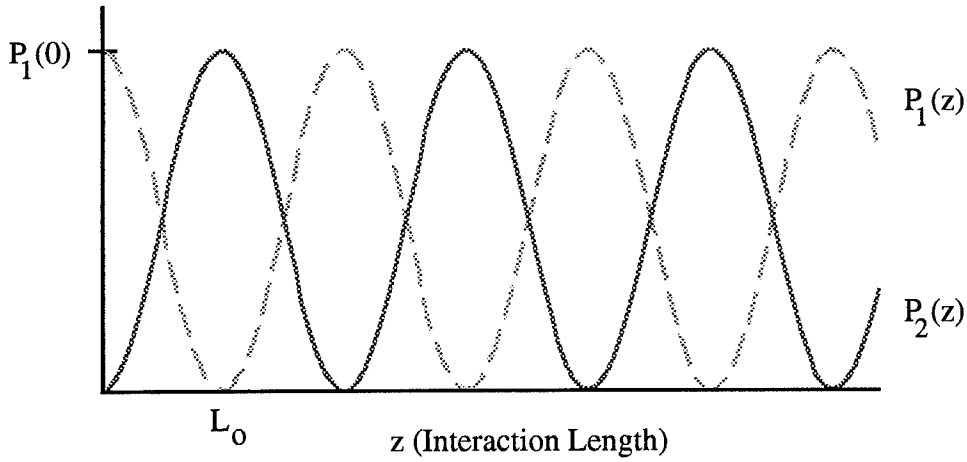

Fig. 2-6. The periodic exchange of power when $\Delta\beta = 0$. This is also called the phase-matched case (after 25:266).

In the case of a directional coupler with an interaction length of L_O, the power-transfer ratio can be defined as the amount of power present in guide 2 at $z = L_O$ divided by the power incident in guide 1 at $z = 0$. This quantity, denoted as $\Im$, is given by (25:267)

$$\Im = \frac{P_2(L_O)}{P_1(0)} = \left(\frac{\pi}{2}\right)^2 \operatorname{sinc}^2\left\{\frac{1}{2}\left[1+\left(\frac{\Delta\beta L_O}{\pi}\right)^2\right]^{1/2}\right\} \tag{2-16}$$

where *sinc(x)* is defined as $sin(\pi x)/(\pi x)$.

A plot of this equation is shown in Fig. 2-7. As can been seen, the power-transfer ratio is a maximum for $\Delta\beta = 0$ (the phase matched case). Also note that no power will be transferred to guide 2 ($\Im = 0$) if $\Delta\beta L_o = \sqrt{3}\pi$. Thus, the amount of optical energy exiting guide 2 can be varied from $P_1(0)$ to zero by controlling the phase mismatch, $\Delta\beta$.

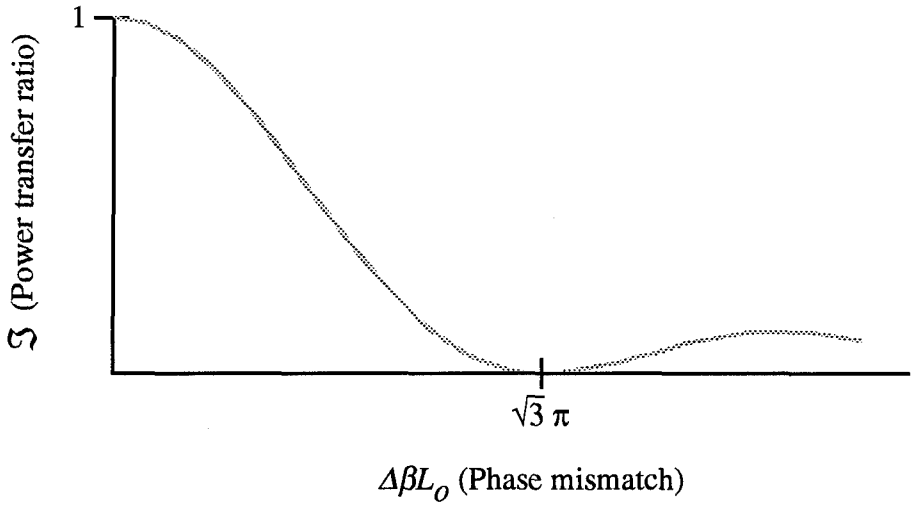

Fig. 2-7. Dependence of the power-transfer ratio, $\mathfrak{I}$, on the phase mismatch. Note that complete coupling occurs only if the phase-mismatch ($\Delta\beta$) is zero (after 25:267).

The amount of power transferred from guide 1 to guide 2 is a function of the guide materials and dimensions (through the coupling coefficient κ), their interaction length, and the difference in the propagation constants (phase mismatch) between the two guides. Any one or all of these parameters may be varied to control the amount of power transferred between the two guides. Of course, once a coupler is fabricated in an IO circuit, the geometry and materials of the coupler are fixed. Note that a directional coupler can be a "passive" device. Here, passive means that no external inputs are needed to induce coupling. Optical energy will transfer from one guide to another simply because the guides are in close proximity and thus coupled.

By changing the refractive index of one or both of the guides the propagation constant mismatch can be dynamically controlled. In the case of lithium niobate or gallium arsenide structures, for instance, this mismatch can be accomplished through the electro-optic effect, where the material exhibits a refractive index that depends on the electric field within the material (25:268). An applied voltage can change the refractive index in one or both of the

guides and thus control the amount of optical power that is transferred from one guide to another. This is the way that electro-optic directional couplers route optical power from one output port to the other output port. Thus, an electrically controlled directional coupler can function as either a switch for optical energy or as an intensity modulator. A directional coupler made from nonlinear material functions in much the same way. Instead of an applied voltage controlling the coupling, the intensity of the light in the waveguides controls the amount of coupling between the two optical waveguides.

Optical Nonlinearity in Polymers

In a **third-order nonlinear** medium, the electric field of an incident monochromatic light beam causes a nonlinear polarization to occur in the material (24:15). One type of third-order nonlinearity is an **intensity-dependent index** of refraction, also called the **optical Kerr effect.** In organic polymers, the source of this intensity-dependent index is loosely bound electrons that are free to move up and down a polymer chain in the presence of an electric field, such as the field of an incident optical beam (24:35-58). This polarization of the atoms or molecules in the material can induce a small change in the optical index of refraction of the material. For more specific information on optical nonlinearity in polymers see, for example, (24).

The change in the index of refraction due to the intensity of an incident beam of light is given by (25:752)

$$\Delta n = n_2 I \tag{2-17}$$

where I is the intensity of the incident light and n_2 is the nonlinear coefficient with units of cm^2/W. This coefficient is related to the material parameters by (25:752)

$$n_2 = \frac{3\eta_o}{n^2 \varepsilon_o} \chi^{(3)} \tag{2-18}$$

where η_o is the impedance of free space, n is the refractive index of the material with no light incident upon it (the "linear" index), ε_o is the permittivity of free space, and $\chi^{(3)}$ is a material parameter that describes the third-order nonlinear properties of the material (25:752, 24:15-19). The refractive index of a nonlinear material is thus a function of the intensity of the light that is traveling through it. This intensity-dependent refractive index is given as (25:752)

$$n(I) = n + n_2 I \tag{2-19}$$

Note that in eqn. (2-18), the sign of $\chi^{(3)}$ can be either negative or positive. A negative value of $\chi^{(3)}$ indicates that the refractive index of the material *decreases* as the intensity of the light increases. If the shape of the beam is Gaussian in nature, this causes a **self-defocusing** effect as seen in Fig. 2-8a. A positive value of $\chi^{(3)}$ means that the refractive index of the material *increases* as the intensity of the light increases, leading to **self-focusing** of a Gaussian light beam as seen in Fig. 2-8b.

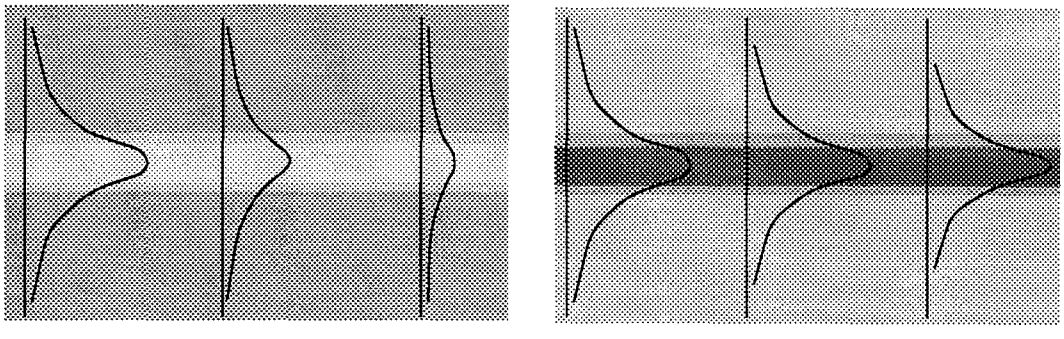

(a) (b)

Fig. 2-8. Self-defocusing and self-focusing in nonlinear materials. In (a), the material has a negative $\chi^{(3)}$. The intensity profile of the beam creates a region of lower refractive index in the middle of the beam and this index gradient makes the beam spread out and become more planar. In (b), the material has a positive $\chi^{(3)}$. The higher intensity toward the center of the beam creates a self-waveguide region and a self-focusing effect (after 25:755).

To illustrate the effect of a self-induced change in refractive index, consider two identical single-mode waveguides made from a nonlinear material having a positive $\chi^{(3)}$ value. The guides are spaced far enough apart that there is negligible coupling between them. Two separate beams, of the same wavelength but different intensities, I_1 and I_2, are launched into the waveguides at the same instant in time. In this case, I_1 is much larger than I_2. At the entrance to the guides the two beams are in phase with one another. This is shown in Fig. 2-9. It should be noted that the following discussion is somewhat qualitative in that the optical beams propagating through the waveguides are treated as plane waves. A more complete analysis would include the self-focusing properties of the material, the effects of modes in the waveguide structure, and the idea of an effective index within the guide (27, 25, 24).

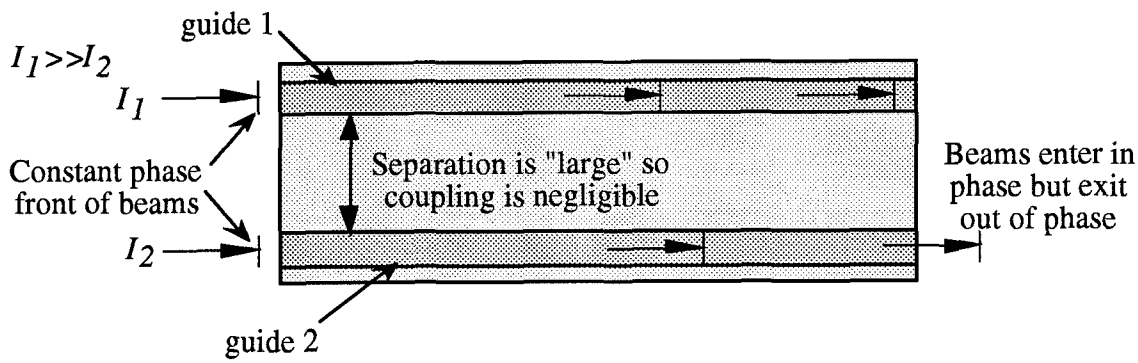

Fig. 2-9. Uncoupled nonlinear waveguides. Two beams of light, with the same wavelength and in-phase but with different intensities ($I_1 >> I_2$), are launched into identical nonlinear waveguides at the same instant. The two beams become out of phase due to the intensity-dependent refractive index of the nonlinear material (after 25:752-753).

Since the guide medium is nonlinear, the index of refraction in the guide depends on the intensity of the wave traveling through it. The guides are identical but the intensity of

the optical energy traveling through them is different, thus each wave "sees" a different index of refraction. These indices are given by (25:752)

$$n_{g1} = n + n_2 I_1 \tag{2-20a}$$

$$n_{g2} = n + n_2 I_2 \tag{2-20b}$$

where n_{g1} is the refractive index seen by the optical energy traveling in guide 1 and n_{g2} is the refractive index seen by the optical energy traveling in guide 2.

The difference in index of refraction between the two guides leads to different propagation constants for each of the waveguides. The mismatch in the propagation constants is give by (25:265)

$$\begin{aligned} \Delta\beta &= \beta_1 - \beta_2 \\ &= \frac{2\pi n_{g1}}{\lambda_o} - \frac{2\pi n_{g2}}{\lambda_o} \\ &= \frac{2\pi}{\lambda_o}(n_{g1} - n_{g2}) \\ &= \frac{2\pi n_2}{\lambda_o}(I_1 - I_2) \end{aligned} \tag{2-21}$$

As can be seen in eqn. (2-21), the amount of mismatch between the guides is directly proportional to the difference in the optical intensity traveling through the guides. Also note that if $I_1 = I_2$ then $\Delta\beta = 0$ and the guides are not phase mismatched. Since the nonlinear coefficient n_2 is usually quite small, the guides are very nearly phase matched if $I_2 = 0$ and I_1 is small enough not to induce significant changes in the index of the guide.

This simplified example of uncoupled nonlinear guides illustrates that the amount of phase mismatch between otherwise identical nonlinear guides can be controlled simply by changing the amount of optical power launched into one of the guides.

Coupling Between Waveguides Made from Nonlinear Media

Previously, the case of two nonlinear waveguides separated by a distance large enough such that there was negligible coupling between them was discussed. The phrase "large enough" implies that the evanescent tails of the modes do not significantly overlap. In this section, it is assumed that the two guides have been brought into physical proximity in the manner illustrated in Fig. 2-4. The previously presented concept of a passive coupler and the phenomenon of an intensity-dependent index of refraction are brought together in this section to explain how a nonlinear optical directional coupler (NLDC) functions. According to *Leutheuser* (19), this analysis was first performed by *Jensen* (13) and *Maier* (20).

It is assumed that the waveguides are identical and single-mode. They are made from a nonlinear material and they are embedded in a nonlinear material of an appropriate index such that guiding occurs (13:1580). The analysis of this geometry leads to the development of four coupling coefficients that account for both the linear and nonlinear field interactions. Like the coupling coefficients in the case of linear coupler, two of these coefficients are a function of the guide geometry and dimensions. The new coefficients arise from the nonlinear interaction of the field with itself and from the nonlinear interaction between the fields of the two waveguides (13:1581).

The analysis carried out by *Jensen* is involved but similar in concept to that of (25) for a linear waveguide. As *Jensen* points out, a special case of interest for all-optical computing is where all of the optical power is initially launched into just one waveguide (guide 1 in this example). For this case, the power in guide 1 as a function of the coupling length is (13:1582)

$$P_1(Z) = P_1(0)\{1 + cn(2Z|m_c)\} / 2 \tag{2-22}$$

where P_1 is the power in guide 1, Z is the direction of propagation normalized by the appropriate coupling coefficient, $P_1(0)$ is power launched into guide 1, and $cn(2Z|m_c)$ is a Jacobi elliptic function (1:573-575). The parameter m_c is a measure of the power incident in guide 1 and is given by (13:1582)

$$m_c = \frac{[P_1(0)]^2}{P_c^2} \tag{2-23}$$

where P_c is the critical power.

The critical power is defined as the input power into guide 1 such that the power is split equally between the two guides after propagating a distance of $Z \approx \pi$ (see Fig. 2-10). This critical power level is a function of the linear and nonlinear coupling coefficients, which are themselves functions of the material parameters and guide dimensions (13:1582).

The Jacobi elliptic function in eqn. (2-22) is periodic. Therefore, due to the intensity-induced phase-mismatch at "high" power levels ($P_1(0) > P_c$), there is coupling to guide 2 but it is not complete (not all of the energy in guide 1 is coupled to guide 2). If the input power is very small ($P_1(0) << P_c$) then $m \approx 0$ and eqn. (2-22) can be approximated as (13:1582):

$$\begin{aligned} P_1(Z) &= P_1(0)\{1 + \cos(2Z)\} / 2 \\ &= P_1(0)\cos^2(Z) \end{aligned} \tag{2-24}$$

Eqn. (2-24) is the form of the power exchange for a linear coupler (13:1582, 25:266).

The amount of power in guide 1 as a function of distance traveled along the coupling region and m_c is shown in Fig. 2-10. The vertical axis shows the amount of power in the guide normalized by the critical power. At lower power levels, the guide functions as a

linear coupler. That is, for low input powers, there is a distance ($Z/\pi \approx 0.5$) where all of the incident power in guide 1 is coupled over into guide 2. As can be seen in Fig. 2-10, when the input power is equal to or greater than the critical power the NLDC no longer functions in a manner similar to a linear coupler. No matter how long the interaction length, the optical energy will not completely couple into the adjacent guide. At incident powers greater than the critical power, only a relatively small percentage of optical power is coupled into guide 2 (27:101, 13:1582).

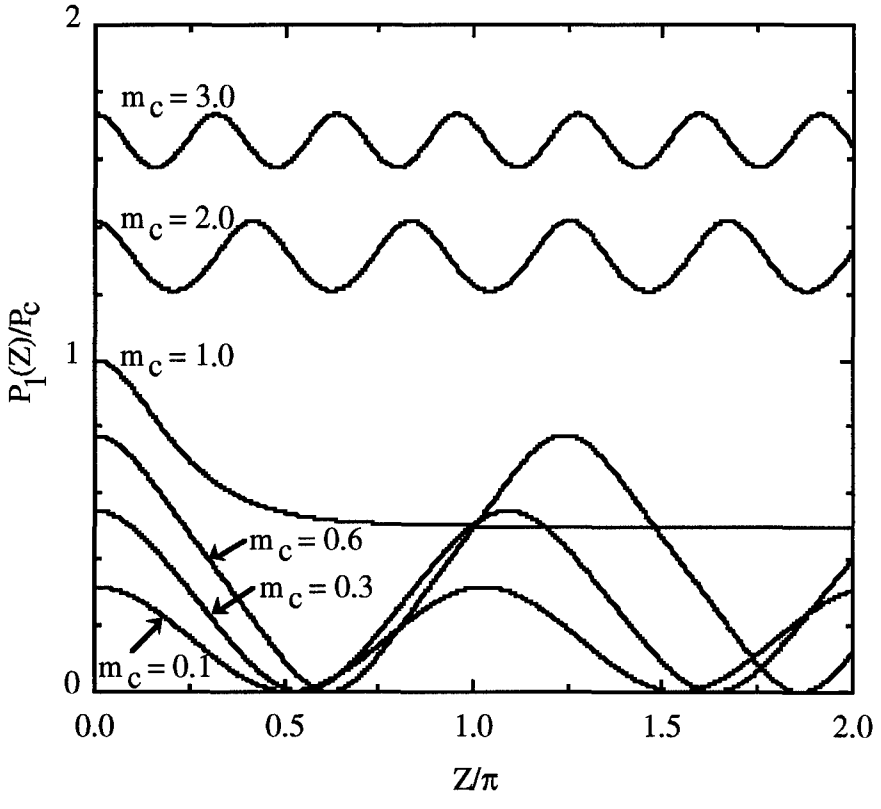

Fig. 2-10. The response of an NLDC to various input powers. This figure illustrates how the coupler makes the transition between acting as a linear coupler (transferring all optical energy over to guide 2 for "low" input powers) and a nonlinear coupler where "high" incident power results in very little power coupled into guide 2 for any interaction length (after 13:1582).

The work by *Jensen* (13) derived the fundamental response of an NLDC using coupled-mode theory. The coupling that occurs between the waveguides in an NLDC can be qualitatively understood in several different ways. As seen in eqn. (2-21), the optical nonlinearity of the material gives rise to an intensity-dependent phase mismatch between the two guides. This "detuning" (13:1582) between the guides changes the coupling between the guides, as was seen in eqns. (2-14) for the case of a linear coupler. So, in this regard, the NLDC can be thought of as a linear coupler that has a mechanism for self-modulation of the phase mismatch. The intensity of the light in the guides controls the phase mismatch between the guides, routing the optical energy from one guide to another in a directional coupler as the input intensity is changed.

Another way to view the functioning of an NLDC centers around the self-focusing or self-defocusing properties of the nonlinear material. Note that the coupled mode theory of *Jensen* is based on the intensity-induced phase mismatch ("detuning") between the guides and does not account for the self-focusing or defocusing material properties. As can be seen in Fig. 2-8, a mode profile of a Gaussian beam traveling through a nonlinear material is altered by the intensity-dependent refractive index changes in the material. For a self-defocusing material (a negative $\chi^{(3)}$ material) the mode spreads out of the guide, resulting in more overlap with the adjacent guide and increased coupling. In a self-focusing material (a positive $\chi^{(3)}$ material) the mode is more confined to the guide through the self-waveguide effect (Fig. 2-8). This increased confinement decreases the coupling between the guides. In this view, the NLDC acts as a linear coupler that has an intensity-dependent coupling coefficient. Thus, the coupling from one guide 1 to guide 2 over a fixed length depends upon the power launched into guide 1.

This intensity-dependent coupling property of NLDCs makes them suitable for all-optical logic devices, such as AND or XOR gates, as in Fig. 2-11 (13:1582-1583). The length of the interaction region is chosen such that most of the input power couples to guide

2 for "low" input powers (say $m_C = 0.1$, $Z/\pi \approx 0.5$ in Fig. 2-10). The intensity that results from the combination of signals 1 and 2 when they are both "high" is greater than the critical power for the coupler ($m_C > 1$). Two simultaneously "high" input signals result in detuning of the guides and the power remains in guide 1. However, if only one "high" signal is present, the signal does not significantly detune the guides and most of the power couples over into guide 2. The relatively large magnitude and fast response time ($\approx 10^{-14}$ sec) of the optical nonlinearity in organic polymers makes these materials strong candidates for IO devices (13:1583, 24:2-6).

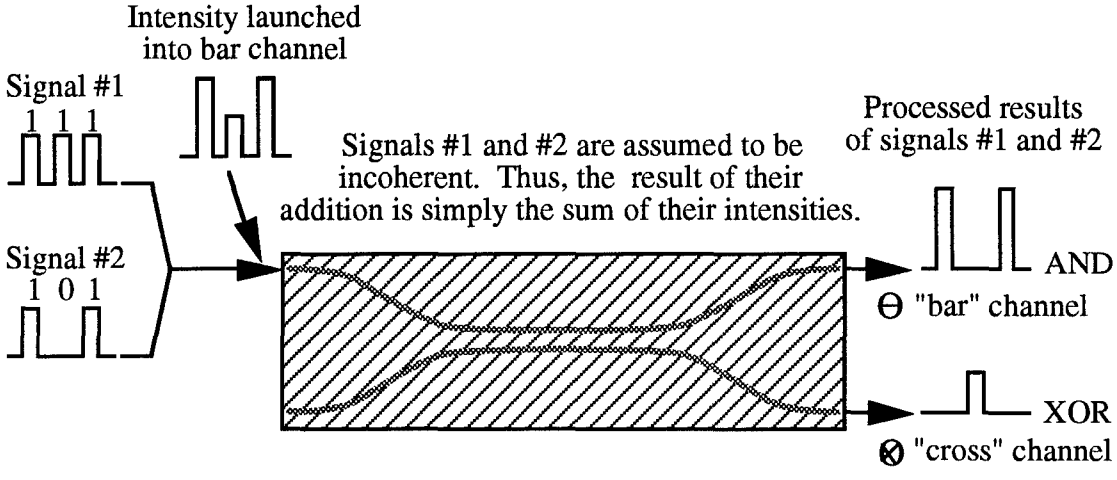

Fig. 2-11. An NLDC functioning as an all-optical logic gate. Light pulses of high intensity, the result of simultaneously "high" input signals, exit the output of the bar channel. Pulses of relatively low intensity, the result of only one input signal being "high," couple to the cross channel. The NLDC thus functions as all-optical logic element.

Another possible mode of operation for the NLDC is in the sub-critical power regime. Note that in Fig. 2-10, the curves for $m_C < 1$ have a relative shift in zero points as the normalized interaction length, Z, increases. This is due to the nonlinear properties of the guides and the $\Delta\beta Z$ phase shift between the guides. A device could be constructed with an interaction length such that complete transfer of power from guide 1 to guide 2 would occur

at low input powers. For this device, a higher input power - but still less than the critical power - would result in a relatively high percentage of the input power exiting guide 1. The device could operate as a logic gate, sensor-overload protector, or signal router at powers less than the critical power (8).

Recently, work has been has been done to refine the coupled-mode theory (2, 6, 22). The results of these investigations indicate that there are small, but perhaps in some cases significant, differences between the coupled-mode approach of *Jensen* and actual device performance. Efforts have been concentrated on accounting for the self-focusing and de-focusing effects of the nonlinear material (6) and incorporating the change in mode field shape as a function of the propagation distance for the strongly coupled case (22). Coupled-mode theory assumes that the interaction between the fields of the waveguides does not affect the shape of the mode, but only the amplitude of the electric field. The authors of (2) show that this is not always a good approximation, particularly when the spacing between guides is small and the interaction length is short, as would be the case in practical IO circuits to be used for all-optical computing.

Refinements of the coupled-mode theory indicate that nonlinear effect on the shape of the mode within the guide region is very small. However, outside of the guide region, were the evanescent tail of the mode propagates, nonlinear effects on mode shape are significant (2). These changes influence the power transfer between guides in a nonlinear directional coupler because the coupling is a function of the overlap between the evanescent tail of the electric field and the adjacent guide region.

The authors of (2) find that, in general, the critical power calculated when the nonlinear evanescent tail effects are accounted for is lower than the value predicted from the standard coupled-mode approximations. They also explicitly demonstrate that the small dimensions required for practical IO circuits lead to nonlinear effects on the shapes of the evanescent tails of the waveguide modes.

III. Design and Modeling of Waveguide and Coupler Structures

In this chapter, the design and modeling of optical waveguides and directional couplers are discussed. The general idea of confinement in two directions is presented. Methods for estimating the electric field profiles of the guided optical energy in various structures of interest are discussed. The calculation of the coupling length between weakly-coupled waveguides and a method for estimating the critical power of an NLDC are presented. Finally, the results of the design and modeling carried out for this research are discussed.

Confinement in Two Dimensions and *Marcatili*'s Method

In the previous discussions concerning the theory of optical waveguides, only the case of confinement in one dimension was considered. Many practical IO circuits use waveguides that confine the energy in two dimensions. These optical pathways can be used much like metal traces on a standard IC, or can be used as structures in IO devices such as phase-modulators or NLDCs (11:36, 25:239-240, 13:1582-1583). The confinement of optical energy in two dimensions can be accomplished by simply surrounding the guide region with media of lesser refractive index on four sides instead of two. Such a structure is sometimes called an embedded guide. The general form of this structure can been seen in Fig. 3-1. Note that the view in Fig. 3-1 is along the direction of propagation, z, with power coming out of the plane of the page, as opposed to a side-view as in Fig. 2-1.

The media surrounding the guide region in Fig. 3-1 does not need to be the same on all four sides to achieve confinement. The surrounding mediums could have several different indices of refraction, provided that the indices of these surrounding mediums are all less than the index of the guide region. The analysis of this general structure is complicated by the geometry and boundary conditions that must be met at each interface

(11:37). *Marcatili* (21) has developed an approximate solution to this general case by assuming that the modes of the structure are well-confined to the guide region. This assumption implies that the field in the surrounding regions decays exponentially away from the guide region interfaces and that the field in the corner regions is negligible (11:38, 21:2073). Because of the small fields in the corner regions, this analysis is sometimes called the **field-shadow method**.

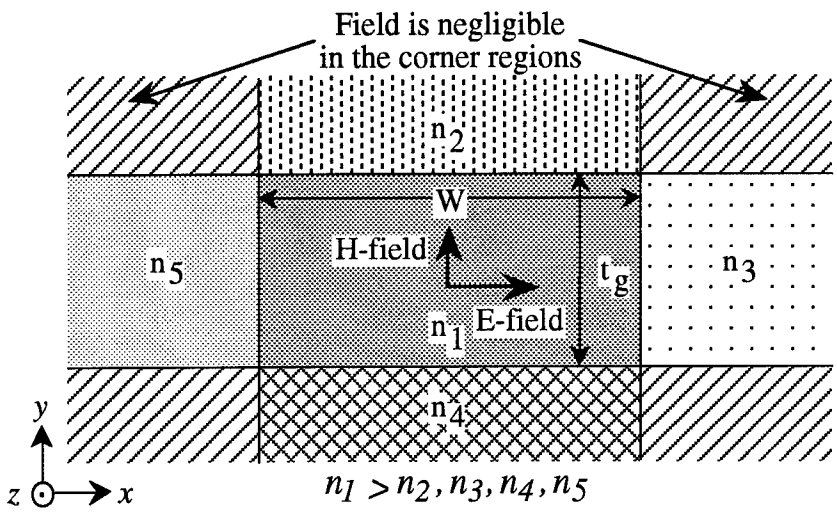

Fig. 3-1. Cross section of a guide region embedded in lower refractive index materials. The view is along the direction of propagation and the geometry is similar to that of the slab waveguide in Fig. 2-1. The main difference between the two guides is that light can be confined in the *x* direction with this structure (after 11:37).

Maxwell's equations are solved by assuming sinusoidal fields in the guide region and exponentially decaying fields in the surrounding regions. The boundary conditions are matched along the four sides of the guide region. *Marcatili* states that if the indices of the surrounding media do not differ by more than 50% from the index of the guide region, the modes are at near grazing angles and are essentially transverse electromagnetic (TEM) in nature. This means that both the electric and magnetic fields of the modes are transverse to

the direction of propagation (9:383, 21:2074, 2096). The electric field has two possible principal polarizations, one with the electric field in the x direction and the other with the electric field in the y direction. All other polarization can be decomposed into combinations of these two directions. For simplicity, only the x direction polarization is considered in this development.

A TEM wave is assumed propagating in the z direction, polarized such that the main transverse field components are E_x and H_y (see Fig. 3-1, 21:2075, 2078). With this polarization and the geometry of Fig. 3-1, the analysis results in the following transcendental equations (21:2079)

$$k_x W = p\pi - \tan^{-1}\left(\frac{n_3^2}{n_1^2} k_x \xi_3\right) - \tan^{-1}\left(\frac{n_5^2}{n_1^2} k_x \xi_5\right) \tag{3-1a}$$

$$k_y t_g = q\pi - \tan^{-1}\left(k_y \eta_2\right) - \tan^{-1}\left(k_y \eta_4\right) \tag{3-1b}$$

where the tan^{-1} functions are to be taken in the first quadrant; k_x and k_y are the propagation constants in the x and y directions, respectively; p and q are mode numbers that correspond to the number of *peaks* in the field distributions in the x and y directions, respectively (thus the fundamental mode in both directions is p, $q = 1$); and where ξ, η are decay coefficients in the regions specified by the subscript and are given by

$$\xi_{3,5} = \left[\left(\frac{\pi}{A_{3,5}}\right)^2 - k_x^2\right]^{-1/2} \tag{3-1c}$$

and

$$\eta_{2,4} = \left[\left(\frac{\pi}{A_{2,4}}\right)^2 - k_y^2\right]^{-1/2} \tag{3-1d}$$

where

$$A_\nu = \frac{\lambda_o}{2\left(n_1^2 - n_\nu^2\right)^{1/2}}, \qquad \nu = 2,\ 3,\ 4,\ 5 \tag{3-1e}$$

The transcendental eqns. (3-1) are solved to find the propagation constants (k_x and k_y) and the decay coefficients for the various regions. The spatial distributions of the fields in the guide and surrounding regions are described by these propagation constants and decay coefficients, in much the same manner as the analysis of eqns. (2-7) through (2-9). See Appendix E for a numerical implementation of *Marcatili*'s analysis.

Marcatili states that this method is based on the assumption that n_1 is only slightly larger than the other indices but that this assumption is not very demanding; the results are valid even when n_1 is 50 percent larger than n_2, n_3, n_4, and n_5 (21:2074). Comparisons of this method with the full numerical solution to the boundary value problem indicate that the field-shadow method of *Marcatili* is most valid for aspect ratios (W/t_g) larger than two (21:2083). This is to be expected because with well-confined modes, larger aspect ratios imply that the field in the shadow regions becomes even less important.

The **channel waveguide**, shown in Fig. 3-2, is a special case of the general structure shown in Fig. 3-1. Confinement of the light in the x direction is provided by the substrate interfaces in that direction. Note that $n_g = n_1$, $n_o = n_2$, and $n_s = n_3$, n_4, and n_5.

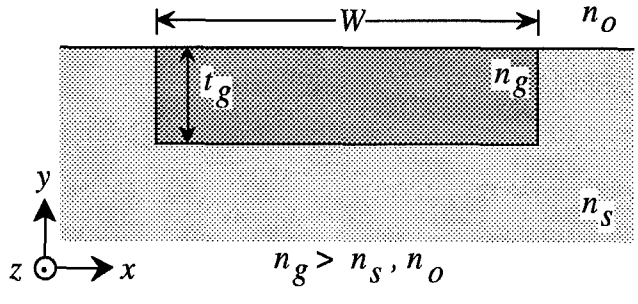

Fig. 3-2. A channel waveguide used for two dimensional confinement of optical energy. Marcatili's method has been used to analyze this structure with good results for aspect ratios (W/t_g) greater than two (after 21:2083).

Effective Index Method

It is possible to achieve confinement in the lateral (x) direction without actually surrounding the guide region with materials of lesser index (11:41). Confinement is achieved by creating a raised structure on top of the guide region, consisting of either a material of lesser index or the guide layer material. Such waveguide structures are often called **strip-loaded** or **rib** waveguides. Some typical structures that confine the light in the lateral direction without embedding the guide region are shown in Fig. 3-3.

The confinement of light in the lateral direction can be most easily explained through the ray-optic interpretation of waveguiding. Consider modes propagating in regions I and II in Fig. 3-3a. Note that the cover layer in this case is not infinite and thus reflections can occur at the n_O/n_C interface. Because of these reflections, the propagation constant of the mode traveling in region I is less than the propagation constant of the mode in region II. The **effective index** of a region - the index that the guide material seems to have based on the group velocity of the mode in that region - is related to the propagation constant of the mode by (11:42)

$$N_{eff} = \frac{\beta_m}{k_o} \tag{3-2}$$

where N_{eff} is the effective index of the region, and β_m is the propagation constant in the z direction of the mth mode in the region.

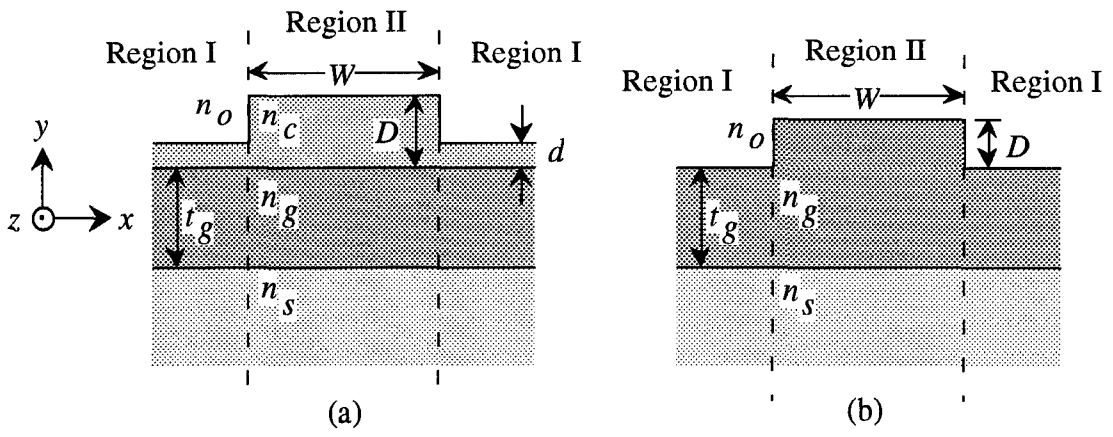

Fig. 3-3. Typical strip-loaded and ridge waveguide structures. The optical energy is traveling in the z direction and is confined to region II of the guide layer. The energy propagating in the guide layer is confined in the lateral (x) direction by the geometry of either the cover layer (a) or the guide material (b). The structure in (a) is a type of *strip-loaded* waveguide while (b) is referred to as a *rib* waveguide (after 11:42).

Since β_m within the strip-loaded region (region II) is greater than β_m outside the loaded region (region I), the effective index of the guide material is greater under the loading strip. This difference in the effective indices leads to confinement in the lateral direction. A similar argument can be applied to the rib waveguide structure of Fig. 3-3b. In the rib waveguide, the effective indices of the two regions are different because of the thicker guide layer in region II. (11:43).

The concept of an effective index is useful in analyzing the structures in Fig. 3-3. The effective index method was first introduced by *Knox* and *Toulios* (15) as a way to avoid the explicit matching of boundary conditions in multi-interface structures such as Fig. 3-3a. The first step in the analysis is finding the propagation constants in the z direction for the modes in the different regions. The development of the dispersion relationship, which relates β_m to the frequency of operation, geometry, and the material parameters, is based on the transverse resonance condition and the Fresnel reflection coefficient at the n_o/n_c interface. *Chuang* gives this dispersion relationship for TE modes as (5:29)

$$k_{gx}t_g = \tan^{-1}\left(\frac{\gamma_s}{k_{gx}}\right) + \tan^{-1}\left(\frac{\gamma_c\left[1-\eta_r \exp(-2\gamma_c t_c)\right]}{k_{gx}\left[1+\eta_r \exp(-2\gamma_c t_c)\right]}\right) + m\pi \tag{3-3a}$$

where

$$\eta_r = \frac{\gamma_c - \gamma_o}{\gamma_c + \gamma_o} \tag{3-3b}$$

$$\gamma_v = \left[\beta_m - \frac{n_v^2\omega^2}{c^2}\right] \quad (v = s,\ c,\ o) \tag{3-3c}$$

$$k_{gx} = \left[\frac{n_g^2\omega^2}{c^2} - \beta_m\right] \tag{3-3d}$$

and t_c is the thickness of the cover layer in the region (either D or d in Fig. 3-3). Note that here m is the familiar mode number, corresponding to the number of *nulls* in the field distribution. Also note that the tan^{-1} functions are to be taken in the first quadrant (15:501).

Solving the transcendental equation, eqn. (3-3a), for β_m gives the propagation constant in the z direction for the allowed modes in the region. The effective index in the region can then be calculated by eqn. (3-2). Appendix C contains a numerical implementation of the effective index method applied to a four-layer waveguide structure such as the strip-loaded guide of Fig. 3-3a. Note that the difference in propagation constants for the regions is a strong function of the cover layer thickness. Often D in region II of Fig. 3-3a is chosen to be much thicker than the penetration depth of light into the cover, making the cover layer in region II essentially infinite. This condition on D is assumed in the following equivalent waveguide model (Fig. 3-4) for the strip-loaded guides. The equivalent waveguide model is also used to analyze the rib waveguide (Fig. 3-3b), with the cover region assumed to infinite.

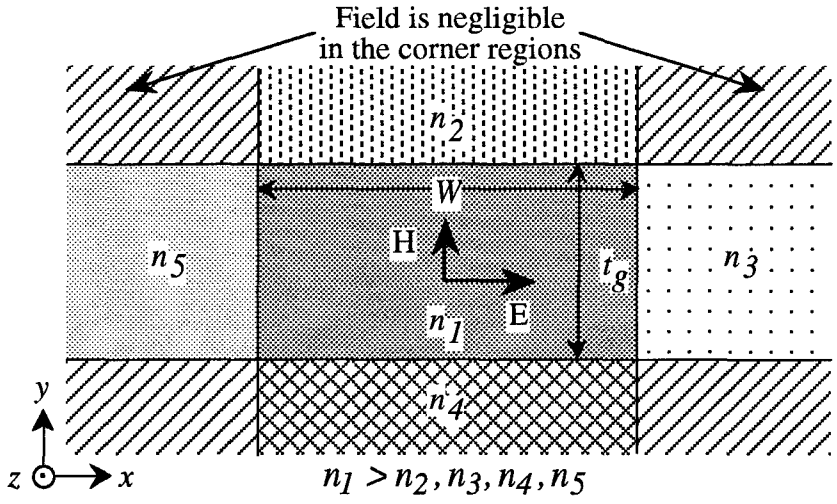

Fig. 3-4. Guide geometry used to analyze the strip-loaded guide by *Marcatili*'s method. The equivalent index is used to calculate the field parameters in the x direction. The cover and substrate regions are assumed to be semi-infinite (after 11:37)

Equation (3-3), developed for a four-layer waveguide structure, can also be used to analyze a three-layer waveguide such as the rib guide of Fig. 3-3b. First, the propagation constant in the z direction is found for the two regions using eqn. (3-3). For this case, $n_C = n_O = 1$ ($\eta_r = 0$). To find the propagation constant in regions I and II, t_C in eqn. (3-3a) is set equal to the actual guide layer thickness (either t_g or $t_g + D$, see Fig. 3-3b). The effective index method is used in Appendix D to determine the effective indices for regions I and II of a rib waveguide. The confinement of light in the x direction can then be modeled using *Marcatili*'s method and an equivalent index in the lateral regions around the guide region (Fig. 3-4). The equivalent index, N_{eq}, used to model index of the lateral regions for both the strip-loaded and rib waveguide structures is given by (7:324)

$$N_{eq} = \left(n_g^2 - N_{II}^2 + N_I^2\right)^{1/2} \tag{3-4}$$

where N_{II} is the effective index in region II, and N_I is the effective index in region I.

Using the values of N_{eq}, n_g, n_c, and n_s, the field distribution parameters for the strip-loaded and rib guides can be calculated using *Marcatili*'s field-shadow method (11:42). Appendix E contains a Mathcad® document that can be used to model strip-loaded and rib waveguide and the coupling between waveguides using the field-shadow method. The principle advantage in using the field-shadow method is that confinement in both directions is accounted for in determining the modal field distribution parameters.

Embedded or channel waveguides suffer under the constraint that the sidewalls must be smooth to reduce losses due to scattering. In both strip-loaded and rib waveguides, most of the field is contained in the guide region, away from the sidewalls that define the structure. Thus, strip-loaded and rib waveguides could exhibit less scattering losses due to side-wall roughness (11:44). Excessive roughness and non-uniformity of the defining ridge sidewalls in strip-loaded or rib guides could, however, have a significant effect on waveguide losses if confinement in the lateral (x) direction is reduced as a result of the ridge side-wall characteristics.

Calculation of Coupling Coefficients

The coupling of light between slab waveguides, such as the ones shown in Fig. 2-4, was examined in Chapter II. The overlap between the spatial distributions of modes in adjacent waveguides was found to be a measure of the coupling between the guides. In this section, the special case of the coupling between two-dimensional, identical, weakly-coupled, adjacent guides that are isolated from other structures is considered (see Fig. 3-5). The basic process is the same as in Chapter II: the field distribution parameters for the two-dimensional guides are used to determine the coupling.

The fabrication process, discussed in Chapter IV, resulted in groups of non-identical, perhaps strongly-coupled, waveguides that were all coupled to each other. This more general case is much more difficult to analyze but is, in principle, similar the case considered in this section; each guide is coupled to its neighbor and the exchange of energy

occurs between adjacent guides. Thus, the special case of isolated waveguides discussed in this section is illustrative of the phenomenon that would be observed in the general case. *Somekh* (26) has analyzed a multi-channel directional coupler consisting of an infinite number of weakly-coupled identical guides.

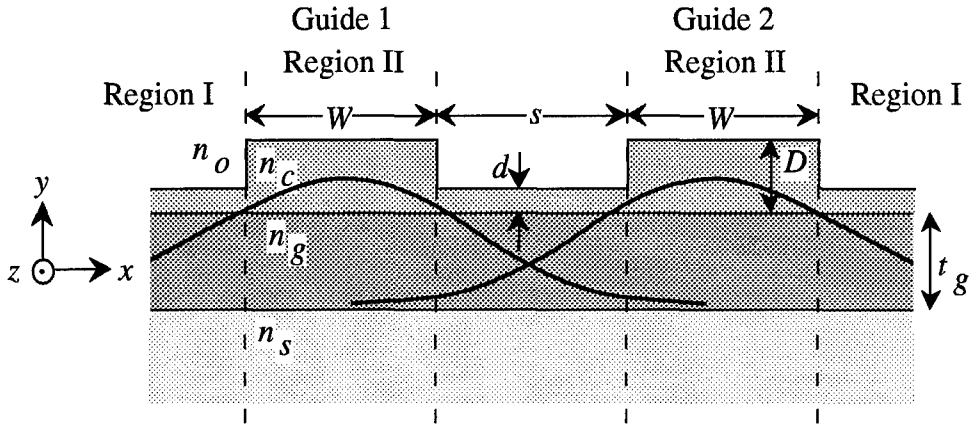

Fig. 3-5. Typical coupled waveguide structure and mode profiles. The energy is traveling in the z direction. The amount of coupling between the guides is determined by the mode profiles and their degree of overlap (after 11:111).

For small input powers, an NLDC functions as a linear coupler (13:1582). That is, if the intensity of the light launched into the guide is small enough such that the refractive index of the guide is not significantly altered, the NLDC can be expected to perform as though it were made of linear materials. Thus, it is useful to calculate the coupling coefficients of an NLDC by assuming that the materials are linear.

The field distribution parameters for the waveguide modes can be used to determine the coupling between guides. Recall that this weakly-coupled approximation implies that the overlap of the evanescent mode-tail in the guide region does not significantly change the overall shape of the mode (11:116). *Marcatili* gives the condition for weakly-coupled guides as (21:2099)

$$\left|sk_{xeq}\right| >> 1 \tag{3-5a}$$

where s is the separation between guides (Fig. 3-5),

$$k_{xeq} = \left[\left(\frac{2\pi}{\lambda_o} N_{eq}\right)^2 - k_z^2 - k_y^2\right]^{1/2} \tag{3-5b}$$

and k_z is the propagation constant in the z direction, which can be calculated using (21:2097)

$$k_z = \left[\left(\frac{2\pi}{\lambda_o} n_g\right)^2 - k_x^2 - k_y^2\right]^{1/2} \tag{3-5c}$$

The case of particular interest assumes identical, weakly-coupled, single-mode waveguides with well confined modes. Using these constraints, the coupling coefficient between guides can be expressed as (21:2101)

$$\kappa = \frac{2k_x^2 t_g \exp\left[\frac{-s}{\xi_{eq}}\right]}{k_z \xi_{eq}\left(t_g + \eta_2 \sin^2\left[k_y t_g\right]\right)\left(W + 2\xi_{eq}\right)\left(k_x^2 + \frac{1}{\xi_{eq}^2}\right)} \tag{3-6a}$$

where κ is the coupling coefficient between adjacent guides; ξ_{eq} is the decay coefficient in the N_{eq} region of Figs. 3-4 and 3-5; and W, s are the coupler dimensions (see Fig. 3-5). In eqn. (3-6a) the assumption that $n_2 > n_4$ has been made. If $n_4 > n_2$ had been assumed, η_2 in eqn. (3-6a) would have been replaced by η_4.

Equation (3-6) is the same as a formula presented by *Marcatili* (21:2101) except for a modification that accounts for modes that are reasonably well confined but perhaps do not meet the strict condition of eqn. (3-5) (26:45-46). The coupling coefficient calculated using eqn. (3-6) is equivalent to the coupling coefficient presented in eqn. (2-11), provided that the proper normalization of the field profiles is accomplished using eqn. (2-12). Good agreement between the two methods for calculating κ were observed during modeling of the waveguide structures (see Appendix E, p. E-8).

For identical guides and modes, the length required for complete coupling of the light from one guide to the other, L_O, is related to the coupling coefficient by (11:115)

$$L_O = \frac{\pi}{2\kappa} \tag{3-7}$$

Recall that the power will be transferred periodically between the two guides, as indicated by eqn. (2-15) and Fig. 2-6.

Estimation of the Critical Power for an NLDC

The critical power for an NLDC is a function of the nonlinearity of the guide material and the mode profile (13:1581). It is assumed here that the interaction length of the coupler is $L_O = \pi/2\kappa$, where κ is the linear coupling coefficient between the guides. By approximating the mode in the guide as a plane wave, an estimate of the critical power for an NLDC can be obtained as (13:1583)

$$P_C = \kappa A \frac{\lambda_O n_g c}{2\pi^2 n_{2esu}} \tag{3-8}$$

where κ is the linear coupling coefficient between adjacent guides, A is the cross-sectional area of a guide, n_g is the linear index of the guide, c is the speed of light in vacuum, and n_{2esu} is the nonlinear coefficient in electrostatic units (*esu*).

From the relationship (in cgs-Gaussian units), $n = n_g + n_{2esu}|E|^2$, where E is the electric field in statvolt/cm, it can been seen that n_{2esu} must have units of cm^2/statvolt^2. These units are equivalent to cm-sec^2/gram. That is, [n_{2esu}] = cm^2/statvolt^2 = cm-sec^2/gram (3:307).

The value of n_{2esu} can be found from the intensity-dependent nonlinear coefficient n_{2mks} (in *mks* units) by (3:308)

$$n_{2esu} = \frac{n_{2mks} n_g}{8.4} \tag{3-9}$$

where n_{2mks} must be expressed in cm^2/kW and n_{2esu} carries units of cm-sec^2/gram.

The critical power estimated with eqn. (3-8) is based on the assumption that the waveguide mode can be approximated by a plane wave. Thus, the estimate is only valid for the fundamental mode and should be regarded as a means of determining the approximate power level at which nonlinear optical effects could be observed in an NLDC.

Note that the assumption was made that the interaction length between the two guides was $L_O = \pi/2\kappa$. Thus for very weakly-coupled guides, where κ is very small, the interaction length between guides can be very long. Since L_O is large, the accumulated phase shift, $\Delta\beta L_O$, can be substantial even for small values of intensity-induced $\Delta\beta$. Thus, only small input powers are needed to achieve switching in a coupler with a very large interaction length. It should be noted, however, that coupler structures with interaction lengths longer than a few millimeters are not practical in IOCs. The critical powers for these structures are essentially meaningless because the coupling between the guides is too weak to achieve switching within reasonable interaction lengths.

Models of Fabricated Coupler Structures

Three different waveguide structures, strip-loaded, rib, and embedded channel, were designed and modeled (see Figs. 3-2 and 3-3). The goal was to design single-mode

waveguides and to model the coupling that occurs between adjacent guides. All modeling was conducted at the nominal wavelength of 0.92 μm. Known parameters such as index and nonlinearity for the materials of interest were used in the design process. The two polymers used in the fabrication process, polythiophene and polyphenylene, have indices of 1.71 and 1.79, respectively, at 0.85 μm (14). The nonlinear coefficient of polyphenylene, n_{2mks}, is 2.03 x 10^{-10} cm^2/kW (n_{2esu} = 4.33 x 10^{-11} cm-sec^2/gram) at 0.85 μm (14). The absorption resonance of polyphenylene is in the UV so the material parameters are approximately constant across the near-infrared spectrum (14). Note that polyphenylene is a self-defocusing material so the sign of the nonlinear coefficient is negative. The loss coefficient of polyphenylene at 0.85 μm has been measured to be 2.3 ± 0.6 dB/cm (14). For simplicity, all materials were modeled as lossless.

An additional design constraint was the use of a pre-existing photolithographic mask. The dimensions of this mask, used in previous work (18), defined the feature sizes of the waveguides. This mask consisted simply of three groups of parallel lines, each group having the same basic features but with the separation between the features differing from group to group. A diagram of the 2" chromium mask used to define the waveguiding structures is shown in Fig. 3-6.

In the case of the strip-loaded structures, the use of negative photoresist resulted in waveguides with nominal dimensions of W = 3, 5, and 10 μm and separation distances of s = 1, 2, and 3 μm. Using positive photoresist in the fabrication of the rib waveguide structures resulted in nominal dimensions of W = 1, 2, and 3 μm and s = 3, 5, and 10 μm. For the channel guide structures, waveguide regions with nominal dimensions of W = 3, 5, and 10 μm and s = 1, 2, and 3 μm were produced by using positive photoresist. More information concerning the fabrication of waveguide structures is contained in Chapter IV.

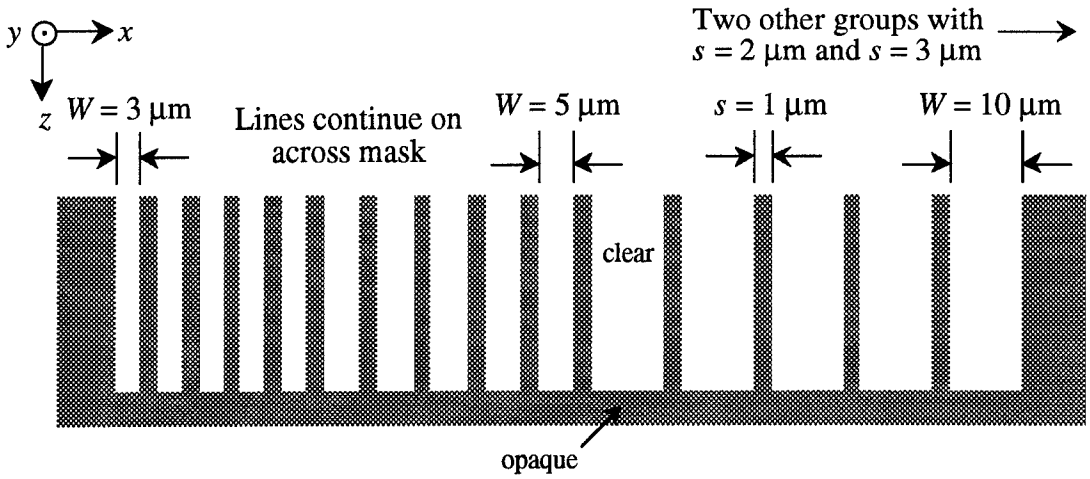

Fig. 3-6. The photolithographic mask used to define the dimensions of the waveguide structures. Note that two different sets of waveguide structures were produced with this mask, differing by the type of photoresist (positive or negative) used in the fabrication process. The groups of guides were separated by approximately 2 mm.

The first step in the design process was the determination of the allowable dimensions for single-mode operation. In the y direction the structures were approximated by equivalent slab waveguides and the Mathcad® document in Appendix A was used to find the minimum and maximum allowable dimensions for single-mode operation. The field-shadow method was used to determine how many modes a structure would support in the x direction by varying the parameter p, the mode number in the x direction. The highest value of p for which a solution to eqn. (3-1a), bounded by the condition that $k_x < k_o$, exists was the number of modes that the structure can support in the x direction.

The profiles of the electric field were modeled using the field distribution parameters calculated by the field-shadow method of *Marcatili*. For simplicity, only the x direction polarization of the TEM modes is considered (see Fig. 3-1). The Mathcad® documents found in Appendices C, D, and E were used to compute and plot these profiles. The field distribution parameters were also used to compute the coupling coefficient and coupling

length for adjacent guides. The critical power, subject to the constraints on eqn. (3-8), was calculated where applicable.

The numerical aperture of the guides was calculated using the indices of the guide material, cover, and substrate layers, as appropriate. Since the guides were asymmetric in the x direction, the index used in the calculation was the larger of either the cover or substrate. This is because the larger index, resulting in a larger critical angle at that interface, is the limiting factor in determining if a ray will be guided. The numerical aperture, NA, was calculated using (25:251)

$$NA = \left(n_g^2 - n_{c,s}^2 \right)^{1/2} \tag{3-10}$$

where $n_{c,s}$ is the index of either the cover or substrate, whichever is larger.

Modeling of Strip-Loaded Waveguides

A waveguide structure like the one shown in Fig. 3-3a was designed and modeled using both the effective-index and field-shadow methods. In this structure, polythiophene was used as the cover layer ($n_c = 1.71$), polyphenylene was used as the guide material ($n_g = 1.79$), and silicon dioxide was used as the substrate layer ($n_s = 1.5$). The minimum and maximum allowable values for t_g were calculated by assuming that the cover and substrate layers were semi-infinite. It was found that the minimum guide thickness needed to avoid cutting-off the fundamental mode was 0.28 μm while the maximum allowable thickness for single-mode operation was 1.15 μm.

Based on post-fabrication inspection of SEM photographs, nominal values of the dimensions D, d, and t_g were found to be 1.2 μm, 0.6 μm, and 0.67 μm, respectively. Using Appendix E, it was found that the $W = 10$ μm waveguides were capable of supporting both the fundamental ($p = 1$) and first odd mode ($p = 2$) in the x direction. The modeling results for the various waveguide widths and separations are shown in Table 3-1.

An example of the field distribution in $W = 10$ μm guides is shown in Fig. 3-7. Only coupling between the fundamental modes is shown in this figure. Likewise, only coupling between identical modes is shown in Table 3-1. In general, there would also be coupling between the fundamental mode in one guide and the first odd mode, if supported, in an adjacent guide.

Table 3-1. Modeling results for the strip-loaded waveguides. The model parameters were: $\lambda_o = 0.92$ μm, $D = 1.2$ μm, $d = 0.6$ μm, $t_g = 0.67$ μm, $NA = 0.53$, $n_{2esu} = 4.33 \times 10^{-11}$ cm-sec^2/gram, N_{eff} outside guide region was 1.743, N_{eff} within the guide region was 1.744, and N_{eq} used in Marcatili's method was 1.789.

		s = 1 μm			s = 2 μm			s = 3 μm	
W (μm)	κ (mm^{-1})	L_o (mm)	P_c (W)	κ (mm^{-1})	L_o (mm)	P_c (W)	κ (mm^{-1})	L_o (mm)	P_c (W)
3	1.8	0.9	214	1.5	1.1	174	1.2	1.3	142
5	1.6	1.0	308	1.2	1.3	230	0.91	1.7	177
10	0.69	2.3	269	0.49	3.2	189	0.34	4.6	133
	0.76†	2.1†	—	0.66†	2.4†	—	0.57†	2.7†	—

†Value is for the first odd mode ($p = 2$) in the x direction. Note that no critical powers are given for the first odd mode because the approximation used to develop eqn. (3-8) is only valid for the fundamental mode. Critical powers are not given for couplers with L_o longer than a few millimeters because they would not be practical devices.

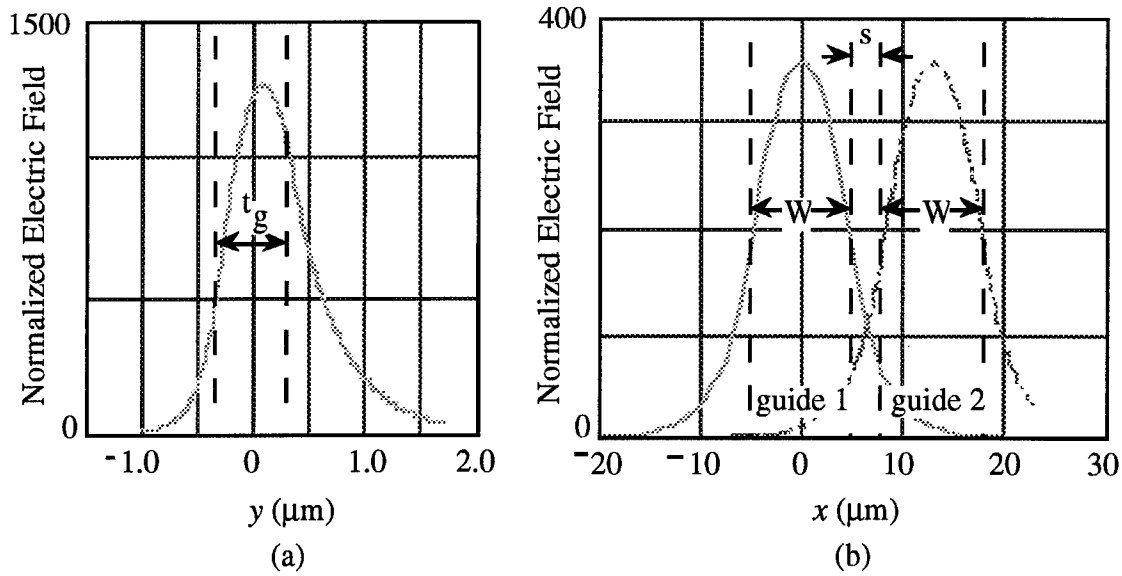

Fig. 3-7. Typical mode profiles in a strip-loaded waveguide. The thickness of the guide material is 0.67 μm, the width of the guides is 10 μm, and the separation between the guides is 3 μm. The zero point on the horizontal axis is the center of the guide in that direction. In (a), the spatial distribution of the electric field in the y direction is shown. Note that the mode is asymmetric about the center of the guide because the indices of the cover and substrate layers are significantly different. The distribution of the electric fields in the x direction and their overlap in a directional coupler structure are shown in (b).

Modeling of Rib Waveguides

Rib waveguides like the one shown in Fig. 3-3b were designed and modeled using the effective-index method and the field shadow method. The material parameters were taken as $n_O = 1$ (air), $n_g = 1.71$ (polythiophene), and $n_S = 1.5$ (silicon dioxide). For this structure, it was found that the minimum guide thickness needed to avoid cutting-off the fundamental mode was 0.17 μm while the maximum allowable thickness for single-mode operation was 0.73 μm. The guide thickness was chosen to be 0.5 μm and, based on modeling by the effective index method, D for design purposes was chosen to be 0.1 μm.

The number of supported modes in the x direction for a given waveguide structure was found using the field-shadow method. The $W = 1$ μm guides were single-mode in the x direction while both the $W = 2$ and $W = 3$ μm were found to support the first odd mode.

Post-fabrication inspection of the rib waveguides indicated that the polythiophene guide layer was not grown thick enough to produce practical waveguides. The fabrication process and inspection results are discussed further in Chapter IV. The modeling results presented in Table 3-2 were calculated using the design values for the guides.

Table 3-2. Modeling results for the rib waveguides. The model parameters were: λ_o = 0.92 μm, t_g = 0.5 μm, D = 0.1 μm, NA = 0.82, $n2_{esu}$ = 4.33 x 10^{-11} cm-sec^2/gram, N_{eff} outside guide region was 1.612, N_{eff} within the guide region was 1.632, and N_{eq} = 1.691.

		s = 3 μm			s = 5 μm			s = 10 μm	
W (μm)	κ (mm^{-1})	L_o (mm)	P_c (W)	κ (mm^{-1})	L_o (mm)	P_c (W)	κ (mm^{-1})	L_o (mm)	P_c (W)
1	1.7	0.94	58	0.19	8.1	7	9x10^{-4}	2x10^3	—
2	0.32	4.9	22	0.018	85	—	2x10^{-5}	1x10^5	—
	2.5†	0.63†	—	1.5†	1.0†	—	0.44†	3.6†	—
3	0.11	14	11	0.005	325	—	2x10^{-6}	8x10^5	—
	1.3†	1.2†	—	0.19†	8.2†	—	0.002†	1x10^3†	—

†Value is for the first odd mode (p = 2) in the x direction. Note that no critical powers are given for the first odd mode because the approximation used to develop eqn. (3-8) is only valid for the fundamental mode. Critical powers are not given for couplers with L_o longer than a few millimeters because they would not be practical devices.

A coupling length, L_o, longer than several millimeters indicates that the guides are essentially uncoupled (see Table 3-2). The critical powers in Table 3-2 were calculated using the value of $n2_{esu}$ for polyphenylene and are given for the fundamental mode of reasonably well-coupled guides. Note that for a given geometry the fundamental mode (p = 1) in the x direction can be uncoupled from adjacent waveguides while the first odd mode (p = 2) can be reasonably well coupled. For instance, with W = 2 μm and s = 10 μm the

fundamental mode has a coupling length of $L_O \approx 1 \times 10^5$ mm while the first odd mode has a much more practical value of $L_O = 3.6$ mm. This great disparity in coupling lengths is because the fundamental mode is very well confined for the mentioned geometry but the first odd mode is nearly cut-off and thus poorly confined. Such a configuration could be used to "strip" the first odd mode from a waveguide, leaving only the fundamental to propagate. Plots of the electric field profiles for the $p = 1$ and $p = 2$ modes illustrate the difference in coupling for the two modes (see Fig. 3-8).

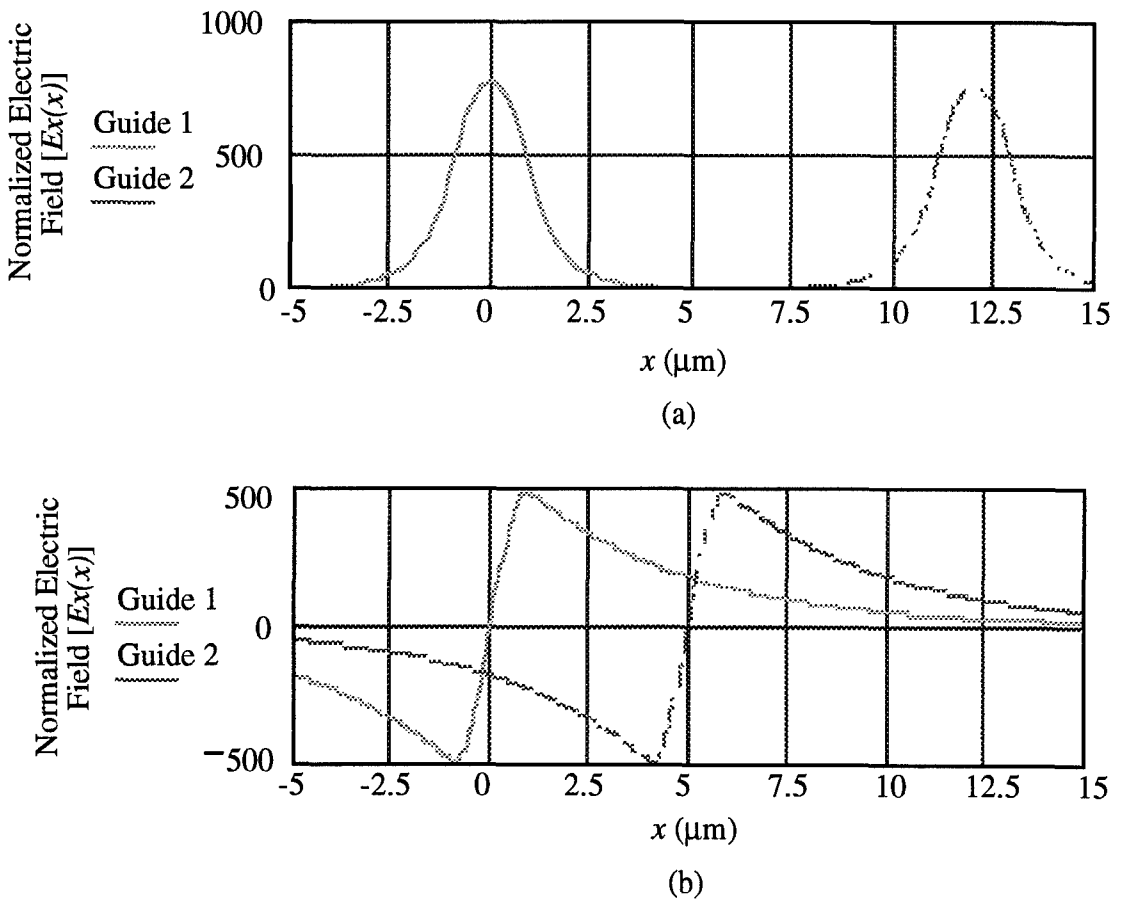

Fig. 3-8. Electric field profiles for $p = 1$ and $p = 2$ in a rib waveguide. The width of a guide is $W = 2$ μm, the separation between guides is $s = 10$ μm. Guide 1 is centered on $x = 0$. Note that the $p = 1$ mode (a) is essentially uncoupled while there is a large degree of overlap (and thus coupling) between modes for the $p = 2$ mode (b).

Modeling of Embedded Channel Waveguides

Channel waveguides like the one shown in Fig. 3-2 were designed and modeled using $n_O = 1$ (air), $n_g = 1.79$ (polyphenylene), and $n_S = 1.5$ (silicon dioxide). The structure was analyzed by using *Marcatili*'s field-shadow method. The thickness of the guiding layer, based on post-fabrication inspection, was 1.8 μm.

Modeling indicates that the guides can support multiple modes in both the x and y directions. For instance, with $W = 10$ μm and $t_g = 1.7$ μm, the guide can support 4 TE modes in the y direction and 22 TE modes in the x direction. All but the very highest modes are essentially uncoupled, even for $s = 1$ μm. Both of these results, multi-mode guides and lack of coupling, are due to the relatively large difference in index between the substrate and guide materials. Using Appendices A and E, the maximum dimensions for single-mode operation are $t_g \approx 0.6$ μm and $W \approx 0.47$ μm. These dimensions imply that coupling light into single-mode guides of this geometry would be very difficult.

Observations Concerning the Modeling of Waveguides

The results of the modeling for strip-loaded, rib, and channel waveguides indicate that the strip-loaded geometry allows the largest dimensions for single-mode operation. The presence of a cover layer with a refractive index close to the guide material refractive index permits the single-mode guide thickness to be larger than it is in the more asymmetric rib or channel guides. The strip-loaded geometry with $d/D \approx 0.5$ weakly confines the energy in the lateral direction. The net result of this weak confinement is that the guide can be relatively large in the lateral direction and still remain single-mode. Also, coupling between guides is enhanced by the weak confinement. The "large" single-mode dimensions of strip-loaded guides make them good candidates for experimental work. The coupling of light into a guide becomes more feasible as the dimensions of the guide are increased.

IV. Fabrication of Waveguiding Structures

This chapter details the fabrication of the three different waveguide structures designed and modeled during this research. Some basic understanding of integrated circuit fabrication techniques is assumed in this chapter; see, for example, (12, 30). Each waveguide structure was fabricated using similar wafer preparation, polymer growth, feature etching, and cleaving techniques. In addition, the features of all three waveguide structures were defined using the same photolithographic mask. The film growth and feature etching techniques were developed during previous work on this topic (18).

The photolithographic mask used for waveguide fabrication was developed during previous work by Kutsche (18:32). The mask was reused in this work to expedite the fabrication process. As mentioned in Chapter III, this mask consisted simply of three groups of parallel lines, each group having the same basic features but with the separation between the features differing from group to group. A diagram of the 2" chromium mask used to define the waveguiding structures is shown in Fig. 4-1.

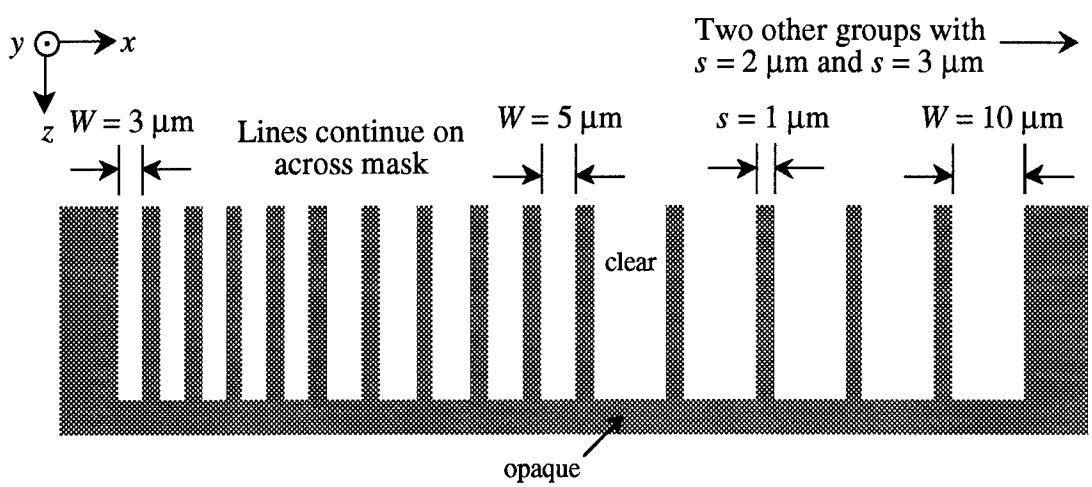

Fig. 4-1. The photolithographic mask used in fabrication of waveguide structures. Note that two different sets of waveguide structures were produced with this mask, differing by the type of photoresist (positive or negative) used in the fabrication process. The groups were separated by approximately 2 mm.

During the photoresist exposure step, the mask was exposed three times across the surface of the wafer, resulting in three copies of the same pattern. This was possible because the mask was a dark-field mask; it blocked the light in the outlying regions, leaving them unexposed. The pattern was repeated across the surface of the wafer to maximize the number of waveguides produced.

All scanning electron microscope (SEM) photographs were taken at relatively low energy (typically one or two keV) to avoid damaging the polymer films. In addition, the samples were coated with approximately 30 Å of tungsten to prevent localized charging of the dielectric materials and enhance resolution of the photographs. All SEM pictures were taken with a Hitachi S-900 Low Voltage High Resolution (LVHR) scanning electron microscope, an instrument well suited for producing high-resolution images under low-energy conditions.

Strip-Loaded Waveguides

The strip-loaded waveguides consisted of two polymer films deposited on a silicon wafer that had been thermally oxidized to form the substrate layer (see Fig. 3-3a). These waveguides were fabricated using negative photoresist resulting in dimensions of $W = 3$, 5 and 10 μm and $s = 1$, 2, and 3 μm. This section details the steps used to fabricate the strip-loaded guides used in this research.

The first step in the fabrication process was the preparation of the silicon wafers. A group of 3" wafers were cleaned by immersing them in a 3:2 solution of sulfuric acid (H_2SO_4) and hydrogen peroxide (H_2O_2) for 25 minutes. They were then rinsed for 20 minutes in a flowing deionized (DI) water bath and blown dry with nitrogen gas. The wafers were then thermally oxidized in a dry oxygen atmosphere for 120 hours at 1100°C. The wafers were slowly inserted (about 1 in/min) into the oxidation furnace to avoid thermal stress-induced warpage of the wafers. The oxidation process resulted in

approximately 2.2 μm of high quality "dry" silicon dioxide (SiO_2) being grown on the surface. This group of oxidized wafers were used as substrates for the strip-loaded guides.

Immediately prior to film growth, the wafer to be used was re-cleaned by immersing it in the 3:2 H_2SO_4:H_2O_2 cleaning solution for 25 minutes, rinsing it in DI water for 25 minutes, blowing it dry with nitrogen, then throughly drying it in a 165°C convection oven for 25 minutes. To avoid contamination of the polymer film the wafer was kept in a silicon wafer carrier until it was inserted in the polymer growth chamber.

The polymer films were deposited through plasma-enhanced chemical vapor deposition (CVD) (18:8-16, 31). Polyphenylene was grown as the guide layer with polythiophene serving as the cover layer. After the wafer to be grown on was inserted, the deposition chamber was allowed to pump-down for three days prior to film growth to remove any traces of water vapor or other out-gassed contaminates. The conditions for growth of the polymer films were as shown in Table 4-1. The substrate temperature was not controlled during the polymer growth process. Polythiophene was grown as the cover layer by changing the monomer gas, replacing the benzene flow with dichlorothiophene (18:10-15).

Table 4-1. Parameters used for growth of polymer thin-films.

Growth Parameter	Value
Total chamber pressure	0.5 torr
Flow rate of argon	100 cc/min
Flow rate of monomer gas†	0.6 cc/min
Forward RF power	100 W
Reflected RF power	84 W

†Benzene for polyphenylene, dichlorothiophene for polythiophene.

During film growth the wafer was rotated at approximately 4 rpm for more uniform deposition across the surface of the wafer. The films were grown without any sort of diffuser on the gas outlet nozzle. Polyphenylene was grown for 28 hours and polythiophene was grown for 55 hours. Post-growth inspection of this deposition indicated growth rates of 0.024 μm/hr for polyphenylene and 0.022 μm/hr for polythiophene. The resulting polymer coated wafer was stored at room temperature in a dry box (< 20% relative humidity) to avoid foreign object contamination and delamination from water vapor (18:36).

The major steps in the fabrication of the strip-loaded guides are diagrammed in Fig. 4-2. The first step in the patterning of the polythiophene cover layer was the plasma deposition of silicon nitride (Si_3N_4) as a passivating layer (18:27-29). The growth conditions for the nitride layer were as follows: a gas mixture of 5% SiH_4 (silane) and 95% N_2 at a flow rate of 168 sccm/min; a separate flow of N_2 at 1250 sccm/min; a flow of NH_3 (ammonia) at 10 sccm/min; forward RF power of 21 W; substrate temperature of 120°C; and a total pressure of approximately 840 millitorr. Growth was monitored by also growing nitride on an otherwise bare wafer and performing post-growth ellipsometry. A total of 0.12 μm of Si_3N_4 was deposited with an observed growth rate of 0.01 μm/min.

After nitride growth, photoresist was spun onto the wafer to prepare for photolithographic masking. Waycoat 28 negative photoresist was spun on to a thickness of approximately 1 μm and soft-baked at 100°C for 5 minutes. The photoresist was then exposed for 8 sec using the photolithographic mask described in Fig. 4-1. The pattern was repeated three times across the wafer surface as previously noted. Note that there was no intimate contact between the mask and the wafer due to the fact that the mask was designed to be used with 2" wafers. This accounts for the rough side-wall features of the resulting waveguides (Fig. 4-3). The photoresist was developed for 25 seconds, rinsed with isopropyl alcohol, and the wafer dried for 3 minutes at 100°C with a contact hot plate.

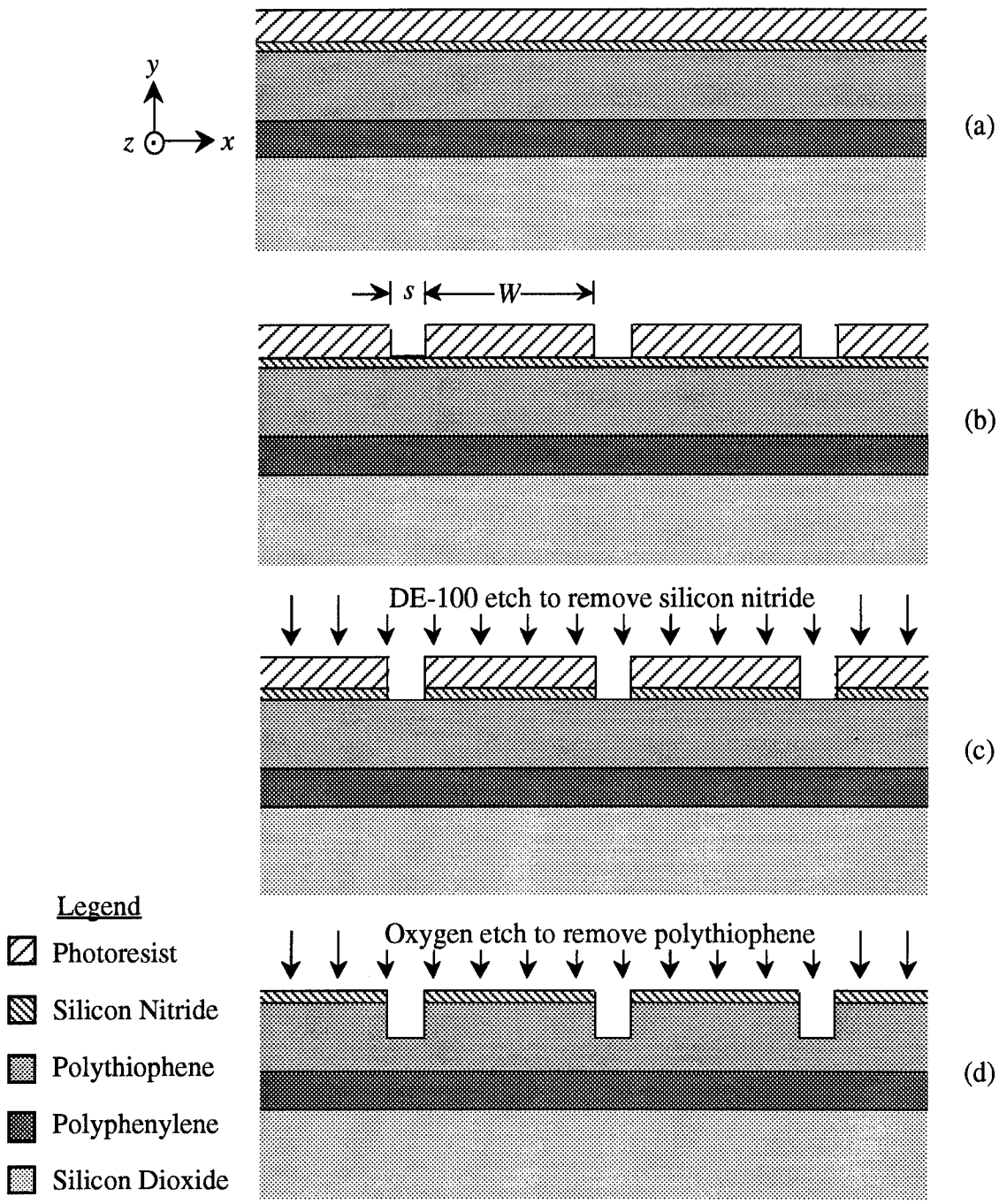

Fig. 4-2. The major steps in the fabrication of strip-loaded waveguide structures. In (a) the substrate is shown coated with polymer films, the silicon nitride passivating layer, and negative photoresist. The photoresist layer is exposed and developed (b) and then the silicon nitride is etched (c). The polythiophene layer is then partially removed with an oxygen etch (d). Note that this step also etches away the remaining photoresist.

The wafer was then placed in the reactive-ion etch (RIE) chamber for partial removal of the cover layer. The nitride layer was removed (where exposed) with a mixture of O_2 and Freon-14 known commercially as DE-100. The nitride was etched for 1.2 minutes at a rate of 0.1 μm/min, completely removing the nitride not protected by the photoresist and leaving the polythiophene exposed. Exposed polythiophene was etched using oxygen with a flow of 50 sccm at a total pressure of 50 millitorr. Note that the photoresist remaining on top of the protected nitride was also etched during the removal of the polythiophene. The RIE was capacitively-coupled with a DC bias of 300 VDC and forward power of 98 W. Polythiophene was etched for a total of 7.5 minutes with an observed etch rate of 0.8 μm/min. This agrees well with previous work (18:47). The sample was removed several times during the polythiophene etch for profilometry as a check on the etch rate. Note that the layer of silicon nitride remaining on the top of the waveguide structures (Fig. 4-2d) could have been removed with another DE-100 etch step but was left to provide some measure of protection against damage by subsequent handling. This layer is thin enough and far enough away from the guiding layer to be ignored in the modeling of the waveguides.

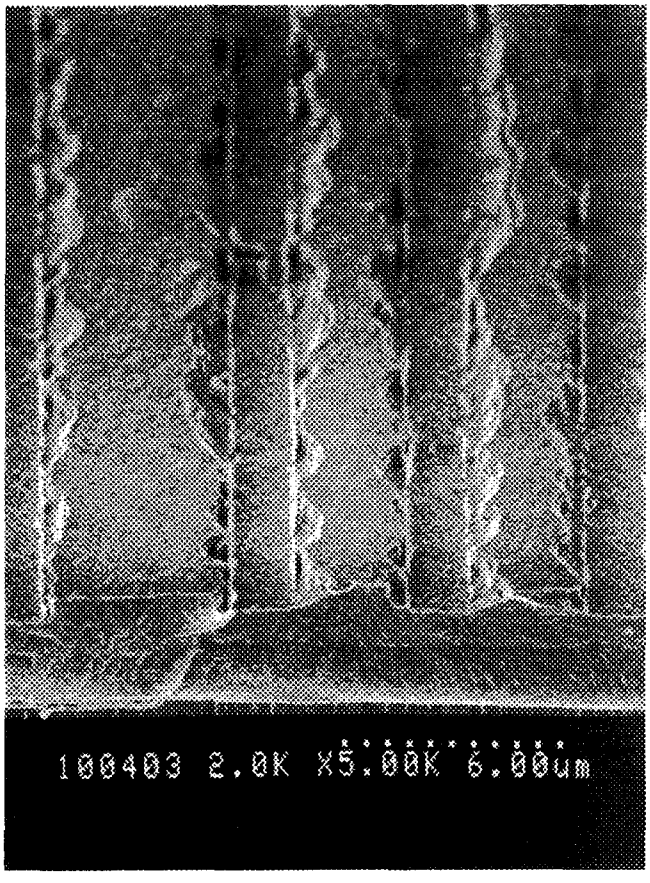

Fig. 4-3. Side wall roughness of the strip-loaded waveguide structures. This top view of the sample shows the very rough side walls in the cover layer of the waveguides. Both 5 μm and 3 μm wide structures are shown. The separation between waveguides in this group is nominally 2 μm.

The wafer was cleaved in order to take cross-section pictures of the resulting waveguide structures. The samples were cleaved both in compression and in tension. "Compression" and "tension" refer to the type of force applied to the polymer film. In compression cleaving, the back of the wafer is scored and broken by applying force to the silicon side of the wafer, with the polymers facing down. Two slightly different methods of tension cleaving were tried. In one case, the wafer was scored across the back (on bare silicon side) and in the other a small tick mark was made on the polymer side of the wafer,

near the edge. In tension cleaving methods, the sample was broken with the polymer films facing up. The different cleaving techniques are shown in Fig. 4-4. A lens tissue was used between the glass slide and the polymer film to lessen the damage to the film.

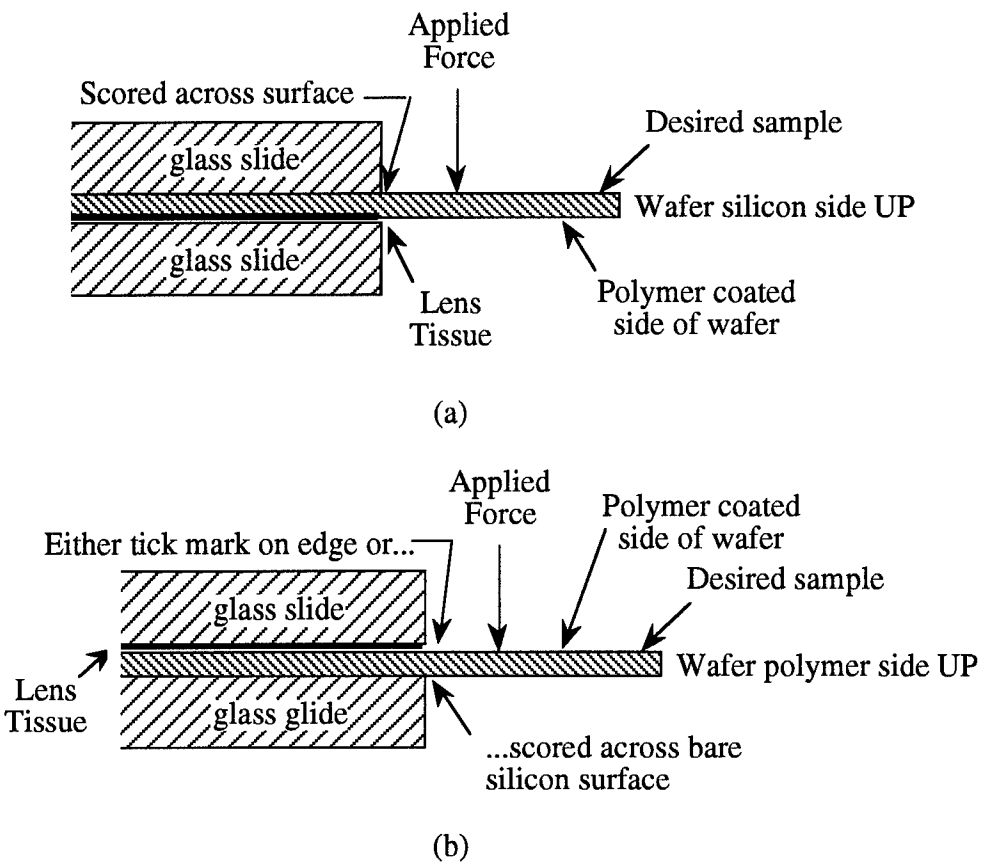

Fig. 4-4. Two different techniques for cleaving of samples. In (a), the polymer film is compressed while it is broken while in (b) the film is cleaved in tension. Note that two different scoring techniques were tried with tension cleaving.

Typical cleaved surfaces produced by the different cleaving techniques are shown in Fig. 4-5. The sample in Fig. 4-5a was broken by the compression technique shown in Fig. 4-4a. In Fig. 4-5b, the sample was broken in tension after being scribed across the

sample on the bare silicon side. Fig. 4-5c shows the results of cleaving the sample in tension after scoring a small "tick" mark near the edge on the polymer side of the wafer.

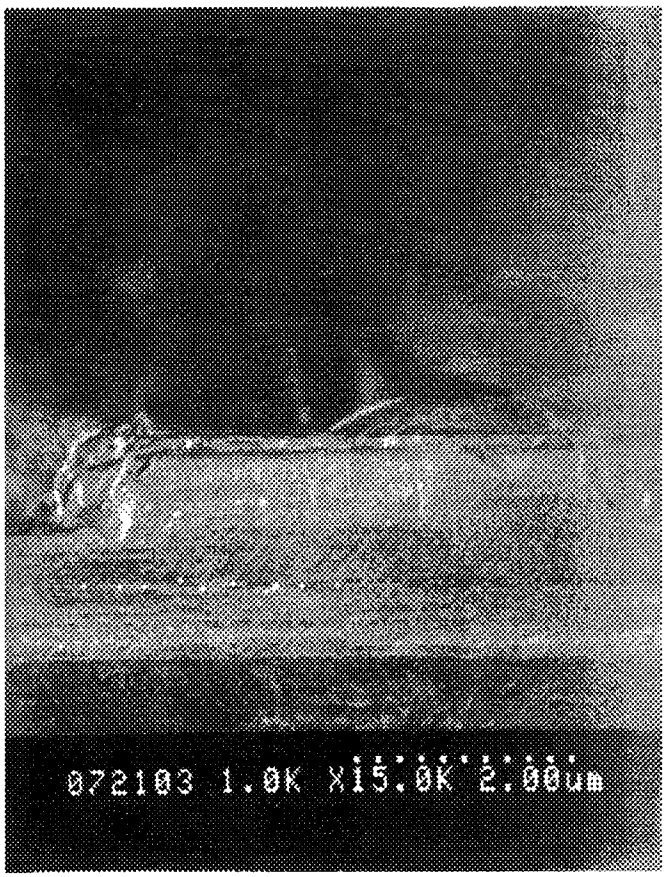

(a)

Fig. 4-5. Resulting sample interfaces for different cleaving techniques. In (a), the sample was cleaved in compression after being fully scored on bare silicon surface. A sample cleaved in tension after being fully scored on the bare silicon surface is shown in (b). In (c), a sample cleaved in tension after being scored with a small "tick" mark on the polymer side of the wafer, near the edge, is shown. The interface quality in (a) and (b) are approximately the same while the interface in (c) shows much more film damage and interface roughness.

The goal of the cleaving process is to produce a smooth, clean, perpendicular edge so that light my be efficiently coupled into the waveguide. The most successful technique

seemed to be cleaving in compression after scoring the back surface of the wafer. Breaking the wafer with the polymer film in tension after fully scoring the bare silicon side of the wafer also produced acceptable results. Observation of samples cleaved with these two techniques did not show marked differences in cleave quality. Both resulted in relatively smooth interfaces for the coupling of light. Cleaving the wafer in tension after scribing only a small "tick" mark near the edge of the wafer resulted in a large degree of film damage and interface roughness (see Fig. 4-5c). This type of interface damage was typical across the sample cleaved in tension by use of the "tick" mark method. The differences in the cleave quality can be seen clearly by comparing Figs. 4-5a and 4-5b with Fig. 4-5c.

(4-5b)

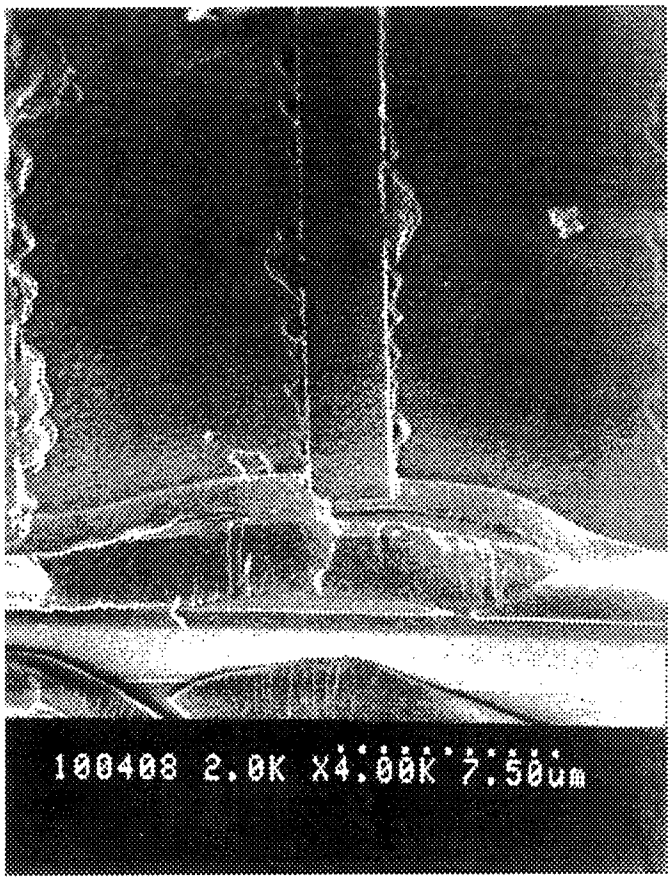

(4-5c)

The physical size of the different layers and features of the strip-loaded waveguide structure were measured from SEM photographs. A typical picture used for making these measurements is shown in Fig. 4-6 and nominal dimensions for the guide features are shown in Table 4-2. No wide-spread delamination of the polyphenylene film was observed during SEM inspection of the samples. The small areas of film damage that were observed seemed to be caused by the cleaving and handling processes, not water vapor or processing chemicals as has been observed in polythiophene (18).

The uniformity of the guiding layer thickness across the wafer was determined by measuring the thickness of this layer on two different samples, one taken from near the center of the wafer and the other taken ≈ 1.3 cm radially away from the center. The variation of the film thickness was observed to be approximately 0.07 μm between the two samples, with the film thickness decreasing away from the center of the wafer. Because the roughness of the side walls precluded accurate measurement of the separation between guides and guide width, the nominal design values were taken for these dimensions.

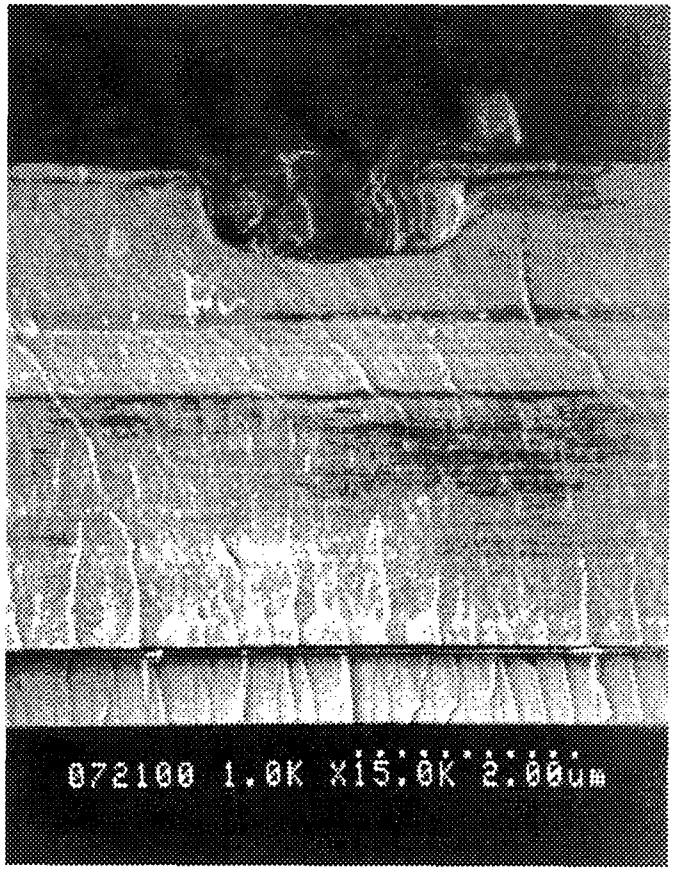

Fig. 4-6. Typical SEM photograph used in the measurement of film thicknesses and waveguide features.

Table 4-2. Nominal dimensions of the strip-loaded waveguide layers and features.

Parameter	Nominal Value (μm)
t_g	0.67
d	0.6
D	1.2
t_s	2.2

Rib Waveguides

The attempted fabrication of rib waveguides was not successful due to insufficient polymer film growth. The wafer used for this process was taken from a stock of polymer coated wafers kept by the growers, WL/MLPJ. The wafer was coated with polythiophene and had a film thickness of ≈ 0.2 μm. This wafer was processed in much the same way as the wafer used in the fabrication of strip-loaded guides. The two major exceptions were that the wafer was 2" in diameter - thus better suited for use with the 2" photolithographic mask - and the processing was done with positive photoresist. The use of positive photoresist resulted in nominal guide widths of $W = 1$, 2, and 3 μm and separation distances of $s = 3$, 5 and 10 μm. The major steps in the processing of this wafer are shown in Fig. 4-7.

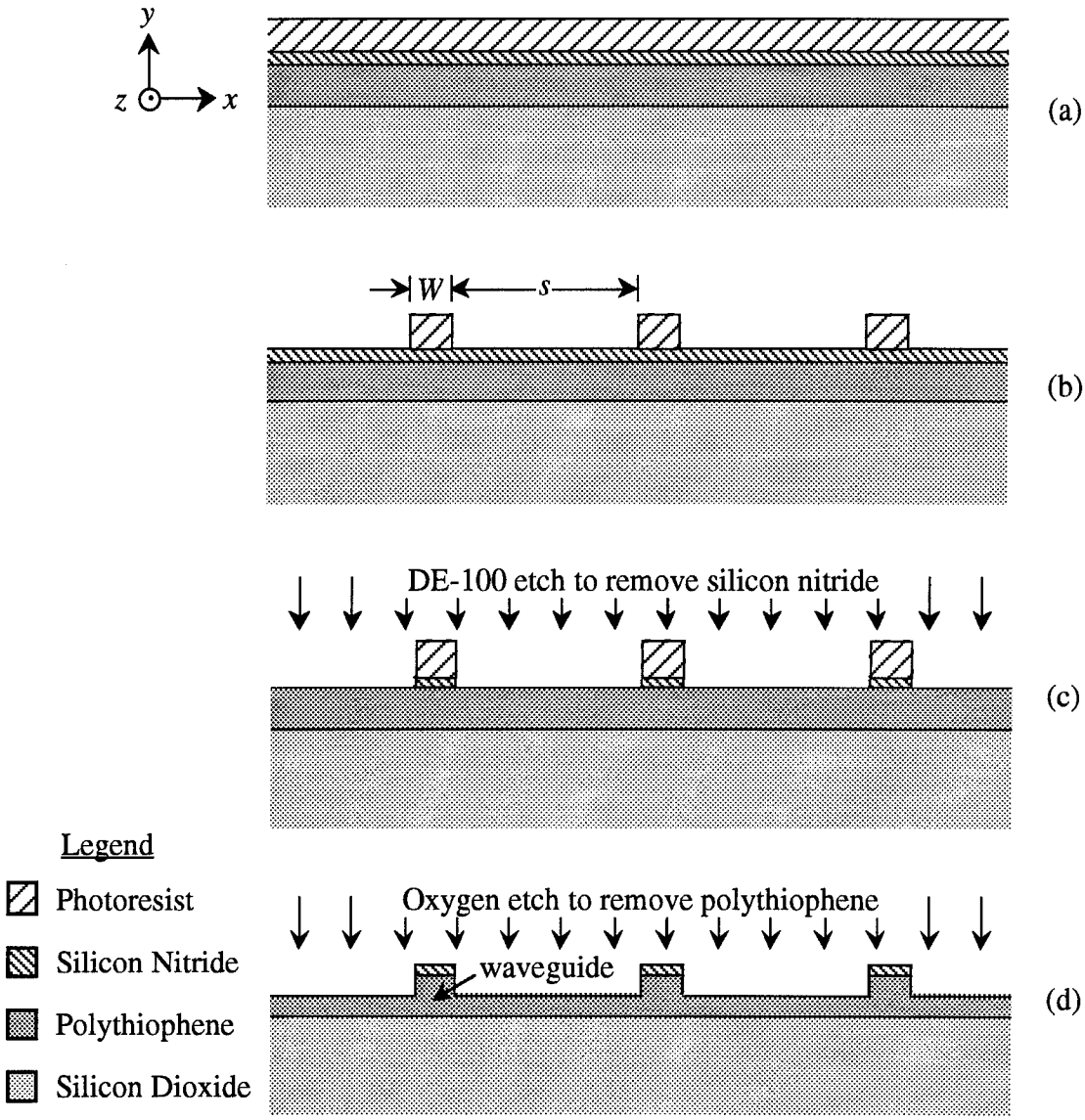

Fig. 4-7. Major steps in the fabrication of the rib waveguide structures. In (a), the silicon substrate is shown coated with polythiophene, silicon nitride, and photoresist. The positive photoresist is exposed and developed (b) and the wafer is etched to remove the nitride layer where exposed (c). An oxygen etch is then carried out (d) to partially remove the polythiophene layer.

Post-processing inspection of the wafer surface using the SEM showed that the film thickness was too thin to fabricate practical waveguides. In addition, delamination of the

polythiophene film was observed in several locations on the wafer. Typical features of the post-processing structures are shown in Fig. 4-8.

(a)

Fig. 4-8. Structures resulting from rib waveguide fabrication attempt. This is a top view of the rib waveguide structures. The W = 2 μm waveguide group is shown in (a). A close-up of the rib waveguide structure and film delamination is shown in (b). Note how much smoother and uniform the sidewalls of the structure are as compared with Fig. 4-3.

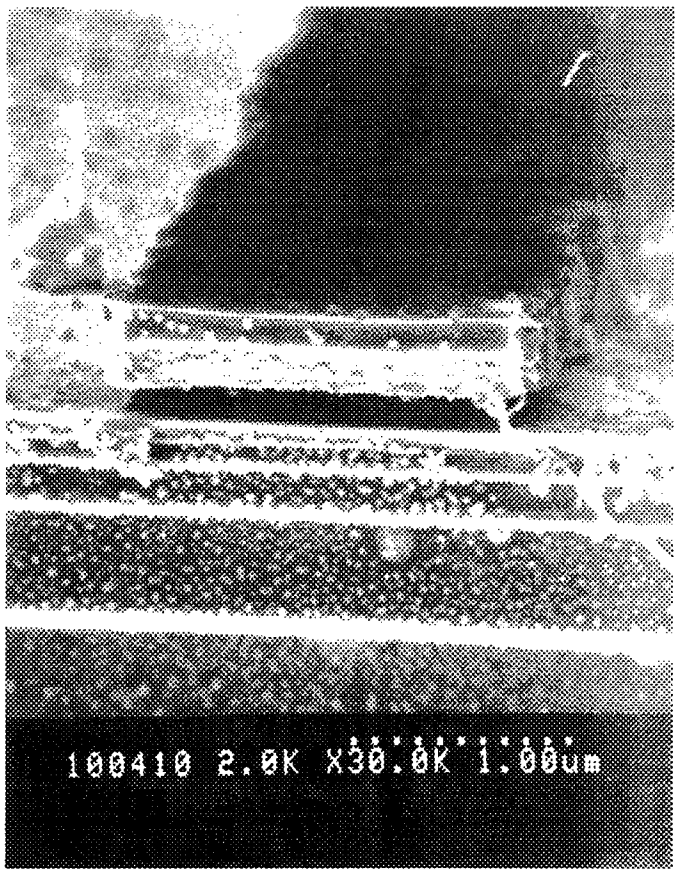

(4-8b)

Fig. 4-8 shows that contact between the mask and wafer during the lithographic process results in waveguide side walls that are much smoother than those obtained during the fabrication of the strip-loaded waveguides (see Fig. 4-3, note the difference in scale between Figs. 4-8 and 4-3). This demonstrates that the RIE process is capable of producing smooth, uniform micron-scale waveguide structures in organic polymer materials. The nature of the small "droplets" or spots on the film is unknown. They could be foreign object contamination or perhaps spalling of the material due to processing steps.

Channel Waveguides

Channel waveguides, similar to the one shown in Fig. 3-2, were fabricated using silicon dioxide as the substrate and polyphenylene for the guide material. Channels were etched into an oxidized 2" wafer using an RIE process. Polyphenylene was then grown over the wafer, filling in the channels and forming waveguides. The major steps in the fabrication of the channel waveguides are shown in Fig. 4-9. Note that the polyphenylene was also deposited on the barriers, making the resulting surface non-planar.

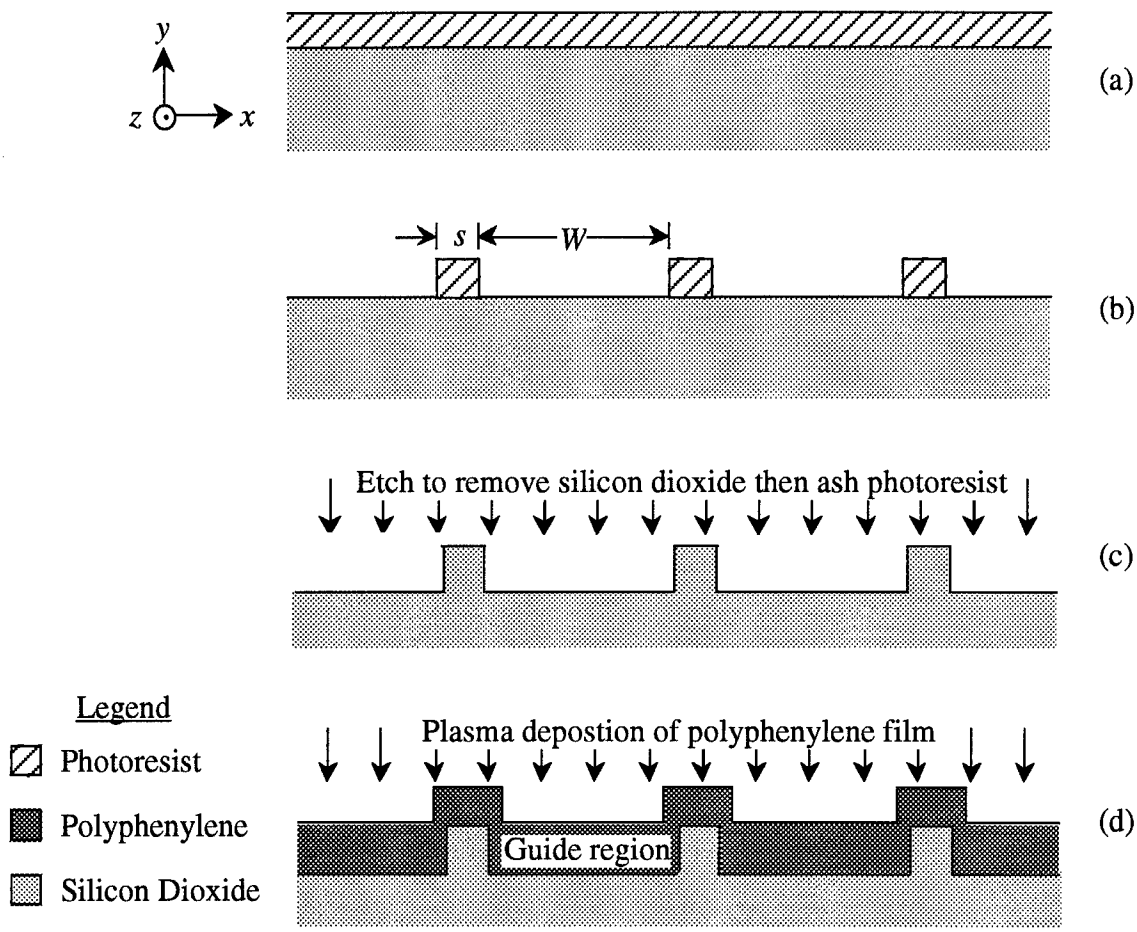

Fig. 4-9. The major steps in the fabrication of channel waveguides. In (a), the oxidized wafer is shown coated with photoresist. The positive photoresist was exposed using the lithographic mask and then developed (b). Channels were etched into the silicon dioxide (c) and then polyphenylene was deposited to form waveguides (d). The waveguides are the regions between the silicon dioxide sidewalls.

The wafer was processed using positive photoresist, resulting in etched channels with $W = 3$, 5 and 10 μm and separating sidewalls of silicon dioxide with $s = 1$, 2 or 3 μm wide. Some undercutting during the etching of the silicon dioxide changed these dimensions, generally decreasing the separation between waveguides and increasing the widths of the guides. The photoresist remaining on the wafer after the etching of the silicon dioxide was removed in a plasma photoresist-ashing chamber. The wafer was then cleaned by immersing it in a 3:2 H_2SO_4:H_2O_2 solution for 25, rinsing it in DI water for 25, blowing it dry with nitrogen, and then throughly drying it in a 165 °C convection oven before film growth began.

Polyphenylene was grown on the wafer surface with a plasma deposition process, resulting in structures as shown in Fig. 4-10. The growth conditions for this film were the same as the polyphenylene grown for the strip-loaded waveguides (shown in Table 4-1). Post-growth inspection of this film indicated a deposition rate of 0.02 μm/hr and that a total of 1.8 μm of film was deposited.

The relative roughness of the deposited film and the poor cleave interface can been seen in Fig. 4-11. The sample was cleaved in tension by scoring fully across the bare silicon (see Fig. 4-4b). The roughness of the silicon dioxide can be attributed to the RIE process. The polyphenylene film deposited during the fabrication of the channel waveguides appears to be physically different from the film grown for the strip-loaded waveguides. The film growth for the strip-loaded guides resulted in what appears to be a dense, smooth, uniform polyphenylene layer. As can be clearly seen in Fig. 4-11, the polymer film in the channel waveguides appears to be much less uniform and smooth. This could be due to the roughness of the silicon dioxide substrate layer in the channel guides; the first layer of polymer follows the contours of the rough silicon dioxide and that roughness is propagated out as the film grows. Another possible cause is contamination, or changes in composition due to time, of the benzene used as the monomer gas. The

history of the distilled benzene used for film growth in these two cases is unknown; perhaps the benzene used for growth of the channel waveguides film was not freshly distilled or contaminated.

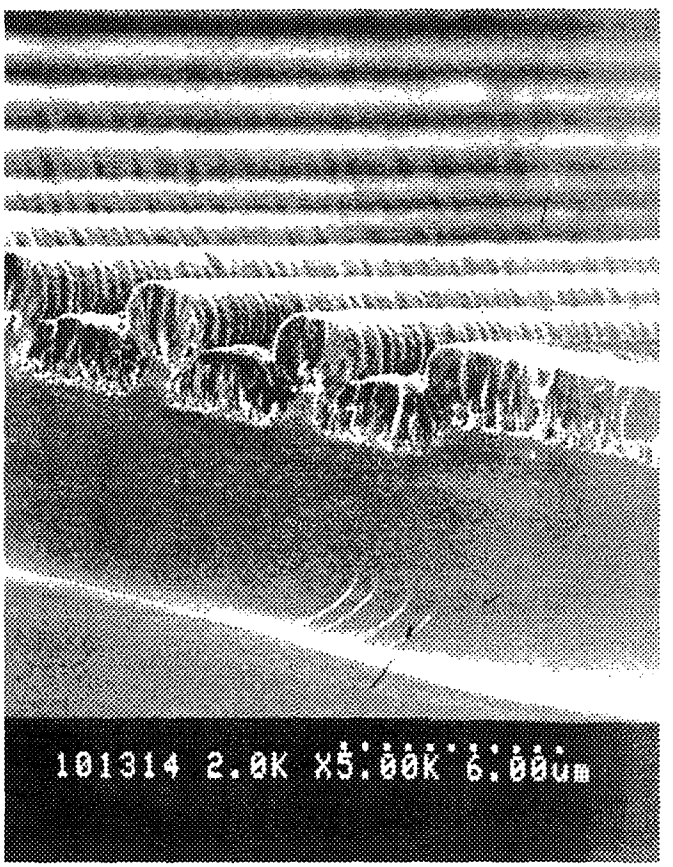

Fig. 4-10. Channel waveguides fabricated by etching silicon dioxide and deposition of polyphenylene. The waveguides are the flat portions between the raised ridges of polymer. The ridges are an artifact of the polymer deposition process.

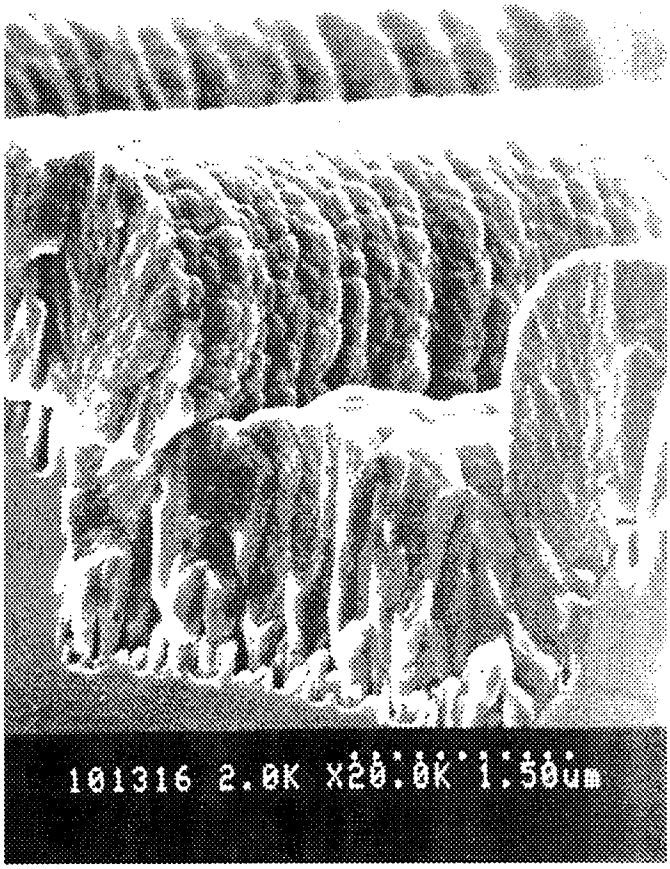

Fig. 4-11. Close-up of the polyphenylene channel waveguides. Note the relative roughness of the top of the waveguide region and the poor cleave interface.

V. Experimental Apparatus

This chapter contains the details concerning the experimental apparatus used to optically characterize the waveguides fabricated during this research. Brief overviews of the techniques used for coupling light into a waveguide and aligning the system are given. Some criteria for component selection are discussed.

End-Fire Coupling Method

The end-fire coupling method was chosen as the technique for launching light into a waveguide because of its flexibility, relative simplicity, and because it is well suited for injecting light into an individual waveguide (11:90-92). The basic geometry of the end-fire coupling method can be seen in Fig. 5-1.

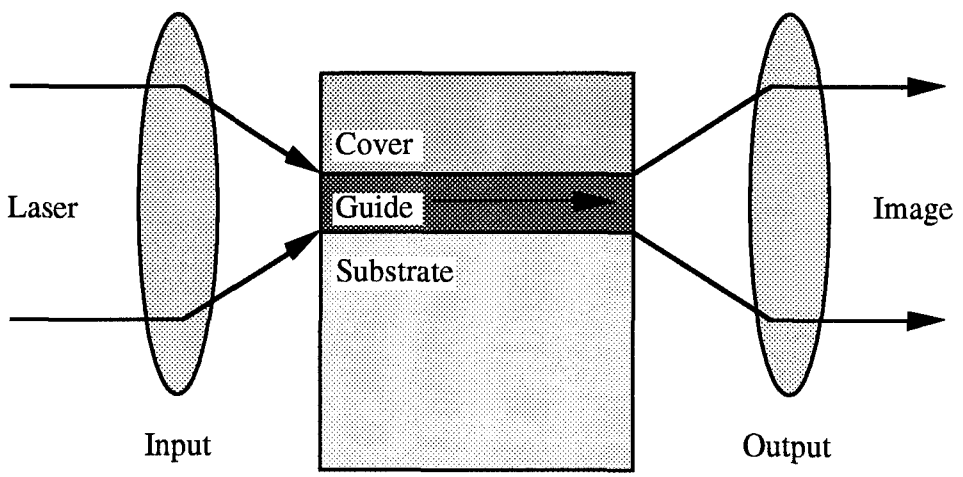

Fig. 5-1. The basic geometry of the end-fire coupling method. On the input side light source is focused down onto the guide layer. Light is coupled into the guide and exits the other side where it is gathered and imaged by the output lens (after 11:91).

For efficient coupling, the spatial profile of the input laser beam should match the shape of the waveguide mode that is to be excited. In addition, the spot size of the focused

beam should closely match the waveguide dimensions. Finally, the numerical aperture (NA) of the input lens and the waveguide should be matched, with the NA of the input lens (NA_i) equal to or less than the NA of the waveguide (NA_g). If $NA_i > NA_g$, some of the light entering the guide will strike the interfaces at less than the critical angle and be lost. If all the above conditions are met and the system is in perfect alignment, the input coupling efficiency could approach 100% (11:92). In practice, however, lower efficiencies are expected due to mismatches in beam profile, spot size, NA, and the difficulties of aligning a system with sub-micron tolerances. Calculations assuming a Gaussian input beam with a waist of 2 μm indicated that input coupling efficiency could be as high as 50% for the strip-loaded guides under investigation. After losses in the optical beam train and any sample misalignment are taken into account, 30% might be a more reasonable estimate for input coupling efficiency.

The spot size for a diffraction-limited input lens can be calculated from (25:131)

$$d_S = 1.22\frac{\lambda_O}{NA} \tag{5-1}$$

where d_S is the diameter of the spot and NA is the numerical aperture of the input lens. Approximately 84% of the beam power is contained within the area of this spot.

Overview of Experimental Apparatus

The equipment used to optically characterize the fabricated devices was assembled and aligned on an optical bench. Fig. 5-2 is a top-view diagram of that equipment. A wavelength tunable argon-pumped Ti:Sapphire laser (ATS), with an output wavelength ranging from ≈ 0.78 μm to ≈ 0.96 μm, was used as the excitation source. Optical characterization was typically performed at an output wavelength of 0.92 μm. In mode-locked configuration, the laser was capable of 2 ps wide pulses with a time between pulses of 13.3 ns. Peak powers in the GW range were obtainable in this mode. Neutral density

filters were used where appropriate to regulate the intensity of the beam (NDW, NDF). An optical isolator (OI) was used to prevent feedback into the laser from the optical setup, and a half-wave plate (POL) was used to reorientate the polarization of the beam to the x direction. An acousto-optic modulator (AOM) was used to divert some of the light to another experiment on the bench. The zero-order beam was used in this setup. Various irises (I) and an alignment plate (AP) were used to align the optics to the beam.

The sample under test (SUT) was mounted on a five-axis stage such that the laser beam excited the guide as shown in Fig. 5-1. The input microscope objective (MO) had a magnification power of 40x and a numerical aperture of $NA_i = 0.65$. Using eqn. (5-1) and an operating wavelength of $\lambda_o = 0.92$ μm, the spot size of this objective was ≈ 2 μm. The output objective was a 20x unit with an NA of $NA_o = 0.4$. The strip loaded guides had an NA of $NA_g = 0.53$. Thus, there were some injection losses incurred because $NA_i > NA_g$. An input objective with an NA larger than NA_g was chosen to decrease the input spot size. Note also that since $NA_g > NA_o$, not all of the light coming from the waveguides was gathered by the output objective. An output objective with a smaller NA was chosen to increase the field of view on the output side of the SUT.

The images of the SUT interfaces were observed with cameras sensitive to the near infrared spectrum and monitors. A personal computer was used to capture and digitize the output of the cameras. A red helium-neon laser (HNL) was aligned to the optical system and used for the initial alignment and imaging of the SUT.

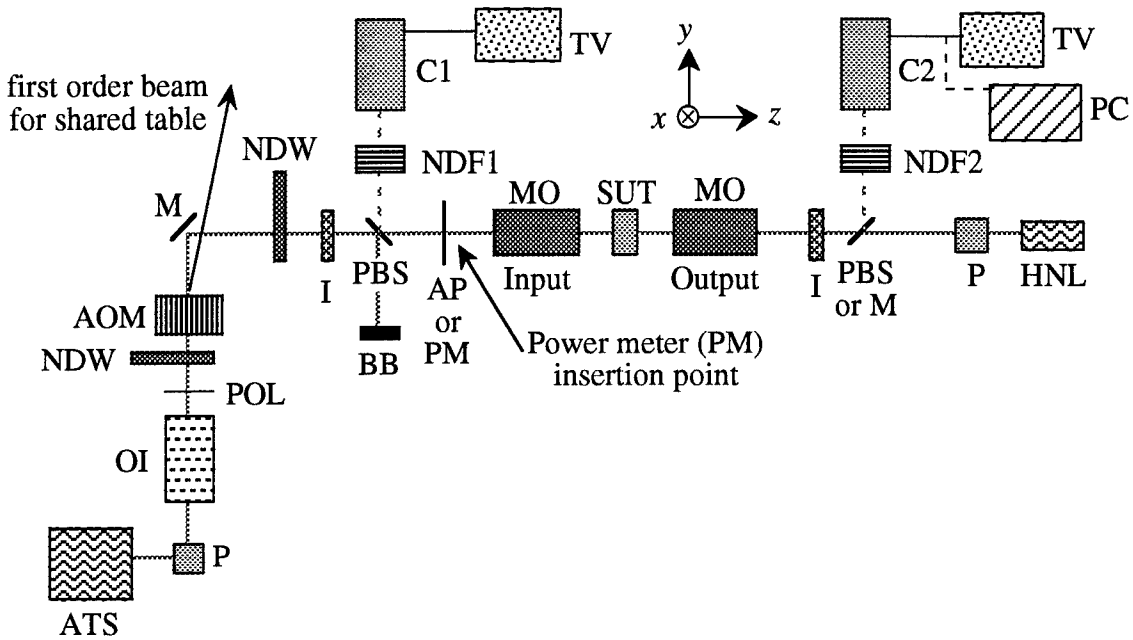

Fig. 5-2. Test setup for the optical characterization of NLDCs. ATS is an argon-pumped tunable Ti:Sapphire laser; P is a periscope arrangement of mirrors; OI is an optical isolator; POL is a half-wave plate used to rotate the polarization of the beam; NDW is a neutral density filter wheel; AOM is an acousto-optic modulator; M is a flat mirror; I is an iris used in the alignment process; PBS is a pellical beam splitter; AP is an alignment plate for aligning the optics to the beam; PM is the power meter head; MO is a microscope objective mounted on a five-axis stage; SUT is the device-under-test mounted on a five-axis stage; BB is a beam block; HNL is a helium-neon laser; NDF1 and NDF2 are sets of neutral density filters; C1 and C2 are cameras for imaging the input and output side of the SUT, respectively; TV is a monitor for observing a camera output; and PC is a personal computer used for frame-grabbing of the camera output.

Alignment of the Optical Components

The alignment of the system was complicated by the number of components and the sub-micron dimensions of the guiding layer. The input microscope objective was aligned with the retro-reflection technique using the AP and an iris in the SUT position. The AP consisted of a polished aluminum plate with several small holes. A hole in the AP was aligned with the center of the input beam and the retro-reflection of the input objective was observed on the AP. The input objective was aligned such that the retro-reflections of both

the front and rear surfaces of the objective coincided with the hole in the AP. The iris in the SUT position was used to check this alignment by changing the z position of the objective and observing the spot on the iris. The output objective was aligned to the beam and the input objective using an iris.

With the pellical beam splitter (PBS) in place on the output side, the HNL was aligned such that its beam retraced the ATS beam. The HNL beam was used to initially image the output side of the sample during installation of the SUT. After this initial alignment, the PBS could be replaced with a mirror (M) to increase the amount of the light reaching the output camera.

VI. Experimental Procedure

This chapter details the procedures used to characterize a sample under test (SUT). The preparation of samples for testing and the alignment of the sample to the input beam are discussed. Capture of images and simple analysis of those images using a personal computer is explained. Only the strip-loaded waveguides were optically characterized due to the poor fabrication results of the other waveguide designs.

Sample Preparation and Alignment

Samples for optical characterization were cleaved from the wafer using the compression technique illustrated in Fig. 4-4. The length of the samples, the z dimension, ranged from 2 to 5 mm. Sample preparation met with varying levels of success. Finding a sample with good interface cleave quality and waveguides unspoiled by handling damage or fabrication flaws along the length of the guides was, at times, a tedious process. Poor guide quality may have been due to a number of factors: excessive losses due to the roughness of the side walls (see Fig. 4-3); the fact that each group of guides was concentrated in an approximately 100 μm wide region and thus susceptible to "mass destruction" by handling damage; or the practice of placing the polymer side down during the cleaving process, thereby causing film and waveguide damage.

After cleaving, a sample was mounted onto a fixture with a small amount of rubber cement. The rubber cement was applied to the fixture surface and the bare silicon side of the sample was pressed into the cement, taking care not to break the wafer, contaminate the interface surfaces with cement, or scrape across a region of the wafer containing guides. The fixture was mounted to a five-axis stage for alignment of the SUT and input beam.

The SUT was placed into the beam train with the input beam blocked and the helium neon laser (HNL) on. All alignments were conducted with the input beam reduced in intensity by the neutral density filter wheels. In addition, neutral density filters were used

as appropriate to reduce the intensity of the images at the cameras. The output side of the SUT was imaged using the output objective and the HNL beam. This step insured that an image of the SUT output edge appeared in the plane of the output camera. The HNL could then be turned off. The input beam was focused on the input side of the wafer. The image from this side of the wafer was limited in extent because of the very small spot size of the input objective.

The SUT was then aligned about the x axis (Fig. 5-2) by tilting the sample until the film-coated edge of the wafer could be seen on both monitors and a "sunrise" pattern was seen on the output side of the wafer. The spot and rings in the "sunrise" pattern of Fig. 6-1 are not an image of the spot on the input side. These features result from the Fresnel diffraction of the input spot by the film edges. This pattern above a waveguide indicates that the beam and sample are aligned such that light will be injected into that waveguide. The sample could be examined by translation along the x axis until waveguide features or waveguiding through the film were observed. The SUT was aligned in the x-z plane about the y axis by maximizing the amount of light coupled through a waveguide. Typically the alignment process was iterative in nature, tilting the sample about both the x and y axis until the SUT was properly aligned.

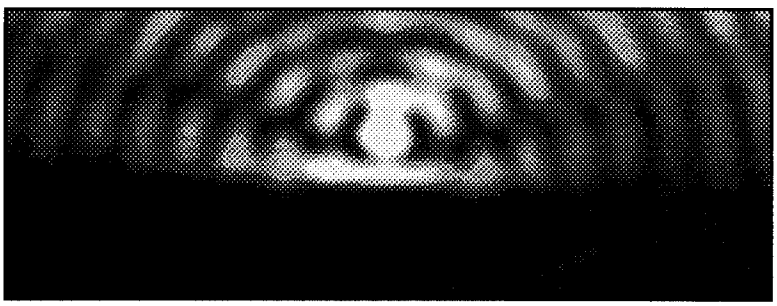

Fig. 6-1. The "sunrise" pattern seen on the output monitor from the diffraction of the input light. This pattern indicates that the SUT is aligned with the input beam and that light will be injected into the guide directly below the spot.

After the sample was aligned, the PBS on the output side could be replaced with a mirror to maximize the amount of light collected by the output camera. By using a mirror in this position, lower input beam powers could be used while still producing an observable image on the output side. With high input powers, the PBS could be put in place again, protecting the output camera from damage.

Input beam power was varied by using the two neutral density wheels. Data collection was conducted with the laser in the mode-locked configuration. This was done principally to protect the polymer film from excessive heating while in CW mode. The focusing power of the input lens made it possible to exceed the optical damage threshold of the polymer film with the laser running in the CW configuration. While the peak power of the mode-locked laser was much greater than the CW power, the sample was only exposed to the power during the "on" portion of the pulse (approximately 2 ps) and was not illuminated for the subsequent 13.3 ns.

Images from the cameras were captured using frame-grabbing software on a personal computer. The intensity profile of a line drawn across the image could also be obtained using this software.

VII. Experimental Results and Analysis

In this chapter, the results of the waveguide optical characterization experiments are presented. Only the strip-loaded waveguides were optically characterized. Guiding of the input beam was observed through the polyphenylene film in an area of the wafer that did not contain waveguide structures. Guiding through waveguides and coupling of optical energy from one waveguide to another was also observed in the sample under test (SUT).

In all experimental observations, the laser was mode-locked at $\lambda_O = 0.9$ μm, with the pulse width ≈ 2 ps, and the electric field of the light polarized in the x direction. The SUT had a length in the z direction of $L = 3$ mm. Because of problems in obtaining a consistent cleave quality, only this length of sample was successfully characterized. Based on modeling and estimations of the losses in the optical beam train, the input coupling efficiency was estimated to be 30%. The actual input efficiency is highly dependent on the interface cleave quality and is thus difficult to quantify.

In all pictures of the output side of the sample the contrast has been altered slightly to enhance the reproduction quality of the figure. All intensity measurements were made prior to the contrast adjustments. Intensity profile plots in the x direction have been smoothed with a three-point moving average. The profile plots are from a single line scan of one video frame. Because of the difficulties in analyzing the general case of a multi-channel directional coupler composed of non-identical waveguides, the results presented in this chapter are qualitative in nature.

Guiding of Light Through a Polyphenylene Slab Waveguide

The guiding of light through polyphenylene was observed in a slab waveguide structure (see Fig. 7-1). The slab waveguide was actually a region of the strip-loaded waveguide wafer that was not near any etched waveguide features. The length of the sample was $L = 3$ mm. The light was confined in the y direction by the cover and substrate

and allowed to diverge in the x direction. Assuming an input beam with a Gaussian profile, a waist of 2 μm, and $\lambda_o = 0.9$ μm, the beam would diverge to a waist of 0.48 mm in 3 mm of travel through the polyphenylene guide layer (33:67). Thus, the guided input beam would spread to fill the field of view in the x direction and appear as a line on the output side (see Fig. 7-1). The changes in observed intensity along the x direction are probably due to variation in the output edge cleave quality for that direction. These intensity variations could also be due to defects in the polymer films or foreign object contamination of the output side edge. Note that since the spot size of the output objective was ≈ 3 μm, the guide layer ($t_g \approx 0.67$ μm) of the SUT was not actually imaged. The image on the output side of the experimental apparatus is a convolution of the spot size of the output objective and the profile of the light coming from the guiding layer. A measured intensity profile in the x direction of the guided light is shown in Fig. 7-2a. The guide is single-mode in the y direction.

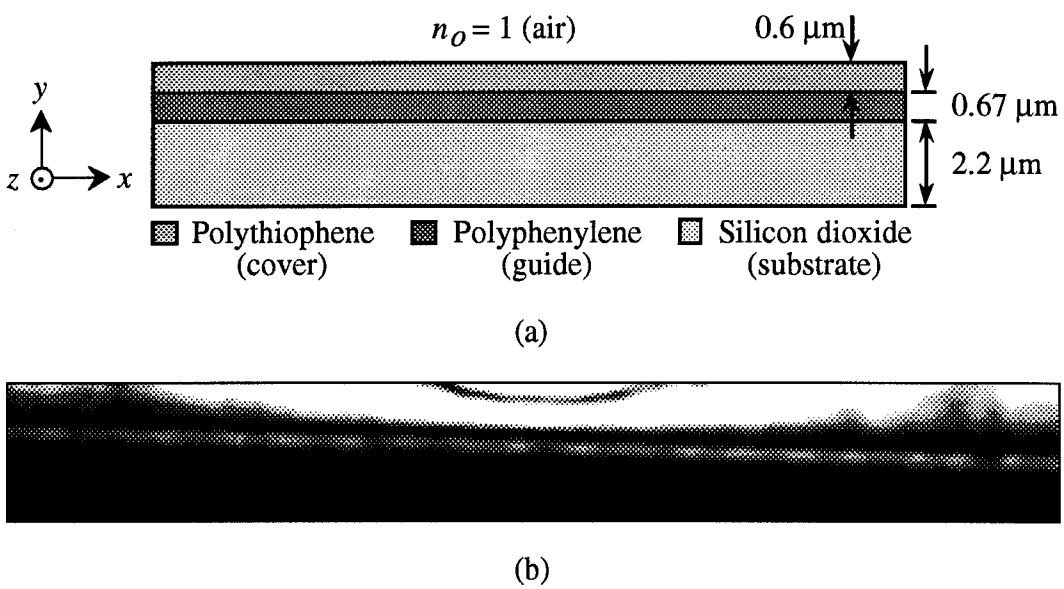

Fig. 7-1. Guiding of light through the polyphenylene film. In (a), a diagram of the slab waveguide structure is shown. In (b), the light band near the center of the picture is light ($\lambda_o = 0.9$ μm) being guided through 3 mm of polyphenylene film.

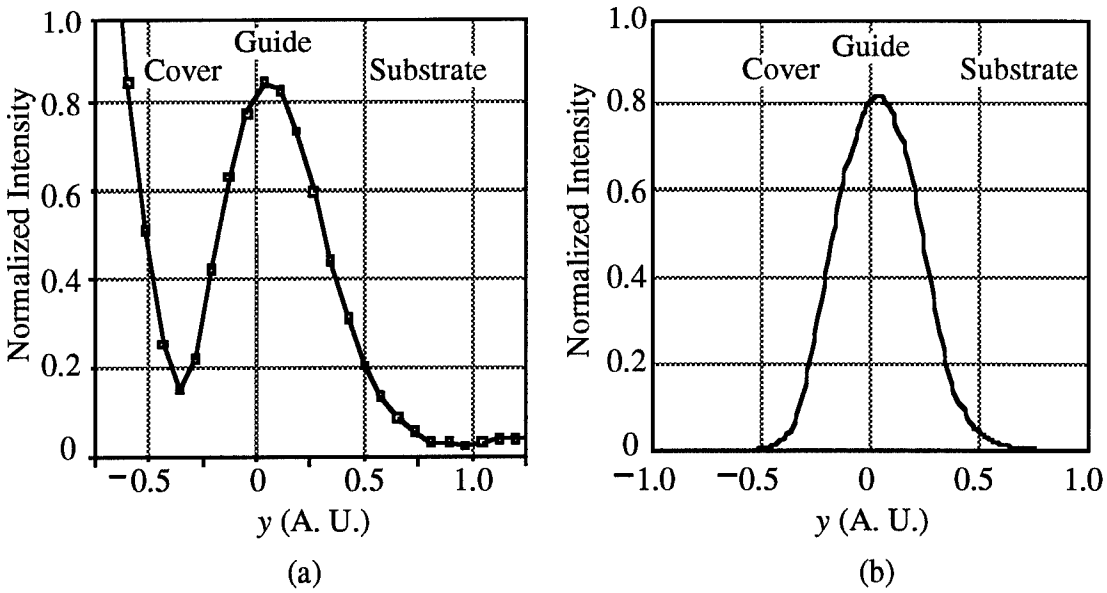

Fig. 7-2. Measured (a) and modeled (b) intensity profiles for a polyphenylene slab waveguide. The large intensity spike in (a) near $y = -0.5$ is due to the light above the cover (see Fig. 7-1b). In both profiles the left hand part of the profile corresponds to the cover region while the right hand part corresponds to the substrate layer. In (b) the $y = 0$ point corresponds to the center of the modeled guide while in (a) the $y = 0$ point is arbitrarily placed.

In agreement with modeling, the mode profile in the y direction is single-mode and asymmetric. The intensity decays more rapidly on the cover side of the guide than on the substrate side. If the cover layer were thick enough to be considered semi-infinite in the y direction, the opposite would be true since the index difference at the cover/guide interface is much smaller than the index difference at the substrate/guide interface (see Figs. 7-1a, 3-7a). However, in the slab waveguide region of the sample, the cover layer is only 0.6 μm thick - thin enough that the electric field profile is influenced by the cover/air interface. The large difference in index between the cover and the surrounding air causes the field to decay rapidly on the cover side of the guide. This geometry was modeled by using the effective index of the guide in a slab waveguide model with air as the cover layer (Fig 7-2b). Note that the shapes of the mode profiles appear to be in good agreement.

Coupling in a Multi-channel Directional Coupler

In a multi-channel directional coupler, such as the groups of strip-loaded guides fabricated as part of this research, the light traveling in a waveguide is coupled to adjacent guides on both sides. Thus, a branching or cascading of the light through the guides is to be expected as the light travels in the z direction (see Fig. 7-3).

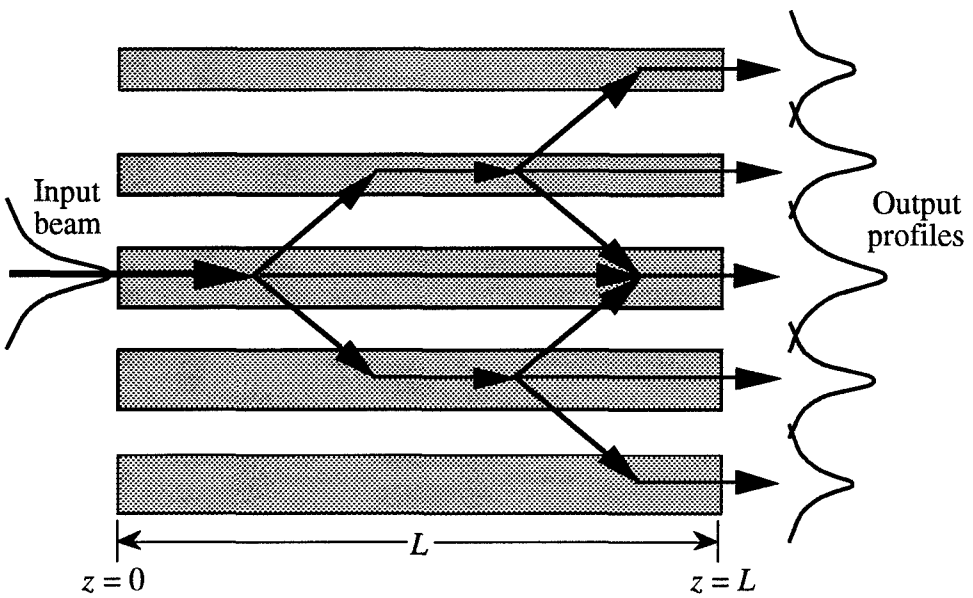

Fig. 7-3. Flow of injected power in a multi-channel directional coupler. The individual guides are not identical but are coupled to both adjacent guides. The input power, initially launched into a single guide, branches out to the other guides in a cascade manner.

Somekh (26) has analyzed a multichannel directional coupler for the special case of an infinite number of parallel, identical guides, each weakly-coupled to only the adjacent guides (26:46-52). Solving the coupled-mode equation for this special case, assuming that light is injected into only one guide at $z = 0$, gives the power flow in the νth guide as (26:48)

$$P_\nu(z) = J_\nu^2(2\kappa z)\exp[-\alpha z] \tag{7-1}$$

where $P_\nu(z)$ is the power flow in the νth guide ($\nu = 0$ is the guide the light is initially launched into), J_ν is the Bessel function of the νth order ($\nu = 0, 1, 2 \ldots$), κ is the coupling coefficient between adjacent guides, z is the direction of propagation, and α is the loss coefficient for the guides.

Thus, given the relative output intensities of the guides for a given distance $z = L$, the coupling coefficient, κ, can be determined. Unfortunately, the guides fabricated in this research did not lend themselves to this analysis. The analysis assumes an infinite number of identical guides but there are only five guides of a given size within a group. Furthermore, the guides are *not* identical, both by design and because of the rough sidewalls of the guides, and thus the coupling coefficient between the guides is not a constant. Because of the rough sidewalls and differing guide dimensions, there is a "built-in" phase mismatch between adjacent guides that varies in an essentially random manner along the direction of propagation. The nature of the waveguides fabricated during this research limits the analysis to qualitative observations.

Lateral Confinement of Light and Coupling Between Guides

The confinement of light in the lateral (x) direction, indicating the guiding of light through the fabricated waveguides, was observed in the strip-loaded waveguides. Coupling of light into the $s = 2$ μm group of guides on a $L = 3$ mm sample was successful. Furthermore, coupling between adjacent guides was observed.

As shown in Fig. 7-4, the guides of the fabricated multi-channel directional couplers are numbered starting with the leftmost guide. Guides G1 - G5 have $W = 10$ μm, G6 - G10 have $W = 5$ μm, and G11 - G15 are the $W = 3$ μm guides.

In Fig. 7-4, light was injected into guide 3 (G3, $W = 10$ μm) on the input side of the sample. Recall that the spot size of the input objective was 2 μm, much smaller than the lateral dimension of the $W = 10$ μm guides. The light is coupled into the adjacent $W = 10$ μm guides and, to a much lesser extent, into the $W = 5$ μm guides. In Fig. 7-4, the

average power at the power meter location (Fig. 5-2) was 0.1 W, indicating a peak power of 665 W at this point in the optics train. Using 30% as the estimated input coupling efficiency, the peak injected power is ≈ 200 W.

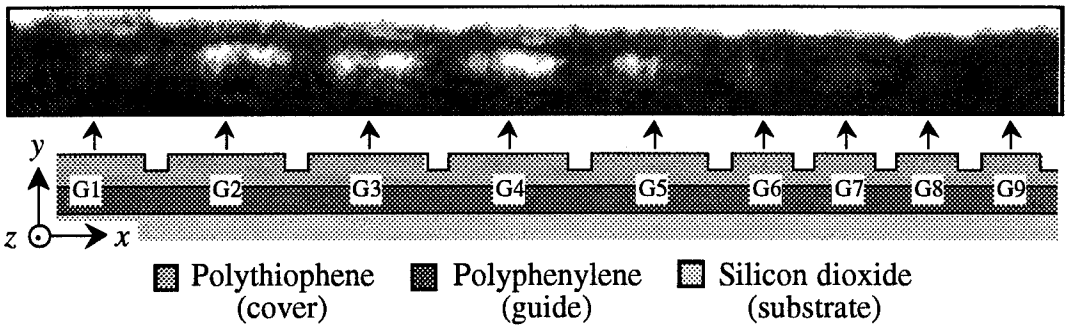

(a)

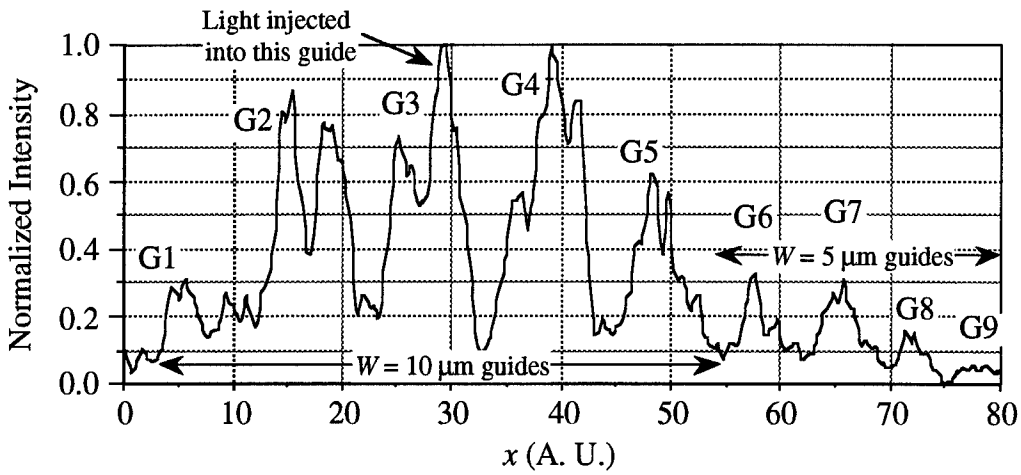

(b)

Fig. 7-4. Observed confinement of light in the lateral direction and coupling between adjacent strip-loaded guides. The nominal separation between guides is $s = 2$ μm. The experimentally observed output side of the sample is shown in (a). A diagram of the guide structure, with arrows pointing to the corresponding guides, is shown for reference. Light is injected into guide 3 (G3) on the input side of the sample. As shown in (b), coupling occurs to the other guides.

It should be noted that while the profiles presented in this chapter represent only one line scan in the x direction, the features of a given profile persisted from frame to frame and did not fluctuate. The intensity peaks and dips of the profiles are not "noise" but rather are indicative of the spatial distribution of the light within the waveguides. Some of these features, mainly the smaller ones, may be due to scattering off of defects in the film or interface cleave. The larger features, such as those seen in G2 and G3 of Fig. 7-4, are most likely evidence of the modes propagating in the waveguides.

In Fig. 7-4, the $W = 10$ μm guides seem to be capable of supporting the first odd mode in the lateral direction, as predicted by modeling in Chapter III. The fundamental mode is excited in the guide by the focused input beam; conversion to the first odd mode occurs from scattering in the guide due to material defects or the roughness of the defining sidewalls. Modeling of the electric field profiles in the guide region indicate that the field near the rough side walls is small. The main influence of the rough side walls is to effectively change the width of the guide along the direction of propagation. These changes in guide width change the mode profiles along the length of the guide, leading to a loss of energy as the light propagates down the guide. The effect is similar to sending an RF signal through a length of connected coaxial cables, each cable having a slightly different characteristic impedance. Reflections due to impedance mismatch result in losses to the RF signal as it propagates along the coaxial cables.

Confinement of the light in the lateral direction and coupling between guides was also observed in the SUT by injecting light directly into the $W = 5$ μm guides of the $s = 2$ μm group. In Fig. 7-5, the average power measured at the power meter insertion point was 50 mW, indicating a peak power of 335 W at this point in the optics train and a peak injected power of $\approx$ 100 W.

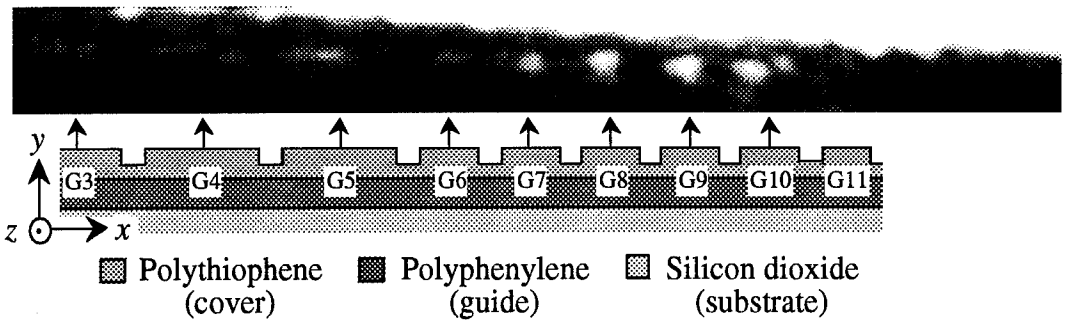

(7-5a)

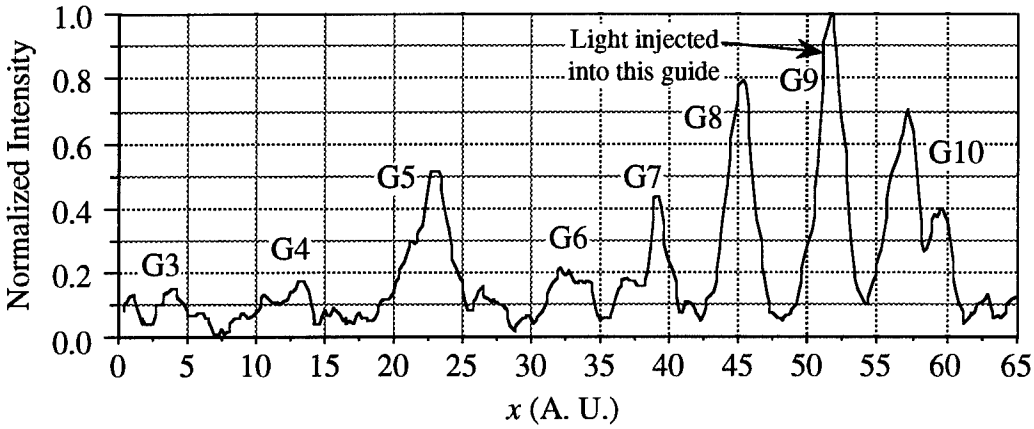

(b)

Fig. 7-5. Observed guiding and coupling of light injected into a $W = 5$ μm strip-loaded waveguide. The nominal separation between guides is $s = 2$ μm. The view is of the output side of the sample. The experimentally observed output side of the sample is shown in (a). A diagram of the guide structure, with arrows pointing to the corresponding guides, is shown for reference. As seen in (b), light injected into G9 on the input side of the sample couples into the adjacent guides in a cascade or branching manner.

No light was observed out of the $W = 3$ μm waveguides. This is probably due to the rough sidewalls of the guides. Because the nominal width of these guides is smaller, the roughness of the sidewalls would have a more drastic effect on the effective width of the guide, resulting in greater losses. Any light coupled into a $W = 3$ μm guide is probably lost before reaching the output.

In agreement with modeling, the $W = 5$ μm guides G8 and G9 appear to be single-mode in the x direction. The first odd mode appears to be excited in G10 and G7. Flaws

along the length of the guides could change the effective width of the guides and allow the first odd mode to propagate for some distance along G10 and G7. These intensity profiles could also be due to contamination of the output coupler edge at these guide locations.

The relatively large amount of coupling from G6, a $W = 5$ μm guide, into G5, a $W = 10$ μm, is to be expected. Modeling indicates that the first odd mode is poorly confined in the $W = 10$ μm guides. Thus the first odd mode in G5 would be well coupled to the fundamental mode of G6. In Fig. 7-5a the light is injected into G9 rather than G8, the center guide of the $W = 5$ μm group, in an attempt to better isolate the $W = 5$ μm guides from the $W = 10$ μm guides.

Another example of coupling between the waveguides is shown in Fig. 7-6. Here, light is injected on the input side into G8. The average power measured at the power meter insertion point was 50 mW, implying a peak injected power of ≈ 100 W. The intensity profiles of guides G6 - G9 in Fig. 7-6 look similar to the corresponding profiles in Fig. 7-5. In both figures the guide into which light was initially launched has the highest relative intensity on the output side of the sample. This is probably due to the built-in phase mismatch between the guides, which decreases the coupling between guides. It is also possible, given the asymmetric and non-identical nature of the waveguides, that a majority of the power has returned to G8 at this particular sample length. The problems associated with waveguide fabrication and cleaving make a complete analysis of this data difficult.

Note that in both G4 and G5 of Fig. 7-6a, the intensity profile is not centered on the waveguide, but rather is shifted spatially to one side. This is probably the result of both the fundamental and first odd modes propagating in the waveguide. If more than one mode is propagating in a waveguide, the electric field in the guide will be the sum of the electric fields of the modes. Within the guide there were will be regions where the electric fields add in such a way as to cancel each other. Likewise, there will be regions where the electric fields of the modes add and reinforce each other. Thus, it is possible that the

fundamental and first odd mode are propagating in G4 and G5, resulting in an overall intensity pattern as shown. Note that both of these guides seem to have good output cleaves, as evidenced in Fig. 7-5. This suggests that the intensity patterns of G4 and G5 in Fig. 7-6a are not due to interface contamination or poor quality of the output cleave.

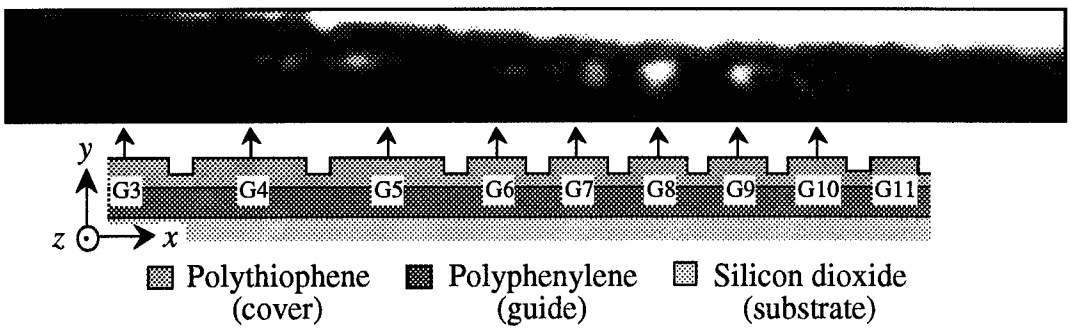

(a)

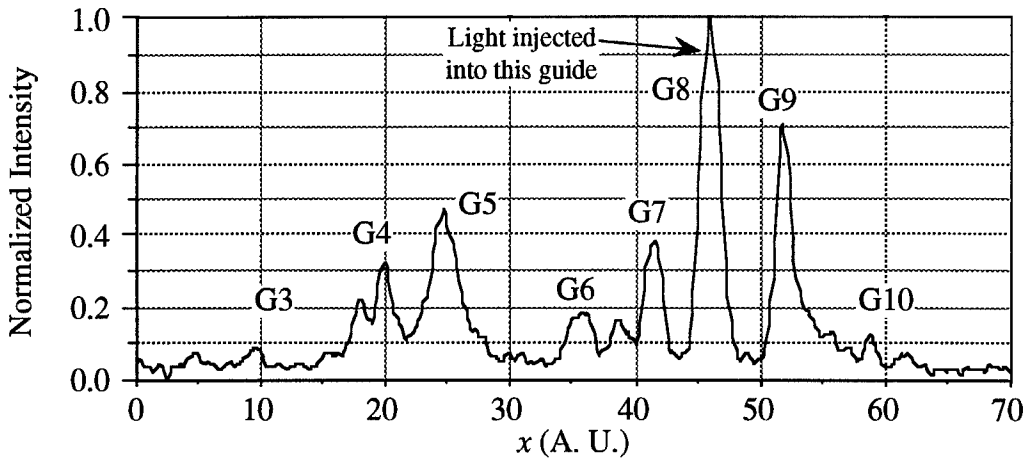

(b)

Fig. 7-6. Coupling of light between adjacent strip-loaded waveguides. The nominal separation between guides is $s = 2$ μm. The experimentally observed output side of the sample is shown in (a), along with a diagram of the guide structure. As seen in (b), light injected into G8 on the input side of the sample couples into the adjacent guides.

Nonlinear Effects

As the power injected into a multi-channel NLDC is increased from a low level to a level large enough to induce nonlinear effects, some variation of the coupling coefficient, κ, and thus the output intensities would be expected. To investigate the nonlinear characteristics of the fabricated structures, the peak power injected into the SUT was varied and the output monitored. Using 30% as the input coupling efficiency, the estimated injected power varied from $\approx$ 41 W to $\approx$ 319 W.

The critical power calculated from eqn. (3-8) does not accurately characterize the nonlinear response of the fabricated multi-channel NLDC because it was developed by assuming a pair of identical, isolated nonlinear waveguides that had an interaction length of L_O. The phase-mismatch of the guides makes the modeling much more difficult (13:1581). At best, the critical powers for the strip-loaded guides found in Table 3-1 can be regarded as only an order of magnitude estimate of the power needed to induce nonlinear effects in the fabricated structure. For reference, the critical power for a pair of identical, isolated strip-loaded guides with $W = 5$ μm and $s = 2$ μm was estimated to be 230 W.

In Fig. 7-7, the output profiles for two different injection powers is shown. It should be noted that the profiles represent only one scan of the output intensities and are thus essentially qualitative in nature. Note that the basic features of the two profiles in Fig. 7-7 are the same. This fact is further evidence that the profile features are representative of the spatial distribution of light within the guides and not "noise." In both profiles the power was initially launched into G9, just as in Fig. 7-5.

As can be seen in Fig. 7-7, there is some shift in the intensity profiles for the two different input powers. In the case of the high injection power, the highest peak intensity was observed out of G8, even though the power was initially launched into G9. This shift in peak output intensity from G9 to G8 could indicate that the coupling between G9 and the adjacent guides changed, as would be expected for an NLDC.

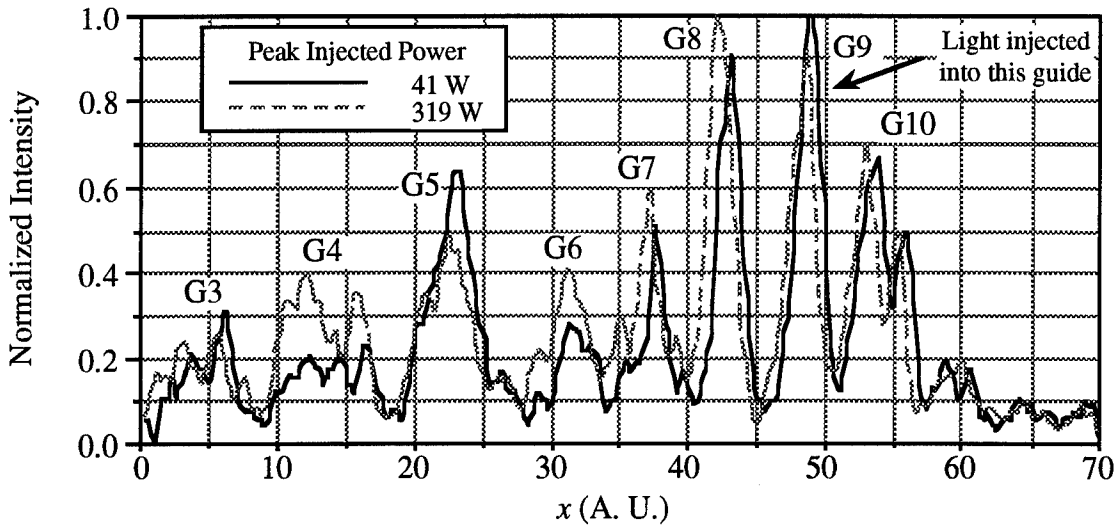

Fig. 7-7. Output intensities for "low" and "high" peak injected powers. In both profiles, all of the light was initially injected into G9. The shifts in the output intensities could be indicative of a nonlinear response but the results are not conclusive.

Arguably, there may be significant shifts in output intensity for G4, G5, and G6, possibly indicating a change in coupling due to higher injection power. However, without a more quantitative analysis, which is made difficult by the multi-channel, non-identical nature of the fabricated guides, no definitive conclusions can be reached concerning the nonlinear response of the SUT. The observation of nonlinear effects would be more straight-forward in devices consisting of a single pair of isolated, identical, single-mode waveguides since the influence of multiple, nonidentical adjacent guides would not be a factor in the analysis. A much more quantitative investigation of nonlinear effects on coupling would be possible with such devices.

Waveguide Losses

Measurements of the waveguide loss were not made due to the difficulty in obtaining consistent cleave quality as the sample length was decreased. The analysis of loss measurements would have been further complicated by the presence of multiple coupled

guides. Measurements could have been made on the channel waveguide structures since they were essentially uncoupled but these measurements would not have been applicable to the analysis of the strip-loaded waveguides. Also, the poor polymer quality observed in the channel waveguide fabrication (Fig. 4-11) indicated that the film may not have had good optical qualities. The scattering losses from this inhomogenous film would have probably dominated over the scattering from the substrate and air interfaces.

VIII. Summary and Recommendations

In summary, this thesis research has resulted in the successful design and fabrication of waveguiding structures in polyphenylene, a recently developed nonlinear organic polymer. Waveguiding, through both a slab waveguide and strip-loaded guides, was observed for the first time in this polymer. The coupling of optical energy from one guide to the adjacent guides in a multi-channel directional coupler was also observed. No definitive conclusions concerning nonlinear effects are possible due to the non-identical, multi-channel nature of the fabricated waveguides. Several design and modeling tools have been developed that should support additional research in this area.

The film growth results for the strip-loaded guides indicate that it is possible to grow both polyphenylene and polythiophene films that are dense, uniform, mechanically and hydroscopically stable, and suitable for fabrication into IOCs. However, the film deposited for the channel waveguides was not of the same quality. Reproducibility of film quality should be quantified with further study. Better attention to substrate roughness and the history of the distilled benzene or dichlorothiophene should help improve film quality.

Another difficulty encountered in the fabrication of waveguides involved the growth rate of the thin polymer films. Slow film deposition rates hinder the fabrication of waveguides. In-situ monitoring of film thickness would greatly enhance the ability to grow films to a specified thickness.

One way to avoid the CVD growth of another polymer as a cover layer (such as the use of polythiophene in the strip-loaded guides) would be to spin-on a layer of photoresist directly on top of the polyphenylene and use it as the cover layer. Most common photoresists have refractive indices of ≈ 1.6 and are essentially transparent to near infrared radiation, making them suitable materials for such an application. The photoresist could simply take the place of the polythiophene layer in Fig. 4-2, be passivated with silicon nitride, and etched with oxygen in a RIE chamber. Alternatively, the photoresist on top of

the polyphenylene could be exposed with a lithographic mask and be developed, leaving the polyphenylene exposed. The large step in index at the polyphenylene /air interface would, however, tend to increase the confinement of light in the lateral direction, decreasing the coupling between guides and the maximum allowable guide width for single-mode operation.

Another concern with using photoresist as a cover layer is its stability when exposed to UV. Unless the photoresist was passivated with silicon nitride or a similar material after waveguide fabrication, the photoresist unexposed during fabrication could become exposed (thus changing its optical and mechanical properties) during subsequent handling and testing. The potential benefit of using photoresist as the cover layer - avoiding the slow CVD growth of another polymer on top of the polyphenylene - justifies an attempt at this fabrication method. The use of a photoresist cover layer should be considered during further research.

The results of this thesis, the successful fabrication of guides and the observation of both guiding and coupling of light, justify further investigation of polyphenylene as a material for IOCs. Perhaps the most important next step in this research is the fabrication of a photolithographic mask more suitable for NLDC research. The mask should contain pairs of single-mode waveguides, coupled to each other but far enough away from other waveguides to be effectively isolated. NLDCs with a variety of guide dimensions, separations, and coupling lengths could be incorporated in the mask, allowing the researcher to more fully characterize the coupling between guides and experimentally confirm the nonlinear optical properties of polyphenylene. Isolated waveguides, for making loss measurements, could also be incorporated in the mask design. An example of such a mask is shown in Fig. 8-1 .

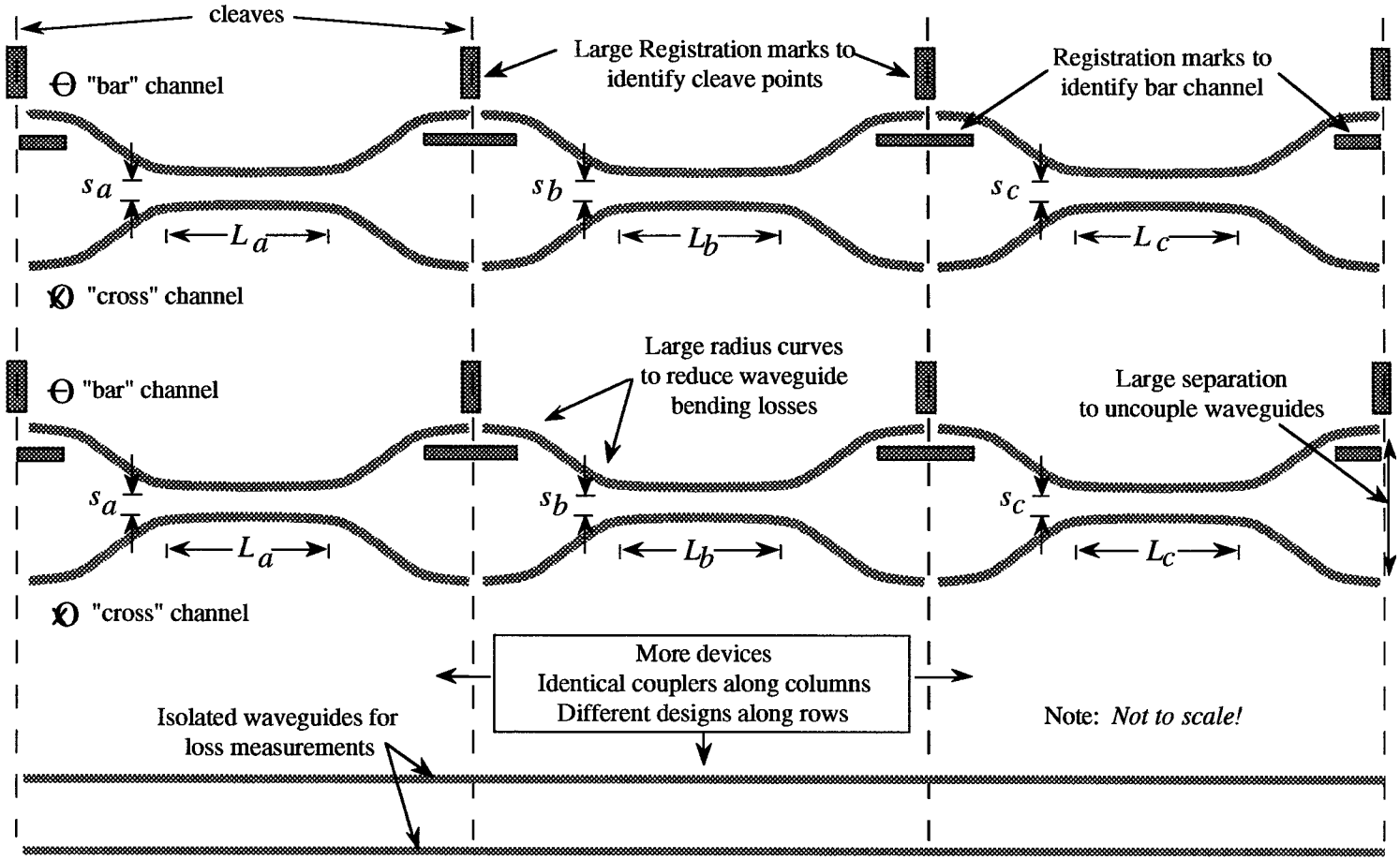

Fig. 8-1. Proposed lithographic mask for further NLDC research. The registration marks serve to identify the proper cleave locations and the bar channels of the devices. The separation between couplers should be large (≈ 20 μm) so that adjacent couplers are isolated. All the couplers in a column could be identical while the couplers along a row could have different guide separations and interaction lengths.

Appendix A: Waveguide Dimensions for Single-mode Operation

This document calculates the min and max waveguide dimensions for a single-mode waveguide. The indicies of the materials and the free-space wavelength of operation must be entered into the document. See Fig. 2-2 for geometry.

Constants

$\mu m := 10^{-6} \cdot m$ $\quad nm := 10^{-9} \cdot m$ $\quad c := 2.998 \cdot 10^{8} \cdot \frac{m}{sec}$

Material and Structure Parameters

$n_c := 1.71$ $\quad \lambda_o := 0.92 \cdot \mu m$ $\quad k_o := \frac{2 \cdot \pi}{\lambda_o}$

$n_g := 1.79$ $\quad \lambda := \frac{\lambda_o}{n_g}$ $\quad \omega := k_o \cdot c$

$n_s := 1.5$ $\quad \lambda = 0.514 \cdot \mu m$

Calculation of Critical Angles

NOTE: "bar" means the completment of the angle.

$\theta_{cgc} := \operatorname{asin}\left(\frac{n_c}{n_g}\right)$ $\quad \theta_{cgc} = 72.806 \cdot deg$ $\quad \theta_{cgc.bar} := \frac{\pi}{2} - \theta_{cgc}$ $\quad \theta_{cgc.bar} = 17.194 \cdot deg$

$\theta_{cgs} := \operatorname{asin}\left(\frac{n_s}{n_g}\right)$ $\quad \theta_{cgs} = 56.928 \cdot deg$ $\quad \theta_{cgs.bar} := \frac{\pi}{2} - \theta_{cgs}$ $\quad \theta_{cgs.bar} = 33.072 \cdot deg$

$\theta_{cgc} := Re(\theta_{cgc})$ $\quad \theta_{cgs} := Re(\theta_{cgs})$

$\theta_{c.limiting.bar} := if(\theta_{cgc} > \theta_{cgs}, \theta_{cgc.bar}, \theta_{cgs.bar})$

$\theta_{c.limiting.bar} = 17.194 \cdot deg$

Note: The larger of the two critical angles limits the number of guided modes in the structure.

At cutoff for a mode, the bounce angle is equal to θc.limiting.bar.

$\theta_{mode} := \theta_{c.limiting.bar}$ $\quad \theta_{mode} = 17.194 \cdot deg$

Goos-Haenchen Phase Shifts

$$\phi_{gs}(\theta) := \operatorname{atan}\left[\frac{\left(n_g^2 \cdot \sin\left(\frac{\pi}{2} - \theta\right)^2 - n_s^2\right)^{\frac{1}{2}}}{n_g \cdot \cos\left(\frac{\pi}{2} - \theta\right)}\right]$$

NOTE: Calculation of the phase shifts upon reflection for the two interfaces. (see Hunsperger, p. 28)

$$\phi_{gc}(\theta) := \operatorname{atan}\left[\frac{\left(n_g^2 \cdot \sin\left(\frac{\pi}{2} - \theta\right)^2 - n_c^2\right)^{\frac{1}{2}}}{n_g \cdot \cos\left(\frac{\pi}{2} - \theta\right)}\right]$$

(for TE mode, E-field in x direction.)

$mode := 0$

$$Mint_g := \mathrm{Re}\left[\frac{mode \cdot \pi + \phi_{gs}(\theta_{mode}) + \phi_{gc}(\theta_{mode})}{(k_o \cdot n_g \cdot \sin(\theta_{mode}))}\right]$$

$Mint_g = 0.276 \cdot \mu m$

NOTE: That there is a MINIMUM thickness for an asymmetric guide structure (where $n_c \neq n_s$).
Below this thickness, the fundamental mode will not propagate. To find the minimum thickness for an asymmetric waveguide, set the variable 'mode' to zero.

$mode := 1$ Set to '1' for max dimension of single mode, '2' for max dimension that will only support modes up to m = 1, etc.

$$Maxt_g := \mathrm{Re}\left[\frac{mode \cdot \pi + \phi_{gs}(\theta_{mode}) + \phi_{gc}(\theta_{mode})}{(k_o \cdot n_g \cdot \sin(\theta_{mode}))}\right]$$

$Maxt_g = 1.146 \cdot \mu m$

Note: take real part to avoid any round-off problems that would result in complex value.

NOTE!!! These are the minimum and maximum dimension of the guide for single mode operation. For well confined modes, the actual design dimension of the guide should be somewhat greater than the minimum and somewhat less than the maximum.

Calculation of numerical aperture of guide:

$n := \mathrm{if}(n_c > n_s, n_c, n_s)$ $\quad NA := \left(n_g^2 - n^2\right)^{\frac{1}{2}}$ $\quad NA = 0.529$

Appendix B: Slab Waveguide Electric Field Profiles

This Mathcad document calculates and plots the profile of the mode in a slab waveguide.

Constants

$\mu m := 10^{-6} \cdot m$ $\quad nm := 10^{-9} \cdot m$ $\quad c := 2.998 \cdot 10^{8} \cdot \frac{m}{sec}$

Material and Structure Parameters

$n_c := 1.71$ $\quad t_g := 0.67 \cdot \mu m$ Guide layer thickness $\quad \lambda_o := 0.92 \cdot \mu m$ Free-space wavelength of operation.

$n_g := 1.79$ $\quad k_o := \frac{2 \cdot \pi}{\lambda_o}$ $\quad \lambda := \frac{\lambda_o}{n_g}$ Wavelength in the guide media

$n_s := 1.5$ $\quad \omega := k_o \cdot c$ $\quad \lambda = 0.514 \cdot \mu m$

Calculation of Critical Angles

NOTE: "bar" means the completment of the angle.

$\theta_{cgc} := \operatorname{asin}\left(\frac{n_c}{n_g}\right)$ $\quad \theta_{cgc} = 72.806 \cdot deg$ $\quad \theta_{cgc.bar} := \frac{\pi}{2} - \theta_{cgc}$ $\quad \theta_{cgc.bar} = 17.194 \cdot deg$

$\theta_{cgs} := \operatorname{asin}\left(\frac{n_s}{n_g}\right)$ $\quad \theta_{cgs} = 56.928 \cdot deg$ $\quad \theta_{cgs.bar} := \frac{\pi}{2} - \theta_{cgs}$ $\quad \theta_{cgs.bar} = 33.072 \cdot deg$

Calculation of Bounce Angles

$$\phi_{gs}(\theta) := \operatorname{atan}\left[\frac{\left(n_g^2 \cdot \sin\left(\frac{\pi}{2} - \theta\right)^2 - n_s^2\right)^{\frac{1}{2}}}{n_g \cdot \cos\left(\frac{\pi}{2} - \theta\right)}\right]$$

NOTE: Calculation of the phase shifts upon reflection for the two interfaces. (see Hunsperger, p. 28)

$$\phi_{gc}(\theta) := \operatorname{atan}\left[\frac{\left(n_g^2 \cdot \sin\left(\frac{\pi}{2} - \theta\right)^2 - n_c^2\right)^{\frac{1}{2}}}{n_g \cdot \cos\left(\frac{\pi}{2} - \theta\right)}\right]$$

Goos-Haenchen phase shifts (for TE polarization, E-field in x direction)

Solve for the Bounce Angle of the Mode

$mode := 0$ Mode to calculate profle. Note that m=0 is the fundamental mode. If a mode is selected that the structure can not support, no solution will be found by the bounce angle calculation.

$\theta := 0.1 \cdot deg$ Initial guess for solve block

given

Transverse Resonance Condition!

$$2 \cdot k_o \cdot n_g \cdot t_g \cdot \sin(\theta) - 2 \cdot \phi_{gs}(\theta) - 2 \cdot \phi_{gc}(\theta) = 2 \cdot mode \cdot \pi$$

$$\theta > 0$$

$\theta_m := find(\theta)$ $\theta_m = 13.036 \cdot deg$ Bounce angle for the mode

$\phi_m := \frac{\pi}{2} - \theta_m$ $\phi_m = 76.964 \cdot deg$ Angle of incidence for the mode

Field Parameters

$\beta_m := n_g \cdot k_o \cdot \cos(\theta_m)$ $\beta_m = 1.191 \cdot 10^7 \cdot m^{-1}$

$q_m := \left(\beta_m^2 - n_c^2 \cdot k_o^2\right)^{\frac{1}{2}}$ $q_m = 2.336 \cdot 10^6 \cdot m^{-1}$

Calculation of field parameters for the mode. (see thesis and Hunsperger pg. 32)

$h_m := \left(n_g^2 \cdot k_o^2 - \beta_m^2\right)^{\frac{1}{2}}$ $h_m = 2.757 \cdot 10^6 \cdot m^{-1}$

$p_m := \left(\beta_m^2 - n_s^2 \cdot k_o^2\right)^{\frac{1}{2}}$ $p_m = 6.074 \cdot 10^6 \cdot m^{-1}$

Calculation of Mode Profiles

$$cover(C_m, y) := C_m \cdot \exp\left[-q_m \cdot \left(y - \frac{t_g}{2}\right)\right]$$

Note: functional forms for mode profile. (see Hunsperger, pg. 31)

$$guide(C_m, y) := C_m \cdot \left[\cos\left[h_m \cdot \left(y - \frac{t_g}{2}\right)\right] - \left(\frac{q_m}{h_m}\right) \cdot \sin\left[h_m \cdot \left(y - \frac{t_g}{2}\right)\right]\right]$$

$$substrate(C_m, y) := C_m \cdot \left[\cos(h_m \cdot t_g) + \left(\frac{q_m}{h_m}\right) \cdot \sin(h_m \cdot t_g)\right] \cdot \exp\left[p_m \cdot \left(y + \frac{t_g}{2}\right)\right]$$

$$\text{tophalf}(C_m, y) := \text{if}\left(y > \frac{t_g}{2}, \text{cover}(C_m, y), \text{guide}(C_m, y)\right)$$

$$\text{eprofile}_x(C_m, y) := \text{if}\left(y < -\frac{t_g}{2}, \text{substrate}(C_m, y), \text{tophalf}(C_m, y)\right)$$

$$\text{Iprofile}(C_m, y) := \text{eprofile}_x(C_m, y)^2$$

Note: $2t_g$ used to approximate infinity. Increase for poorly confined modes.

$$\text{Normalization}(C_m) := \int_{-2\cdot t_g}^{2\cdot t_g} \text{eprofile}_x(C_m, y)^2 \, dy$$

See Saleh, pg. 253

$C_m := 485\cdot m^{-0.5}$ initial guess for normalization constant

given

$C_m > 0\cdot m^{-0.5}$

$\text{Normalization}(C_m) = 1$

$C_m := \text{find}(C_m)$

$C_m = 961.145\cdot m^{-0.5}$ $\quad$ $\text{Normalization}(C_m) = 1$

Plot mode profile in x direction

$y := -2\cdot t_g, -1.95\cdot t_g .. 2\cdot t_g$

Electric Field Profile

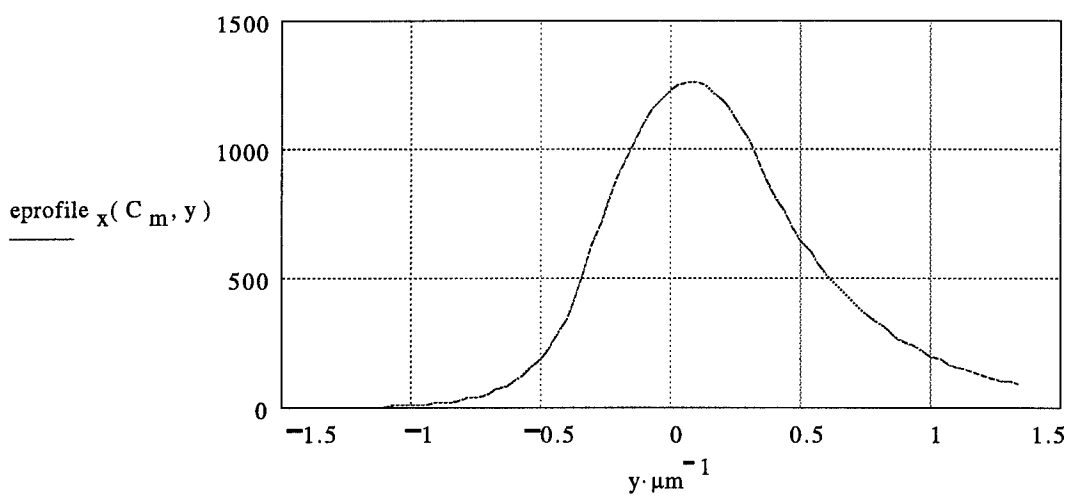

guide thickness: $t_g = 0.67\cdot\mu m$

mode = 0

Note that zero on horzontal scale is the middle of the guide region. Positive y is the upper part of guide and cover region, negative y is the lower half of guide and substrate region.

Appendix C:
Effective Index Method for Strip-Loaded Waveguides

This document uses the effective index method to calculate the effective index of Regions I and II for the strip-loaded waveguide structure shown below.

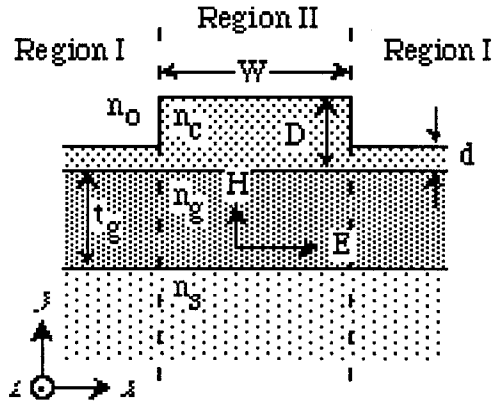

Constants

$\mu m := 10^{-6} \cdot m$ $\quad$ $nm := 10^{-9} \cdot m$

$c := 2.998 \cdot 10^{8} \cdot \frac{m}{sec}$

Material and Structure Parameters

$n_c := 1.71$ $\quad$ $t_g := 0.67 \cdot \mu m$ Guide layer thickness $\quad$ $\lambda_o := 0.92 \cdot \mu m$ Free-space wavelength of operation.

$n_g := 1.79$ $\quad$ $D := 1.2 \cdot \mu m$ $\quad$ $\lambda := \frac{\lambda_o}{n_g}$ Wavelength in the guide media

$n_s := 1.5$ $\quad$ $d := 0.6 \cdot \mu m$

$n_o := 1.0$ $\quad$ $k_o := \frac{2 \cdot \pi}{\lambda_o}$ $\quad$ $\omega := k_o \cdot c$ $\quad$ $\lambda = 0.51 \cdot \mu m$

$m_y := 0$ The mode for which you are seeking the propagation constant. Note that m_y=0 is the fundamental mode.

Calculation of the propagation constant in the z direction

(see Chuang, pg. 21-33)

$$\gamma_s(\beta) := \sqrt{\beta^2 - \frac{n_s^2 \cdot \omega^2}{c^2}} \qquad \gamma_c(\beta) := \sqrt{\beta^2 - \frac{n_c^2 \cdot \omega^2}{c^2}} \qquad \gamma_o(\beta) := \sqrt{\beta^2 - \frac{n_o^2 \cdot \omega^2}{c^2}}$$

$$\eta(\beta) := \frac{\gamma_c(\beta) - \gamma_o(\beta)}{\gamma_c(\beta) + \gamma_o(\beta)} \qquad k_{gy}(\beta) := \sqrt{\frac{n_g^2 \cdot \omega^2}{c^2} - \beta^2}$$

Trancendental equations to be solved for beta. Note: absolute value of argument because of 1st quadrant!

$$\text{RegionIILHS}(\beta) := k_{gy}(\beta)\cdot t_g$$

$$\text{RegionIIRHS}(\beta) := \text{atan}\left(\left|\frac{\gamma_s(\beta)}{k_{gy}(\beta)}\right|\right) + \text{atan}\left[\left|\frac{\gamma_c(\beta)\cdot(1-\eta(\beta)\cdot\exp(-2\cdot\gamma_c(\beta)\cdot D))}{k_{gy}(\beta)\cdot(1+\eta(\beta)\cdot\exp(-2\cdot\gamma_c(\beta)\cdot D))}\right|\right] + m_y\cdot\pi$$

$$\text{RegionILHS}(\beta) := k_{gy}(\beta)\cdot t_g$$

$$\text{RegionIRHS}(\beta) := \text{atan}\left(\left|\frac{\gamma_s(\beta)}{k_{gy}(\beta)}\right|\right) + \text{atan}\left[\left|\frac{\gamma_c(\beta)\cdot(1-\eta(\beta)\cdot\exp(-2\cdot\gamma_c(\beta)\cdot d))}{k_{gy}(\beta)\cdot(1+\eta(\beta)\cdot\exp(-2\cdot\gamma_c(\beta)\cdot d))}\right|\right] + m_y\cdot\pi$$

Finding beta for region II (under the loading strip).

$$\beta := n_o\cdot k_o, 1.05\cdot n_o\cdot k_o .. n_g\cdot k_o$$

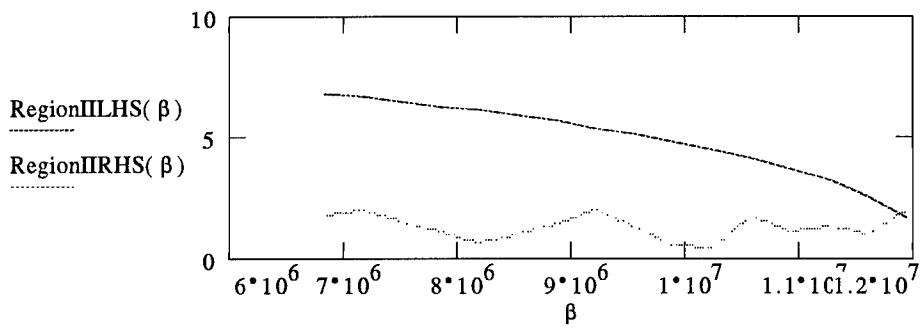

$$\text{RegionIIDiff}(\beta) := |\text{RegionIILHS}(\beta) - \text{RegionIIRHS}(\beta)|$$

$\beta := 1.19\cdot 10^7\cdot m^{-1}$ NOTE: The initial guess is critical to the success of this routine. Use the above graph to pick a beta that is very close to the value at intersection.

given

$\beta < n_g\cdot k_o$

$\beta > n_o\cdot k_o$

$\text{RegionIIDiff}(\beta) < 0.001$

$\text{RegionII}\beta_m := \text{find}(\beta)$ $\quad \text{RegionII}\beta_m = 1.1909\cdot 10^7\cdot m^{-1}$

$\text{RegionIIN}_{eff} := \dfrac{\text{RegionII}\beta_m}{k_o}$ $\quad \text{RegionIIN}_{eff} = 1.7438$

Finding beta for region I (outside loading strip).

$\beta := n_o \cdot k_o, 1.05 \cdot n_o \cdot k_o .. n_g \cdot k_o$

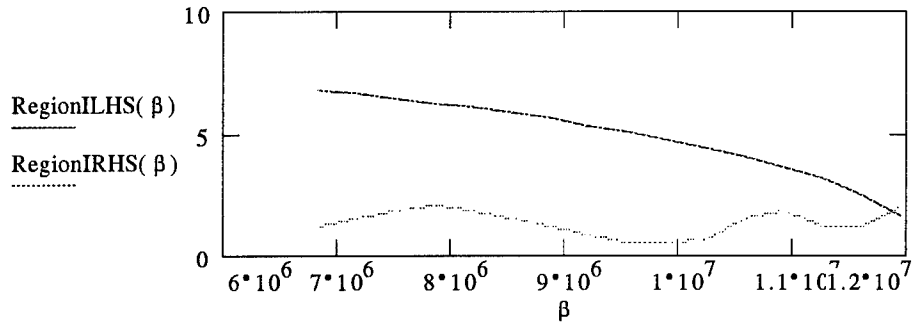

$\text{RegionIDiff}(\beta) := |\text{RegionILHS}(\beta) - \text{RegionIRHS}(\beta)|$

$\beta := 1.19 \cdot 10^7 \cdot m^{-1}$

NOTE: The initial guess is critical to the success of this routine. Use the above graph to pick a beta that is very close to the value at intersection.

given

$\beta < n_g \cdot k_o$

$\beta > n_o \cdot k_o$

$\text{RegionIDiff}(\beta) < 0.001$

$\text{RegionI}\beta_m := \text{find}(\beta)$

$\text{RegionI}\beta_m = 1.1903 \cdot 10^7 \cdot m^{-1}$

$\text{RegionIN}_{eff} := \dfrac{\text{RegionI}\beta_m}{k_o}$

$\text{RegionIN}_{eff} = 1.7428$

$\text{RegionIIN}_{eff} = 1.7438$

$m_y = 0$

Mode number in the x direction for which these numbers were found. They ARE mode dependent!

Calculation of equivalent index for strip-loaded guide

$N_{eq} := \left(n_g^2 - \text{RegionIIN}_{eff}^2 + \text{RegionIN}_{eff}^2\right)^{\frac{1}{2}}$

$N_{eq} = 1.78904$

NOTE: This is the value that should be substituted for n_3 and n_5 in Marcatili's method.

Appendix D:
Effective Index Method for Rib Waveguides

This document uses the effective index method to calculate the effective index of Regions I and II for the rib waveguide structure shown below.

Constants

$\mu m := 10^{-6} \cdot m \qquad nm := 10^{-9} \cdot m$

$c := 2.998 \cdot 10^{8} \cdot \frac{m}{sec}$

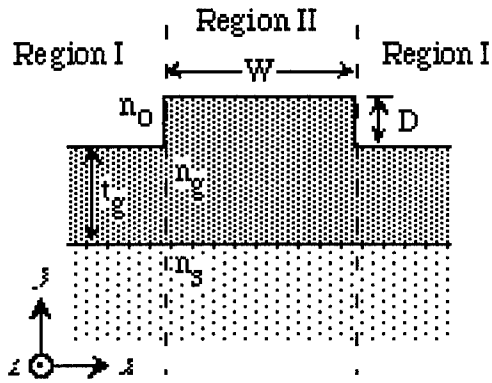

Material and Structure Parameters

$n_g := 1.71$	$t_g := 0.5 \cdot \mu m$	Guide layer thickness	$\lambda_o := 0.92 \cdot \mu m$	Free-space wavelength of operation.
$n_s := 1.5$	$D := 0.1 \cdot \mu m$	Rib height	$\lambda := \frac{\lambda_o}{n_g}$	Wavelength in the guide media
$n_o := 1.0$	$W := 3 \cdot \mu m$	Guide width	$\lambda = 0.54 \cdot \mu m$	
$k_o := \frac{2 \cdot \pi}{\lambda_o}$	$\omega := k_o \cdot c$			

$mode_y := 0$ The mode in the y direction for which you are seeking the propagation constant.
NOTE: mode = 0 is the fundamental mode.

Calculation of the propagation constant in the z direction

(see Chuang, pg. 21-33)

$$\gamma_s(\beta) := \sqrt{\beta^2 - \frac{n_s^2 \cdot \omega^2}{c^2}} \qquad \gamma_o(\beta) := \sqrt{\beta^2 - \frac{n_o^2 \cdot \omega^2}{c^2}} \qquad k_{gy}(\beta) := \sqrt{\frac{n_g^2 \cdot \omega^2}{c^2} - \beta^2}$$

Trancendental equations to be solved for beta. Note: absolute value of argument because of 1st quadrant!

$$RegionIILHS(\beta) := k_{gy}(\beta)\cdot(t_g + D)$$ Under the rib

$$RegionIIRHS(\beta) := atan\left(\left|\frac{\gamma_s(\beta)}{k_{gy}(\beta)}\right|\right) + atan\left(\left|\frac{\gamma_o(\beta)}{k_{gy}(\beta)}\right|\right) + mode_y\cdot\pi$$

$$RegionILHS(\beta) := k_{gy}(\beta)\cdot t_g$$ Outside the rib

$$RegionIRHS(\beta) := atan\left(\left|\frac{\gamma_s(\beta)}{k_{gy}(\beta)}\right|\right) + atan\left(\left|\frac{\gamma_o(\beta)}{k_{gy}(\beta)}\right|\right) + mode_y\cdot\pi$$

Finding beta for region II (under the loading strip).

$$\beta := n_o\cdot k_o, 1.01\cdot n_o\cdot k_o .. n_g\cdot k_o$$

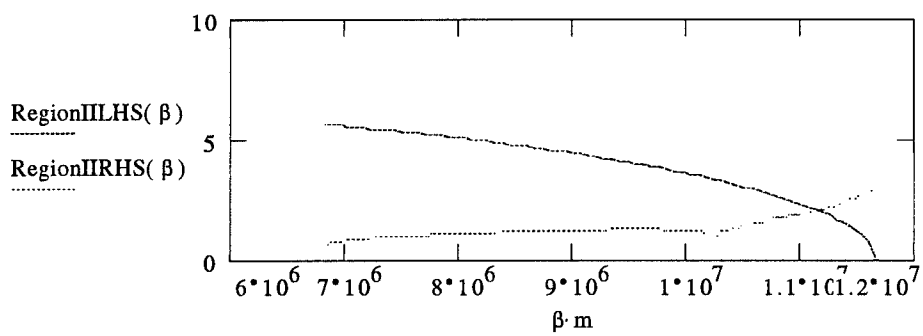

$$RegionIIDiff(\beta) := |RegionIILHS(\beta) - RegionIIRHS(\beta)|$$

$\beta := 1.114\cdot 10^7\cdot m^{-1}$

NOTE: The initial guess is critical to the success of this routine. Use the above graph to pick a beta that is very close to the value at intersection. If Mathcad has a problem finding a solution that obviously exists, try increasing the tolerance of the Diff(Beta) function in the Given block.

given

$\beta < n_g\cdot k_o$

$\beta > n_o\cdot k_o$

$RegionIIDiff(\beta) < 0.0001$

$RegionII\beta_m := find(\beta)$

$RegionII\beta_m = 1.115\cdot 10^7\cdot m^{-1}$

$$RegionIIN_{eff} := \frac{RegionII\beta_m}{k_o} \qquad RegionIIN_{eff} = 1.632$$

Finding beta for region I (outside loading strip).

$\beta := n_o \cdot k_o, 1.05 \cdot n_o \cdot k_o .. n_g \cdot k_o$

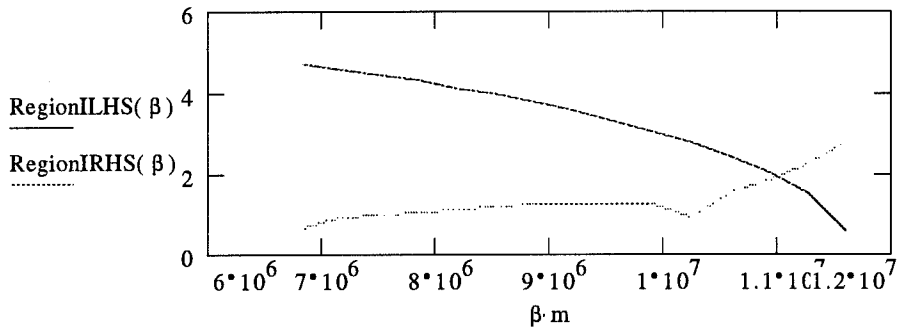

$\text{RegionIDiff}(\beta) := |\text{RegionILHS}(\beta) - \text{RegionIRHS}(\beta)|$

$\beta := 1.09 \cdot 10^7 \cdot m^{-1}$

given

$\beta < n_g \cdot k_o$

$\beta > n_o \cdot k_o$

$\text{RegionIDiff}(\beta) < 0.0001$

NOTE: The initial guess is critical to the success of this routine. Use the above graph to pick a beta that is very close to the value at intersection. If Mathcad has a problem finding a solution that obviously exists, try increasing the tolerance of the Diff(Beta) function in the Given block.

$\text{RegionI}\beta_m := \text{find}(\beta)$

$\text{RegionI}\beta_m = 1.101 \cdot 10^7 \cdot m^{-1}$

$\text{RegionIN}_{eff} := \dfrac{\text{RegionI}\beta_m}{k_o}$

$\text{RegionIN}_{eff} = 1.612$

$\text{RegionIIN}_{eff} = 1.632$

$\text{mode}_y = 0$

Mode number in the x direction for which these numbers were calculated. They ARE mode dependent!!

$N_{eq} := \left(n_g^2 - \text{RegionIIN}_{eff}^2 + \text{RegionIN}_{eff}^2\right)^{\frac{1}{2}}$

$N_{eq} = 1.691$

Note: This is the value that should be substituted for n_3 and n_5 in Maracatilli's method.

Appendix E: Marcatili's Method for Embedded Guides

This MathCAD document calculates and plots the profile of the transverse modes in a general waveguide structure like the one shown below.

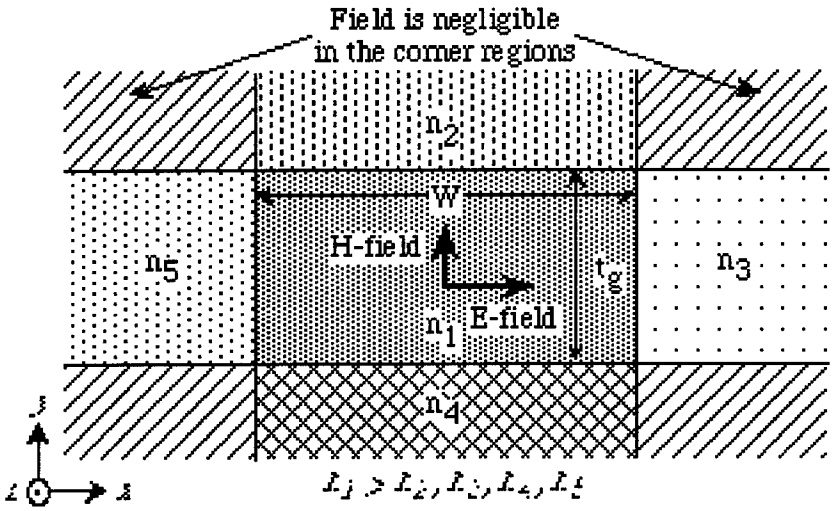

Constants

$\mu m := 10^{-6} \cdot m$ $\quad nm := 10^{-9} \cdot m$ $\quad c := 2.998 \cdot 10^{8} \cdot \frac{m}{sec}$

$kW := 10^{3} \cdot watt$ $\quad GW := 10^{9} \cdot watt$ $\quad gram := 10^{-3} \cdot kg$

Material and Structure Parameters

$n_1 := 1.79$ $\quad W := 5 \cdot \mu m$ $\quad \lambda_o := 0.92 \cdot \mu m$ $\quad k_o := \frac{2 \cdot \pi}{\lambda_o}$ $\quad \omega := k_o \cdot c$

$n_2 := 1.71$ $\quad t_g := 0.67 \cdot \mu m$ $\quad Area := t_g \cdot W$

$s := 2 \cdot \mu m$ guide separation in coupler

$n_3 := 1.789$

$aspect := \frac{W}{t_g}$ $\quad aspect = 7.463$

$n_4 := 1.5$

Note: Method works best for aspect ratios greater than 2.

$p := 1$ for modes in x direction

$n_5 := 1.789$

$q := 1$ for modes in y direction

Mode numbers. Note that p = q =1 is the fundamental mode.

$n_{2mks} := 2.03 \cdot 10^{-10}$ <- NOTE: n2 MUST be in units of cm^2/kW
This is the value for polyphenylene.

$n_{2esu} := \frac{n_{2mks} \cdot n_1}{8.4} \cdot cm \cdot \frac{sec^2}{gram}$

See formula A5.13b from (3), pg 306-308
These are the ESU units used by Jensen.
n = no+n2esu*|E|^2 so n2esu has units of 1/E^2 in
ESU units: cm^2/statvolt^2 = cm*sec^2/gram

$n_{2esu} = 4.326 \cdot 10^{-11} \cdot cm \cdot \frac{sec^2}{gram}$

Solve transcendental equation to find propagation constants

$$A_2 := \frac{\lambda_o}{2\cdot\sqrt{n_1^2 - n_2^2}} \qquad A_3 := \frac{\lambda_o}{2\cdot\sqrt{n_1^2 - n_3^2}}$$

From Marcatili

$$A_4 := \frac{\lambda_o}{2\cdot\sqrt{n_1^2 - n_4^2}} \qquad A_5 := \frac{\lambda_o}{2\cdot\sqrt{n_1^2 - n_5^2}}$$

$$\eta_2(k_y) := \left[\left(\frac{\pi}{A_2}\right)^2 - k_y^2\right]^{-\frac{1}{2}} \qquad \xi_3(k_x) := \left[\left(\frac{\pi}{A_3}\right)^2 - k_x^2\right]^{-\frac{1}{2}}$$

$$\eta_4(k_y) := \left[\left(\frac{\pi}{A_4}\right)^2 - k_y^2\right]^{-\frac{1}{2}} \qquad \xi_5(k_x) := \left[\left(\frac{\pi}{A_5}\right)^2 - k_x^2\right]^{-\frac{1}{2}}$$

$$LHS_y(k_y) := k_y\cdot t_g$$

Equations to solve for propagation constants, from Marcatili.

$$RHS_y(k_y) := q\pi - \mathrm{atan}(\,|k_y\cdot\eta_2(k_y)|\,) - \mathrm{atan}(\,|k_y\cdot\eta_4(k_y)|\,)$$

$$LHS_x(k_x) := k_x\cdot W$$

$$RHS_x(k_x) := p\cdot\pi - \mathrm{atan}\left[\left|\left(\frac{n_3}{n_1}\right)^2\cdot k_x\cdot\xi_3(k_x)\right|\right] - \mathrm{atan}\left[\left|\left(\frac{n_5}{n_1}\right)^2\cdot k_x\cdot\xi_5(k_x)\right|\right]$$

$$k_y := 0\cdot m^{-1}, 500000\cdot m^{-1} .. k_o$$

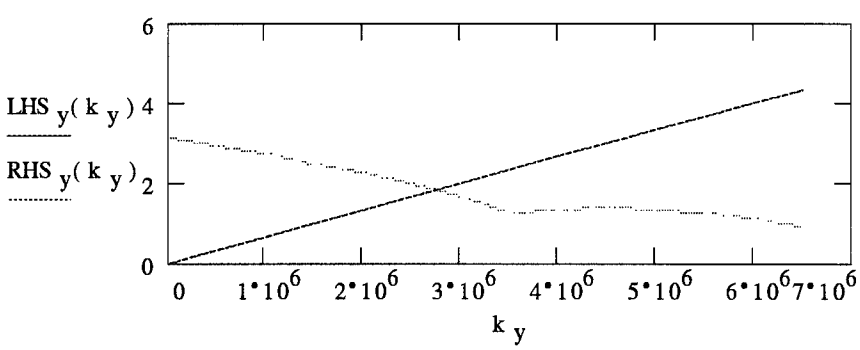

$Diff_y(k_y) := |LHS_y(k_y) - RHS_y(k_y)|$

$k_y := 3.5 \cdot 10^6 \cdot m^{-1}$ NOTE: The initial guess is critical to the success of this routine. Use the above graph to pick a beta that is very close to the value at intersection.

given

$k_y > 0 \cdot m^{-1}$

$k_y < k_o$

$Diff_y(k_y) < 0.0001$

$k_y := find(k_y)$ $k_y = 2.758 \cdot 10^6 \cdot m^{-1}$ Propagation constant in y direction

$k_x := 0 \cdot m^{-1}, 20000 \cdot m^{-1} .. 0.5 \cdot k_y$

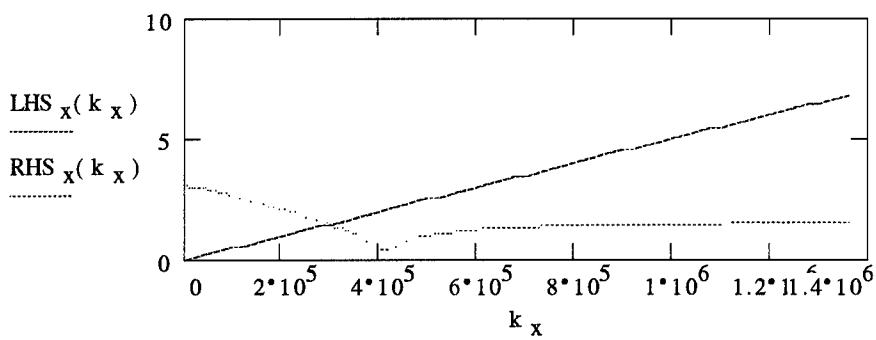

$Diff_x(k_x) := |LHS_x(k_x) - RHS_x(k_x)|$

$k_x := 4 \cdot 10^5 \cdot m^{-1}$ NOTE: The initial guess is critical to the success of this routine. Use the above graph to pick a beta that is very close to the value at intersection.

given

$k_x > 0 \cdot m^{-1}$

$k_x < k_o$

$Diff_x(k_x) < 0.0001$

$k_x := find(k_x)$ $k_x = 2.995 \cdot 10^5 \cdot m^{-1}$ Propagation constant in x direction

Plot profile of mode in y direction

$R2_{G1}$ = region 2 for guide 1
$R1y_{G1}$ = region 1 in y for guide 1
(follows this pattern, see figure aat beginning of document for region locations.)

$$R2_{G1}(y, C_y) := C_y \cdot \exp\left[-\frac{\left(y - \frac{t_g}{2}\right)}{\eta_2(k_y)}\right]$$

$$R1y_{G1}(y, C_y) := C_y \cdot \left[\cos\left[k_y \cdot \left(y - \frac{t_g}{2}\right)\right] - \left(\frac{1}{k_y \cdot \eta_2(k_y)}\right) \cdot \sin\left[k_y \cdot \left(y - \frac{t_g}{2}\right)\right]\right]$$

$$R4_{G1}(y, C_y) := C_y \cdot \left[\cos(k_y \cdot (-t_g)) - \left(\frac{1}{k_y \cdot \eta_2(k_y)}\right) \cdot \sin(k_y \cdot (-t_g))\right] \cdot \exp\left(\frac{y + \frac{t_g}{2}}{\eta_4(k_y)}\right)$$

$$R1R2_{G1}(y, C_y) := \text{if}\left(y > \frac{t_g}{2}, R2_{G1}(y, C_y), R1y_{G1}(y, C_y)\right)$$

$$\text{yeprofile}(y, C_y) := \text{if}\left(y < -\frac{t_g}{2}, R4_{G1}(y, C_y), R1R2_{G1}(y, C_y)\right)$$ profile of electric field

$$\text{Normalization}_y(C_y) := \int_{-3 \cdot t_g}^{3 \cdot t_g} \text{yeprofile}(y, C_y)^2 \, dy$$ See Saleh, pg. 251

$C_y := 960 \cdot m^{-0.5}$ initial guess for normalization constant

given

$C_y > 0 \cdot m^{-0.5}$

$\text{Normalization}_y(C_y) = 1$

$C_y := \text{find}(C_y)$

$C_y = 960.383 \cdot m^{-0.5}$ $\text{Normalization}_y(C_y) = 1$

Plotting the electric field profile

$y := -1.5 \cdot t_g, -1.45 \cdot t_g .. 2.5 \cdot t_g$

Electric Field Profile

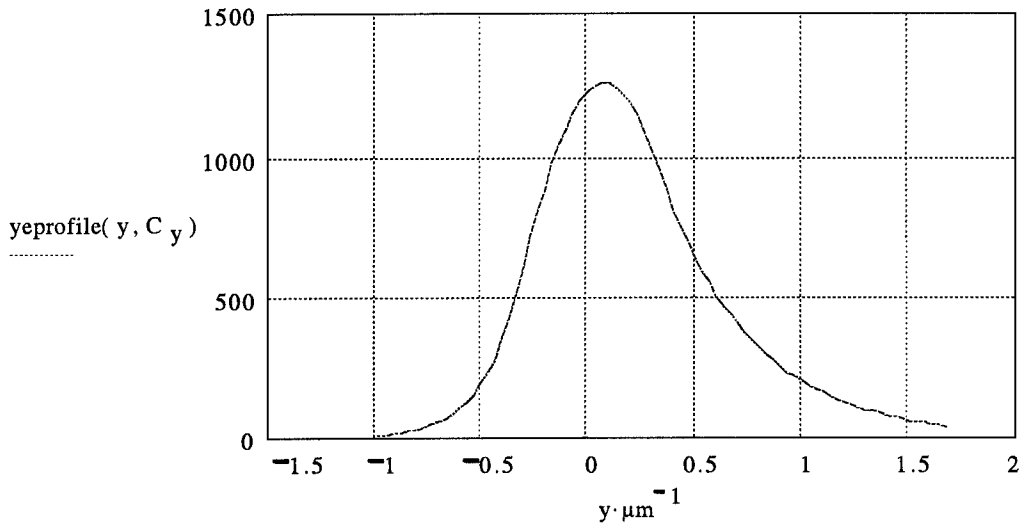

guide thickness is: $t_g = 0.67 \cdot \mu m$

Note: y = 0 is center of guide. Positive y values are upper half of guide and cover. Negative y values are lower half of guide and substrate.

mode number in y direction is: $q = 1$

Note: q = 1 is fundamental mode

Plotting profile of mode in x direction

$$R3_{G1}(x, C_x) := C_x \cdot \exp\left[-\frac{\left(x - \frac{W}{2}\right)}{\xi_3(k_x)}\right]$$

$$R1x_{G1}(x, C_x) := C_x \cdot \left[\cos\left[k_x \cdot \left(x - \frac{W}{2}\right)\right] - \left(\frac{1}{k_x \cdot \xi_3(k_x)}\right) \cdot \sin\left[k_x \cdot \left(x - \frac{W}{2}\right)\right]\right]$$

$$R5_{G1}(x, C_x) := C_x \cdot \left[\cos(k_x \cdot (-W)) - \left(\frac{1}{k_x \cdot \xi_3(k_x)}\right) \cdot \sin(k_x \cdot (-W))\right] \cdot \exp\left(\frac{x + \frac{W}{2}}{\xi_5(k_x)}\right)$$

$$R1R3_{G1}(x, C_x) := \text{if}\left(x > \frac{W}{2}, R3_{G1}(x, C_x), R1x_{G1}(x, C_x)\right)$$

$$xeprofile1(x, C_x) := \text{if}\left(x < -\frac{W}{2}, R5_{G1}(x, C_x), R1R3_{G1}(x, C_x)\right)$$

$$\text{Normalization}_x(C_x) := \int_{-2\cdot W}^{2\cdot W} \text{xeprofile1}(x, C_x)^2\, dx$$ from Saleh

$C_x := 180\cdot m^{-0.5}$ initial guess for normalization constant

given

$C_x > 0\cdot m^{-0.5}$

$\text{Normalization}_x(C_x) = 1$

$C_x := \text{find}(C_x)$

$C_x = 297.605\cdot m^{-0.5}$ $\text{Normalization}_x(C_x) = 1$

Plotting the electric field profile

$x := -2\cdot W, -1.9\cdot W .. 2\cdot W$ Electric Field Profile

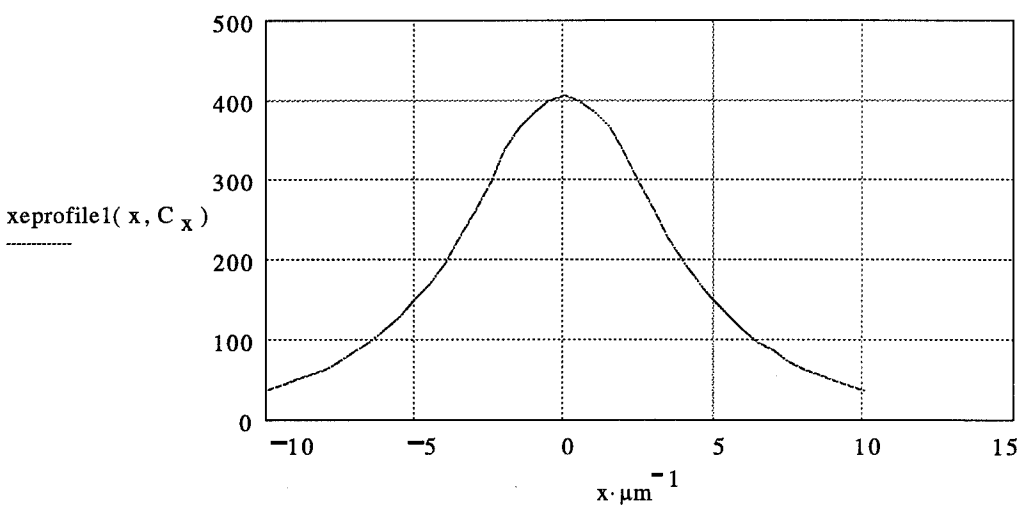

guide width is: $W = 5\cdot\mu m$ Note: x = 0 is center of guide. Positive x values are right half of guide and cover. Negative x values are left half of guide and substrate. (see figure at beginning of document)

mode number in x direction is: $p = 1$ Note: p = 1 is fundamental mode.

Calculation of coupling between guides

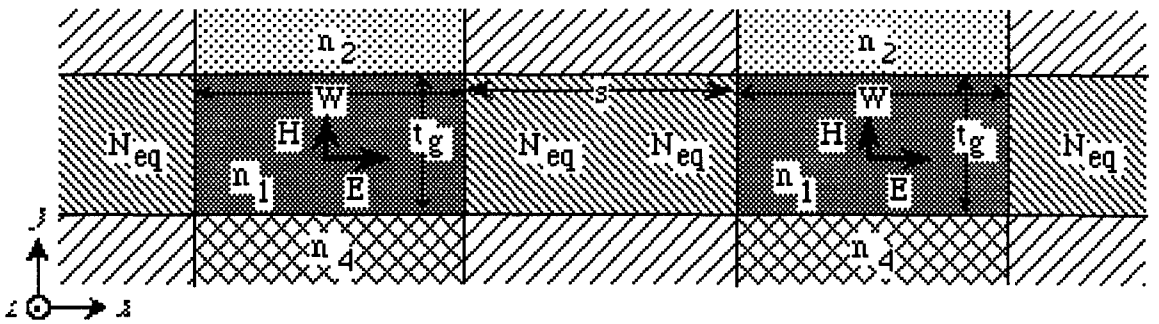

Field profile for second guide, centered on x = s + W

$$R3_{G2}(x) := C_x \cdot \exp\left[-\frac{\left(x - \frac{W}{2} - s - W\right)}{\xi_3(k_x)}\right]$$

$$R1x_{G2}(x) := C_x \cdot \left[\cos\left[k_x \cdot \left(x - \frac{W}{2} - s - W\right)\right] - \left(\frac{1}{k_x \cdot \xi_3(k_x)}\right) \cdot \sin\left[k_x \cdot \left(x - \frac{W}{2} - s - W\right)\right]\right]$$

$$R5_{G2}(x) := C_x \cdot \left[\cos(k_x \cdot (-W)) - \left(\frac{1}{k_x \cdot \xi_3(k_x)}\right) \cdot \sin(k_x \cdot (-W))\right] \cdot \exp\left(\frac{x + \frac{W}{2} - s - W}{\xi_5(k_x)}\right)$$

$$R1xR3_{G2}(x) := \text{if}\left[x > \left(s + \frac{3}{2} \cdot W\right), R3_{G2}(x), R1x_{G2}(x)\right]$$

$$xeprofile2(x) := \text{if}\left[x < \left(s + \frac{1}{2} \cdot W\right), R5_{G2}(x), R1xR3_{G2}(x)\right]$$

$$xIprofile2(x) := xeprofile2(x)^2$$

$$x := -5 \cdot \mu m, -4.9 \cdot \mu m .. 15 \cdot \mu m$$

Electric Field Profiles

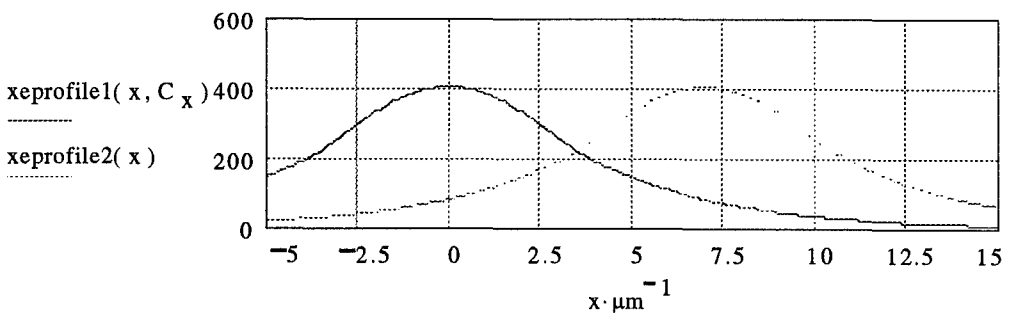

guide width is: W = 5 •μm

guide separation is: s = 2 •μm

Note: p = 1 is the fundamental mode.

Note: x = 0 is the center of guide 1.

mode number in x direction: p = 1

Closely Coupled Calculation Marcatili, pg. 2075, 2099

$$N_{eq} := n_3 \qquad k_z := \left(k_o^2 \cdot n_1^2 - k_x^2 - k_y^2\right)^{\frac{1}{2}} \qquad k_z = 1.191 \cdot 10^7 \cdot m^{-1}$$

$$k_{xeq} := \left[(k_o \cdot N_{eq})^2 - k_z^2 - k_y^2\right]^{\frac{1}{2}}$$

$\left|s \cdot k_{xeq}\right| = 0.556$ The guides are weakly coupled if this quantity is >>1.

$$\kappa_m := \frac{2 \cdot k_x^2 \cdot \frac{1}{\xi_3(k_x)} \cdot t_g \cdot \exp\left(-\frac{s}{\xi_3(k_x)}\right)}{k_z \cdot \left(t_g + \sin(k_y \cdot t_g)^2 \cdot \eta_2(k_y)\right) \cdot (W + 2 \cdot \xi_3(k_x)) \cdot \left(k_x^2 + \frac{1}{\xi_3(k_x)^2}\right)}$$

$\kappa_m = 0.741 \cdot mm^{-1}$

$$\kappa := \left| \frac{1}{2} \cdot \left(n_1^2 - n_3^2\right) \cdot \frac{k_o^2}{k_z} \cdot \int_{-\frac{W}{2}}^{\frac{W}{2}} xeprofile1(x, C_x) \cdot xeprofile2(x)\, dx \right|$$ Using Saleh's equation

$\kappa = 1.185 \cdot mm^{-1}$ $W = 5 \cdot \mu m$ $s = 2 \cdot \mu m$

$p = 1$ mode number in x direction

$$L_o := \frac{\pi}{(2 \cdot \kappa)} \qquad L_o = 1.326 \cdot mm$$

Calculation of Critical Power

$$P_{cJ} := \kappa \cdot Area \cdot \frac{\lambda_o \cdot n_1 \cdot c}{2 \cdot \pi^2 \cdot n_{2esu}}$$

$P_{cJ} = 229.51 \cdot watt$

Bibliography

1. Abramowitz, M. and I. A. Stegam. *Handbook of mathematical functions.* Washington, D.C.: GPO, Mar. 1965.

2. Ankiewicz, A., and G. D. Peng, "Effects of nonlinear mode field changes in optical switching using directional couplers," *J. Opt. Soc. Amer. B*, vol. 9, pp. 1341-1349, Aug. 1992.

3. Butcher, Paul N., and D. Cotter. *The elements of nonlinear optics.* Cambridge, England: Cambridge University Press, 1990.

4. Carter, G. M., Y. J. Chen, and S. K. Tripaythy, "Intensity dependent index of refraction in organic materials," *Opt. Engr.*, vol. 24, pp. 609-612, July 1985.

5. Chuang, Chih-Li. *Semiconductor nonlinear waveguide devices and integrated mirror etalons.* PhD dissertation. University of Arizona, Tucson AZ, 1991.

6. Fraile-Pelaex, F. J., G. Assanto, and D. R. Heatley, "Sign-dependent response of nonlinear directional couplers," *Opt. Commun.*, vol. 77, pp. 402-406, July 15, 1990.

7. Furuta, Hirosuke, H. Noda, and A. Ihaya. "Novel optical waveguide for integrated optics," *App. Optics*, vol. 13, pp. 322-326, Feb. 1974.

8. Grantham, Jeffrey W. Associate Professor of Physics, Air Force Institute of Technology, Wright-Patterson AFB OH. Personal interview. 8 Sep 94.

9. Hayt, Jr., W. *Engineering electromagnetics.* New York: McGraw-Hill, 1981.

10. Holzmann, Gerard J. and Björn Pehrson, "The first data networks," *Scientific American*, vol. 270, pp. 124-129, Jan. 1994.

11. Hunsperger, R. G. *Integrated optics: Theory and technology.* Berlin: Springer-Verlag, 1991.

12. Jaeger, Richard C. *Modular series on solid state devices: Vol. V, Introduction to microelectronic fabrication.* Eds. G. Neudeck and R. Pierret. Reading, MA: Addison-Wesley Publishing Company.

13. Jensen, S. M. "The nonlinear coherent coupler," *IEEE J. Quantum Electron.*, vol. QE-18, pp. 1580-1583, Oct. 1982.

14. Jiang, Hao. Personal interview.

15. Knox, R. M. and P. P. Toulios. "Integrated circuits for the millimeter through optical frequency range," in *Proceedings of the symposium on submillimeter waves, Volume XX.* Ed. Jerome Fox. Brooklyn, NY: Polytechnic Press of the Polytechnic Institute of Brooklyn, 1971.

16. Kogelnik, H. "Theory of dielectric waveguides," in *Integrated Optics.* Ed. T. Tamir. New York: Springer-Verlag, 1985.

17. Koshiba, M. *Optical waveguide analysis*. New York: McGraw-Hill, 1992.

18. Kutsche, Carl A. *Lithographic micropatterning of polythiophene thin-films*. MS thesis, AFIT/GE/ENG/91D-32. School of Engineering, Air Force Institute of Technology (AU), Wright-Patterson AFB OH, December 1991.

19. Leutheuser, V., U. Langbein, and F. Lederer, "Optical response of a nonlinear bent directional coupler," *Opt. Comm.*, vol. 75, pp. 251-255, Mar. 1, 1990.

20. Maier, A. A. "Optical transistors and bistable devices utilizing nonlinear transmission of light in systems with unidirectional coupled waves," *Sov. J. Quantum Electron.*, vol. 12, pp. 1490-1494, Nov. 1982.

21. Marcatili, E. A. J. "Dielectric rectangular waveguide and directional coupler for integrated optics," *Bell Sys. Tech. J.*, vol. 48, pp. 2071-2102, Sep. 1969.

22. X. J. Meng and N. Okamoto, "Improved coupled mode theory for nonlinear directional couplers," *IEEE J. Quantum Electron.*, vol. 27, pp. 1175-1181, May 1991.

23. Möhlmann, G. R., W. H. G. Horsthuis, C. P. J. M. van der Vorst, A. McDonach, M. Copeland, C. Duchet, P. Fabre, M. B. J. Diemeer, E. S. Trommel, F. M. M. Suyten, P. Van Daele, E. Van Tomme, and R. Baets, "Recent developments in optically nonlinear polymers and related electro-optic devices," *Proc. SPIE, Nonlinear Optic. Properties Organic Mater. II*, vol. 1147, pp. 245-255, Aug. 1989.

24. Prasad, P. N. and D. J. Williams, *Introduction to nonlinear optical effects in molecules & polymers*. New York: John Wiley & Sons, Inc., 1991.

25. Saleh, B. E. A. and M. C. Teich, *Fundamentals of photonics*. New York: John Wiley & Sons, Inc., 1991.

26. Somekh, Sasson R. *Theory, fabrication, and performance of some integrated optical-devices*. PhD dissertation. California Institute of Technology, Pasadena CA, 1974.

27. Stegeman, G. I. and E. M. Wright, "All optical waveguide switching," *Optical Quantum Electronics*, vol. 22, pp. 95-122, Mar. 1990.

28. Stegeman, G. I., C. T. Seaton, and R. Zanoni, "Organic films in non-linear integrated optics structures," *Thin Solid Films*, vol. 152, pp. 231-263, Sep. 28, 1987.

29. Syms, R. and J. Cozens, *Optical guided waves and devices*. London: McGraw-Hill, 1992.

30. Sze, S. M. *Semiconductor devices: Physics and technology*. New York: John Wiley & Sons.

31. Tomaru, S., K. Kubodera, and S. Zembutsu, "Optical third-harmonic generation from polydiacetylene thin films deposited by vacuum evaporation," *Electron. Lett.*, vol. 23, pp. 595-596, May 21, 1987.

32. Van Tomme, E., P. P. Van Daele, R. G. Baets, and P. E. Lagasse, "Integrated optic devices based on nonlinear optical polymers," *IEEE J. of Quantum Electron.*, vol. 27, pp. 778-787, Mar. 1991.

33. Verdeyen, J. T. *Laser electronics* (Second Edition). Englewood Cliffs, NJ: Prentice-Hall, Inc.

34. Yariv, A. "Coupled-mode theory for guided-wave optics," *IEEE J. of Quantum Electron.*, vol. QE-9, pp. 919-933, Sep. 1973.

Vita

John Berry was born 18 July, 1967 in Marion, Indiana. He was raised in the nearby communities of Fairmount and Gas City. He graduated from Mississinewa High School, Gas City, Indiana, in May of 1985 and attended Rose-Hulman Institute of Technology (RHIT), Terre Haute, Indiana with a Reserve Officer's Training Corps (ROTC) scholarship. He graduated from RHIT and was commissioned as a second lieutenant in the United States Air Force in May, 1989. His first assignment was to the Phillips Laboratory, Kirtland AFB, New Mexico. While stationed at Kirtland AFB, Captain Berry conducted research on state-of-the-art electro-optical components in radiation environments, including the post-flight analysis of the first active fiber-optic data links flown in a space environment, M0004 - Space Environment Effects on Operating Fiber Optic Systems, flown aboard the Long Duration Exposure Facility (LDEF). Captain Berry was also responsible for the design, fabrication, and testing of the 10 kW electrical power system for the High Altitude Balloon Experiment (HABE) payload while stationed at Kirtland AFB. He entered the Air Force Institute of Technology in June of 1993. Captain John Berry married the former Miss Laurel M. McCulley on 17 June 1994 in Albuquerque, New Mexico. Upon graduation from AFIT, Captain Berry accepted an assignment to the Electrical Engineering faculty of the United States Air Force Academy, Colorado Springs, Colorado.

Captain Berry is a member of Eta Kappa Nu, Tau Beta Pi, and IEEE. His permanent address is: 219 E. S. "F" St., Gas City IN 46933.

REPORT DOCUMENTATION PAGE

Form Approved
OMB No. 0704-0188

Public reporting burden for this collection of information is estimated to average 1 hour per response, including the time for reviewing instructions, searching existing data sources, gathering and maintaining the data needed, and completing and reviewing the collection of information. Send comments regarding this burden estimate or any other aspect of this collection of information, including suggestions for reducing this burden, to Washington Headquarters Services, Directorate for Information Operations and Reports, 1215 Jefferson Davis Highway, Suite 1204, Arlington, VA 22202-4302, and to the Office of Management and Budget, Paperwork Reduction Project (0704-0188), Washington, DC 20503.

1. AGENCY USE ONLY *(Leave blank)*

2. REPORT DATE
December 1994

3. REPORT TYPE AND DATES COVERED
Master's Thesis

4. TITLE AND SUBTITLE
Design, Fabrication, Modeling, and Optical Characterization of Organic Polymer Nonlinear Directional Couplers

5. FUNDING NUMBERS

6. AUTHOR(S)
John Nathan Berry, Capt, USAF

7. PERFORMING ORGANIZATION NAME(S) AND ADDRESS(ES)
Air Force Institute of Technology, WPAFB OH 45433-6583

8. PERFORMING ORGANIZATION REPORT NUMBER
AFIT/GEO/ENP/94D-01

9. SPONSORING/MONITORING AGENCY NAME(S) AND ADDRESS(ES)
RL/OCPB, Rome Laboratory, 25 Electronic Pkwy,
Griffiss AFB NY 13441-4515
WL/MLPJ, Bldg. 651, Wright Laboratory,
WPAFB OH 45403

10. SPONSORING/MONITORING AGENCY REPORT NUMBER

11. SUPPLEMENTARY NOTES

12a. DISTRIBUTION/AVAILABILITY STATEMENT
Distribution Unlimited

12b. DISTRIBUTION CODE

13. ABSTRACT *(Maximum 200 words)*

This research was an investigation into the suitability of a recently developed polymer, polyphenylene, as a material for integrated optical circuits (IOCs). Polymers show great promise in the area of IOCs because of material processing advantages, compatibility with most existing integrated circuit technology, and relatively strong nonlinear optical characteristics. This thesis contains an overview of: dielectric waveguides, linear and nonlinear directional coupler theory; various models useful in the design and analysis of optical waveguides; the fabrication of three different waveguide designs; the experimental apparatus and procedure used to optically characterize the waveguides; and the experimental results of the characterization.

Waveguiding of near infrared light through polyphenylene, in both a slab waveguide and strip-loaded guides, was observed for the first time in this polymer. Coupling of light between guides of a multi-channel directional coupler was also observed. No definitive conclusions concerning nonlinear effects are possible due to the non-identical, multi-channel nature of the fabricated waveguides. The results of this research indicate that polyphenylene is a candidate for use in IOCs and that the polymer should be the topic of further research.

14. SUBJECT TERMS
Nonlinear, Directional Coupler, NLDC, Organic Polymers, Polyphenylene, Integrated Optical Circuits, OIC, Optical Waveguides

15. NUMBER OF PAGES
134

16. PRICE CODE

17. SECURITY CLASSIFICATION OF REPORT	18. SECURITY CLASSIFICATION OF THIS PAGE	19. SECURITY CLASSIFICATION OF ABSTRACT	20. LIMITATION OF ABSTRACT
UNCLASSIFIED	UNCLASSIFIED	UNCLASSIFIED	UL